Computational framework for studying charge transport in high-voltage gas-insulated systems

Shailendra Singh

Computational framework for studying charge transport in high-voltage gas-insulated systems

SHAILENDRA SINGH

Division of Electric Power Engineering
Department of Electrical Engineering
Chalmers University of Technology
SE-41296 Gothenburg
Sweden
Telephone + 46 (0) 31-772 1000

Computational framework for studying charge transport in high-voltage gas-insulated systems

SHAILENDRA SINGH
Department of Electrical Engineering
Chalmers University of Technology

Abstract

Electrical switchgear industry dealing with transmission and distribution of power is strongly affected by the changing dynamics of climate control. Their main contribution to the global warming is through SF_6 gas, having a GWP of 23500 (times of CO_2). SF_6 plays an important role in providing electrical insulation for these high voltage systems. So, there is a need to find an alternative 'green' insulation system. The search is hindered because of lack of design criteria for dielectric withstand in highly inhomogeneous fields, as seen typically in gas-insulated switchgears (GIS). This needs a physical understanding of charge transport and dynamics under such electric fields. Additionally, the replacement gases are characterized by lower dielectric withstand performance and hence needs solid insulation together with gaseous insulation to enhance the electrical insulation properties. This raises a need to develop combined gas-solid physical framework for charge transport and interaction in such systems. This includes initiation and propagation of electrical discharges in gas phase, interactions of produced gas discharge plasma with solid dielectric surfaces, charge transport though solid material, etc. The thesis focuses on developing a numerical simulation framework of discharge initiation and propagation, incorporating various charge generation processes for different insulation systems under highly inhomogeneous electric fields.

The mathematical model of non-thermal electrical discharges in the present thesis is composed of a set of time dependent highly non-linear partial differential equations (PDEs) describing charge transport by drift and diffusion under the influence of electric field incorporating various reactions (electron impact ionization, electron attachment, recombination, etc.). The reaction rate coefficients are calculated by two term Boltzmann approximation of the electron energy distribution function. Another coupled set of PDEs for radiative transport process (photoionization), provides additional reaction sources. Solid insulation modeling includes additional PDEs for electron and hole transport inside the solid insulation. Charge injection from the gaseous medium together with charge accumulation at the solid-gas interface is accounted for. The PDEs are solved by a custom finite element logarithmic weak formulation with Petrov-Galerkin stabilization. This method is implemented in a commercial code (COMSOL-Mathematical module). Adaptive mesh refinement techniques are used to speed up the calculation time. The developed method is validated against the reference experimental data (nanosecond resolved) and published cases. Later, non-axial discharges, 3d branching, hybrid insulation study cases are presented

Keywords: high voltage, gaseous dielectrics, gas discharge, low temperature plasma, streamer propagation, drift diffusion equation, barrier discharge

Acknowledgments

I would like to thank my examiner Prof. Stanislaw Gubanski, for giving me the opportunity to pursue the PhD study at Division of Electric Power Engineering at Chalmers University of Technology. I am very grateful to my supervisor Prof. Yuriy Serdyuk for providing an excellent guidance. He has always been available for discussing any issues and sharing valuable ideas. His guidance and encouragements has made this thesis possible.

Colleagues from High Voltage Engineering group were always there for the brainstorming sessions, for which I am extremely thankful.

My parents, Umed Singh and Parwati Devi are sincerely thanked for all the support and encouragement.

Shailendra Singh

Göteborg, Sweden

July. 2017

Table of Contents

1 Introduction

Non-thermal electrical discharges in air under atmospheric pressure are of considerable interest for a wide range of applications, in particular, for high voltage insulation design. Non-thermal electrical discharges in air at high-pressures (atmospheric and above) typically appear in the form of filamentary plasma channels known as streamers. This kind of discharge have been subject of numerous experimental and theoretical investigations aiming at elucidating their fundamental features as well as creating a basis for evaluations of their characteristics (inception and propagation fields, transported charge and current, etc.) that are of interest for many practical applications. The latter cover various technologies including ozone production, exhaust gas and water treatments, ignition of flammable gases, etc. Extensive studies of streamers have been conducted in connection with the development of high voltage insulation technology, where appearance of such discharges are considered as highly undesirable since they are predecessors of a complete electrical breakdown in gaseous as well as hybrid gas-solid insulation systems. Dynamics of charged species in such discharges is often described utilizing hydrodynamic approximation comprising transport of the charge carriers through insulation media driven by space-charge controlled electric fields and associated with various reactions.

In gas medium under zero-field conditions, the particles are randomly moving and colliding. In order to represent this random motion of the particles, a concept of velocity distribution is used which is a function of spatial coordinates, velocity coordinates and time. Small number of particles in a differential volume at a given spatial coordinate having velocity between u and $u+du$ is proportional to the local velocity. Integration over the spatial and velocity space gives Boltzmann-Maxwell distribution for the equilibrium systems [1] . The velocities of these particles depend on temperature and density.

$$\frac{dN_u}{N} = \frac{4}{\sqrt{\pi}} \left(\frac{u}{u_p} \right)^2 \left[e^{-\left(\frac{u}{u_p} \right)^2} \right] \frac{du}{u_p} \qquad (1.1)$$

where u is the velocity of a fraction of particles N_u out of total particle density N, u_p is the most probable velocity. A typical velocity distribution is shown in the Figure 1.1 [1]. The assumptions for estimating the distribution are that there are large number of particles of the same size moving in all the possible directions. The density is low enough to have mean distance between collisions to be larger than the particle diameter. The velocity distribution and the density of particles can be used to calculate the mean free path, which is the distance travelled between collisions

$$\bar{\lambda} = \frac{1}{N\sigma} \qquad (1.2)$$
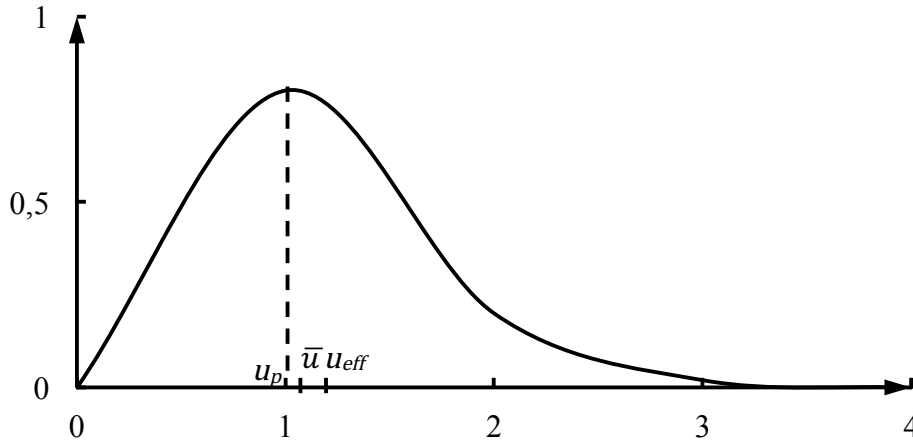
Figure 1.1: Velocity distribution where $\overline{u}$ and u_{eff} are the average and effective velocities, respectively ($\overline{u} = 1.128u_p, u_{eff} = 1.224u_p$)

Here, $\overline{\lambda}$ is the mean free path, and σ is the collision cross section. The above equation is a simplified representation without considering the motion of the target particle.

Collisions among the gas particles (for e.g. electrons, neutrals) can be classified as elastic or inelastic. The former case is associated with the kinetic energy transfer among the particles while in the latter, a part of the kinetic energy is transferred into the internal potential energy of the particles-targets. The probability of the collisions can be characterized by so-called effective cross sections for the processes. Thus if a fraction of the collisions P_i leads, e.g., to the ionization, then the effective cross section for the ionization is represented by $Q_i = P_i N\sigma$ [1]. The collision frequency for this reaction is $V_e Q_i$ and the reaction rate is $n_e V_e Q_i$, where V_e is the mean electron velocity and n_e is the electron density.

Presence of charged species in the gas (regardless of their sources) exposed to an electric field leads to great variety of processes due to the energy supply from the field to the charge carriers. Thus, collisions between charged and neutral particles in gas may, in particular, result in [2-5]

- Excitation $e^- + A_2 \rightarrow A_2^* + e^-$

This happens if an electron e^- with a sufficient energy collides with a gas molecule A_2 in inelastic way that results in a transition of the gas molecule to a higher vibrational or rotational excited state A_2^*, where it stays for a certain time.

- Electron impact ionization $e^- + A \rightarrow A^+ + 2e^-$

This is the main process of generation of electrons in gas discharges. Thus in air at normal temperature and pressure, approximately 10^3 free electrons are available in 1 cm^3 due to cosmic radiation and natural radioactivity [6]. Being exposed to an electric field, they accelerate and may gain kinetic energy along their free path high enough to cause ionization of a neutral molecule upon impact that results in the appearance of a new electron and a positive ion A^+.

- Electron attachment $e^- + A \rightarrow A^-(+hv)$

Some gas atoms or molecules are characterized by so-called electron affinity and can accommodate electrons in their outer electronic shell. Such particles have lower potential energy for negative ions than that of the ground state. In the case of air, main electronegative components are molecules O_2, CO_2, H_2O. Free electrons in the gas can be captured during the attachment process to form the negative ions.

- Photoionization $A + h\nu \rightarrow A^+ + e^-$

Being exposed to an electric field, the neutral gas molecules can be excited, e.g. by electron impact. As a result of quenching of the excited states, photons are produced, the energy of which $h\nu$ (h is the Planck's constant, ν is the radiation frequency) corresponds to the molecule's excitation energy. The photons can be absorbed by nearby molecules leading to their excitation followed by quenching and radiation of photons and so on in a chain manner. Such process is called resonance radiation transport and is typical for discharges in pure gases e.g. nitrogen. In the mixtures, the energy of photons released by excited molecules of a certain sort may be higher than the ionization potential of the molecules of another type. Hence, absorption of the photon by such a particle may lead to its ionization which is indicated by the formula above. This process is typical for air where molecules of Oxygen can be ionized by the photons released from the excited molecules of the Nitrogen.

- Recombination, e.g., $A^+ + e^- \rightarrow A + h\nu$

This is the process leading to the losses of charge carriers in the gas. Recombination may take place between the positive ions and the electrons, as indicated by the formula, or between the positive and the negative ions if the latter exist in gas as in the case of the air. The excess energy of the reaction can be transferred to a photon and to a third particle participating in the process.

Such microscopic processes take place in all types of electrical discharges, which in practice are caused by application of a sufficiently high voltage to the electrodes placed inside a fluid (gas/liquid) or solid dielectric media that leads to the generation of significant amounts of free charge carriers (electrons and ions), if the applied field exceeds the gas ionization threshold. These charged species move along (or opposite, depending upon the charge sign) the direction of the electric field and may eventually cause further ionization forming gas discharge plasma. If the local charge can distort the initial background field, but the ions and electrons are not in a local thermal equilibrium and the temperature of neutrals does not change, then this type of plasma discharge is known as streamer. The magnitude of the applied voltage (to be more precise, the structure and strength of the resulting electric field) decides if the plasma has enough charge generation potential that it can bridge the gap to the ground terminal. The timescale of streamer propagation is in nanoseconds for the distance length scale in centimeters. If the power source is stiff (i.e. capable of supplying current without significant drop of the output voltage), then the plasma channel is thermalized and can be transformed into an electrical arc.

Plasma associated with electrical discharges is composed of charged species, radicals, excited and ground state species. The type of discharge considered in the present study belongs to the class of non-thermal plasmas. This means that the heating effect of the background gases can be neglected as the thermal energy provided by the discharge current is not high enough to raise

the gas temperature and, hence, do not enhance the plasma production rate. Strictly speaking, there is no local thermal equilibrium among the particles constituting the discharge plasma. Moreover, the electrons and other species can have different temperatures based on their velocity distribution and repeated collisions (Te/Ti ~ 10) under the influence of an electric field. Active energy transfer can take place from the electrons to the ions and other particles, but needs multiple collisions and usually not seen in the observation timeframe. In general, however, plasmas are quasi-neutral, except for near the electrode surface, due to the electrostatic interaction and having the characteristic length greater than the Debye length (length scale of the charge shielding).

According to the commonly accepted concept, streamers in the air originate from regions in the gas volume where the density of space charges becomes so high (~10 uC/cm^3 and above) that the charge generated electric field strength is comparable with (or even higher than) the external applied field. This creates conditions for the transition of a discharge in the gas (e.g. Townsend's or multi-avalanche discharges) to a self-sustained mode in which its development is governed mainly by the dynamics of the space charges and the rates of production of the secondary electrons (e.g., by photo-ionization of the neutral molecules). Interestingly, particular mechanisms providing the initial space charges are not crucial for the streamer inception. This may be enhanced by the electron impact ionization of the neutral molecules as in the case of strongly inhomogeneous electric field, where seeding charges are produced by electron avalanches at the sharp electrodes (needles, rods, wires). Alternatively, initial charges may be provided by the secondary discharges as in the case of a three-electrode system [7, 8] or by focusing an intensive laser beam at a particular location in the inter-electrode space [9, 10]. Either type of the inception leads to a channel type of discharge, development of which can be considered as a propagation of an ionization wave converting neutral gas into the low temperature plasma. In the case of air, such wave is associated with electric field strength as high as ~100 kV/cm at its front (also called the streamer head), which has characteristic width in the order of tens of micrometers. Its phase velocity/group velocity is usually in the range of 10^7 - 10^8 cm/s and the density of the charge carriers in the channel is typically between 10^{12} cm$^-$^{3} and 10^{15} cm^{-3}. Due to the relatively high electrical conductivity of the discharge plasma behind the streamer head, the field strength within the channel is much weaker than ahead of the propagating front and its main role is to provide flow of the produced charge carriers (electric current). Being self-sustained discharges, streamers can develop for significant distances up to several tens of centimeters, provided that a relatively weak background field (4–10) kV/cm (depending upon streamer polarity) exists in the direction of the propagation. Note that the mentioned magnitudes of the parameters are typical for pure air and may change in the case of presence of the solid insulating materials [11, 12].

The multi-scale dynamic nature of streamer discharges makes measurements of their internal characteristics (e.g., space charge densities and the associated field strength) challenging. Therefore, numerical simulations have been introduced as an alternative method of analysis and the results of the computational studies have been widely reported, see e.g. review [13]. The majority of the numerical models presented in the literature employ so-called hydrodynamic (or drift-diffusion) formulation of the motion of the charge carriers in the gas under electric fields accounting for various processes of their generation and losses. Such approach incorporates

partial differential equations (PDEs) describing the transport of the charged species which are coupled with the Poisson's equation for the electric potential as discussed in detail in the following section. The resulting set of PDEs are strongly non-linear and the transport part, consisting of hyperbolic type of PDEs, is heavily dominated by the advection. Thus in case of electrons, typical Peclet numbers Pe (the ratio of the convective flux and the diffusive flux) may reach $\sim 10^6$. This leads to a necessity of utilizing special numerical techniques for solving the equations (e.g., so-called flux-corrected transport [14-16]) in order to preserve the positivity of the densities of the transported carriers and to minimize effects of the numerical artifacts. Solutions of the PDEs yield spatial distributions of the densities of the charged species at a particular instant of the discharge development which are utilized as the inputs for the Poisson's equation (by the forming of corresponding space charge density profile). The latter yields electric field distribution in the domain which is used further for obtaining kinetic and rate coefficients for the transport equations to be solved with the new parameters for the next instant and so on. Time step in the simulations is limited by the Courant-Friedrichs-Lewy (CFL) condition, which is defined by a function of the electronic drift velocity (highest as compared to that of ionic species) and the computational mesh size. Typically, the values of the Courant number<1 are used in the explicit formulation for numerical stability. As a result, the time steps in the simulations are restricted and may vary from tens of picoseconds to hundreds of nanoseconds depending upon particular conditions affecting the electron drift velocity. By taking into account that the time intervals of discharge development may reach milliseconds, the number of computational steps may become extremely high. Thus, to achieve simulation results within a reasonable time, efficient numerical algorithms are needed, especially for solving the Poisson's equation (an elliptic PDE) that is known to be the most computationally demanding procedure.

The drift-diffusion model of the streamer discharges based on this approach is considered in the present study focusing on a numerical solution of the partial differential equations. It is suggested that the main numerical issues arising in the solution process, namely positivity of the solution for the densities of the charge carriers and its overall stability, can be resolved by utilizing a logarithmic formulation of the equations stabilized by the streamline upwind Petrov-Galerkin method. Implementation of this formulation as a weak contribution to the problem is presented. Performance of the proposed method is examined in number of numerical tests. Further, the developed approach is utilized to study the propagation of streamers in air in symmetric (needle-plane) and non-symmetric (edges of flat discs), electrode arrangements. The model is further extended to include the solid-gas (barrier) insulation system. Finally, 3d streamer propagation and branching model is also presented.

The complexity of the problem and the special requirements set on by the numerical algorithms and techniques do not allow direct use of the software packages available in the market for simulations of the streamer discharges. It is however highly demanded within the involved scientific community that such an approach becomes available, as the currently observed situation when each computational study of streamer discharges conducted by means of own made computer codes makes the solutions unique and hardly reproducible. Moreover, own made codes are typically limited in their general functionalities, e.g., in introducing, handling

de-featuring and cleaning up the real world geometries, generating proper computational meshes and implementing dynamic mesh refinement, post-processing, etc. Commercial packages available today are (at least partially) free of such drawbacks. However, a majority of them lacks stabilized methods for solving systems of non-linear and strongly coupled hyperbolic and elliptic PDEs. In addition, it is not often possible to define own set of PDEs independently of the inbuilt physical interfaces. In the present research, an attempt to overcome these latter obstacles is undertaken by implementing modifications in the mathematical description of the original model as well as in the numerical algorithms.

The numerical model is verified against the multiple steep gradient and advection tests. Furthermore, the validity of the approach is demonstrated by comparing features of 1 cm long streamer in the air computed with the proposed method and those reported in [17] (chosen for benchmarking as being one of the most cited studies within the subject).

1.1   Aim and objectives

The general objective of the PhD project is to study the physical phenomena associated with the actual processes of the migration of the charged species in gas-solid high-voltage insulation systems under the influence of strong electric fields. The work focuses on developing a computational framework implementing the models of charge transport in the gases and on the gas-solid interfaces within the temporal and spatial scales typical for the existing gas insulated switchgear (GIS) designs. The insulation medium is taken as air rather than SF6 (common to the existing GIS) so as to prepare for the upcoming SF6 free solutions. The primary aims are (i) to implement the simulation model of gas discharges leading to a dielectric breakdown based on the first principle approaches (hydrodynamic plasma physics model, etc.), and (ii) to introduce solid insulating elements in the form of dielectric barriers to simulate the behaviour of the electrical discharges in the hybrid insulation systems.

The model of the discharge processes is formulated in terms of intensities of the microscopic reactions (ionization, recombination, electric drift, energy transfer, etc.), which take place between the charged and the neutral species. Simulations with the model are performed for several study cases representing the problems of scientific and practical interests and allowing for comparison of the calculated and the experimental data for the verification purposes. In addition, the target of the part of the research related to the implementation of the model is to develop an algorithm providing reasonable computational time for the practical usage. The pre-existing simulation model have calculation time of several weeks for a 2 dimensional analysis, which is reduced to less than twenty four hours for inter-electrode dimensions of 50 mm (as seen in the existing designs). Such verified and highly efficient model forms the basis of computational framework, which allowed for the analyses of the effects of the solid insulating elements, interfacial phenomena (charge trapping/de-trapping on the gas-solid interfaces), chemical reactions, heavy species interactions and the excited particles interactions in the discharge volume.

1.2 Outline of the thesis

The thesis is organized in nine chapters. Chapter 1 provides an introduction and scope of the work. Non-thermal discharge principles from the kinetic theory of the gases are introduced. Streamers, a class of plasma discharges, which is the focus of the study are introduced in the context of the insulation media properties. The study focuses on the numerical simulation strategy to understand the streamer discharges. The issues related to the PDEs used to model the transport phenomena are highlighted and the objectives of the work are formulated.

Chapter 2 presents an overview of the fundamental processes in the gas discharges starting from their phenomenology and continuing with the introduction of a hydrodynamic model. The concept of electron energy distribution function and its formulation in the context of two-term Boltzmann approximation is presented. Further, the hydrodynamic model is introduced and associated quantities (source terms and kinetic coefficients) are discussed. Typically, kinetic coefficients are dependent on the energy distribution and the cross sections of the various processes. Therefore, the rates of the reaction taking place in the atmospheric pressure air plasma (impact ionization, attachment, etc.) are presented. Implementation of the photoionization source term in the hydrodynamic model is also described.

Issues related to the numerical solution of the charge transport equations and the inherent problems due to their highly non-linear nature and advection dominated flows of the charge carriers are tackled in the chapter 3. It is shown that the Galerkin finite element weak formulation becomes unstable for the advection dominated flows. Streamline upwind Petrov-Galerkin stabilization is introduced for the transport PDE. Additionally, logarithmic formulation of the transport PDE is presented, which is useful when steep gradients are involved in the transported scalar quantity. A mathematical verification of this formulation in several 1-d and 2-d numerical tests is also presented.

Chapter 4 deals with the applications of the formulated equations for simulating streamers in needle-plane electrode system. The performance of the developed computational framework is compared with the reference cases. The advantage of using an adaptive mesh refinement for reducing the calculation domain is also discussed. Study cases include 3 cm inter-electrode gap in a needle-plane system and 1 cm inter-electrode gap.

Chapter 5 deals with the extension of the model to the non-axial discharges typically seen inside the gas insulated switchgears. A parallel discs electrode system with 6 cm gap is simulated to study the development of simultaneous cathode and anode directed streamer discharges.

Chapter 6 presents an extension of the model to the 3d space to study the streamer branching phenomenon. The challenges associated with the exponential rise in the number of elements for 3d cases are handled by the developed adaptive numerical formulation. Firstly, a brief overview of different branching schemes is presented and they are critically examined. Further, spontaneous streamer branching theory based on the space charge accumulation is analyzed.

Chapter 7 introduces solid insulation enhancement for gaseous dielectric media. The charge transport theory inside the solid insulation is presented. Different physical phenomena including trapping, injection, accumulation are explained in detail. The numerical modeling of the charge

accumulation on the solid-gas interface is introduced. The importance of the charge carriers flux balance at the interface and its contribution to the Poisson equation is presented. Finally, the model is verified against several experimental test cases representing needle-plane electrode systems with dielectric barriers. Nanosecond resolved streamer propagation for these test cases are discussed.

Chapter 8 summarizes the accomplished studies and provides conclusions including those drawn from comparisons of the numerical models with the available experimental data.

Proposals for the future work are formulated in the chapter 9. This includes modeling of the thermal arc using single fluid model, modeling of the streamer-to-leader transition, swarm parameters estimations from the molecular dynamics simulation etc.

1.3   List of publications

The thesis is based on the following publications:

1. M. Ramesh, R. Summer, S. Singh, Y. Serdyuk, S. Gubanski, S. Kumara, Application of streamer criteria for calculations of flashover voltages of gaseous insulation with solid dielectric barrier, Proc. 18th Int. Symp. High Voltage Eng., Aug. 25-30, 2013, Seoul, Korea, pp. 1258-1263.

    In this paper the streamer inception criterion is applied to sphere-sphere gaps employing dielectric barrier in dry air. For such an arrangement, an optimal location of the barrier should exist, where the breakdown voltage becomes maximum. This barrier effect is usually thought of being caused by charging of the barrier. In recent publications the streamer criterion was applied to the shortest path in the air circumventing a barrier. There it was evaluated on the undisturbed electrical background field. Here, charging of the barrier due to a pre-breakdown streamer is considered. The approach of applying the breakdown criterion to the undisturbed electrical field is compared to its application on different model charging conditions of the barrier at the moment just before the breakdown. The dependence of the breakdown voltage on the barrier position is examined and its magnitude is compared with the experimental values of the AC breakdown voltage.

2. S. Singh, Y. Serdyuk, R. Summer, Adaptive numerical simulation of streamer propagation in atmospheric air, Proc. 2013 COMSOL Conference, Rotterdam, the Netherlands.

    In this paper, a 2D axisymmetric numerical model of the streamer-type discharge process in atmospheric air, as it can be implemented into COMSOL Multiphysics is reported. The charge conserving Boltzmann drift-diffusion equations are solved in a logarithmic representation for improved numerical stability, whilst reducing the need for the artificial diffusion terms. A charge density adaptive mesh is utilized and the calculation domain is reduced to the relevant dimensions for improved numerical performance. Results of the so obtained numerical simulations of a nanosecond discharge are analyzed and compared with the previously published experimental data.

3.   S. Singh, Y. Serdyuk, R. Summer, Streamer propagation in air in non-axially symmetric electric field, Proc. 19th Int. Symp. High Voltage Eng., 2015, Pilsen, Czech Republic.

In this paper, development of non-axial streamer discharges in air between the disc-electrodes are studied. Discharge inception and propagation between the edges of the two flat discs is treated with the so-called drift-diffusion model. Partial differential equations constituting the model are solved utilizing a custom developed stabilized finite element procedure implemented in a commercial software. The results of the performed simulations show that the discharge inception takes place in the regions of enhanced electrostatic fields at the curved edges of both the electrodes and two streamers propagate in the air gap towards each other. Quantitative analysis of the dynamics of the charge carriers' densities, generated space charges and the magnitudes of the electric fields during the streamer initiation and propagation is presented. The effect of the space charges and their influence on the streamer propagation path is discussed.

4.   S. Singh, Y. Serdyuk, R. Summer, Streamer propagation in hybrid gas-solid insulation, Proc. IEEE conf. on elec. insulation and dielec. Phen.(CEIDP), 2015, Ann Arbor, United States.

The influence of a solid dielectric barrier on the development of an electrical discharge in air between the needle and plane electrodes is analyzed. The computational model describing the formation and the propagation of a streamer in the atmospheric air and accounting for the charge transport and trapping on the barrier surfaces is presented. The results of the simulation performed for a 5 cm air gap containing a solid barrier (plate) inserted between the needle and the plane electrodes are discussed focusing on the discharge dynamics and the associated electric fields.

5.   S. Singh, Y. Serdyuk, R. Summer, Streamer branching in air: physical model and simulations in fully 3D spatial domain, Proc. Int. Conf. Prop. Appl. of Diel. Materials (ICPADM), 2015, Sydney, Australia.

In this paper a fully coupled self-consistent model of the streamer branching is presented. The model incorporates inhomogeneities in the gas media representing, e.g., large molecular clusters, micro dust particles, etc., which act as centers for the localized space charge build-up. The results of the performed simulations show that the charge accumulation at such centers leads to their electrostatic interactions with the streamer head and causes its splitting. Quantitative analysis of the dynamics of the charge carriers densities, generated space charges and the magnitudes of the electric fields associated with the branching process is presented.

6.   S. Singh, Y. Serdyuk, S. Gubanski, Simulations of streamer discharges in air between edges of curved electrodes, IEEE Trans. Plasma Sci., submitted, 2017.

In this paper the logarithmic stabilized method for the streamer discharge is examined in a number of numerical tests. The developed approach is verified by conducting simulations of a positive streamer in air in a needle-plane electrode system and the results are compared

with those available in the literature. Further, results of the simulations of a non-axially-symmetric double-headed discharge developing between the edges of the flat disc electrodes are presented and discussed.

7. S. Singh, Y. Serdyuk, Simulations of non-thermal electrical discharges in air over solid insulating barrier, J. Appl. Phys., submitted, 2017.

    Non-thermal plasma discharges in the form of streamers propagate through the gaseous insulation media when a high enough voltage is applied across the electrodes. Usually the dielectric strength of this system can be enhanced by introducing a solid insulation in the form of a barrier. There are studies dealing with either the experimental enhancement or the numerical simulation of the barrier touching the electrode. The paper deals with the simulation of hybrid gas-solid insulation system in which the barrier is not in contact and is perpendicular to both the electrodes. Additionally, full charge transport in solid and gas medium is considered. The developed model is used in explaining the initiation and propagation of the streamer discharge over the inter-electrode distance of 1, 6 and 8 cm. The simulation model is validated against experimental nanosecond resolved data. At the gas-solid interfaces Dirac function is used for the charge accumulation.

    Publications not considered in the thesis:

8. B. Bagheri, J. Teunissen, U. Ebert,…., S. Singh, Y. V. Serdyuk, Comparison study of different simulation codes for positive streamers propagating into a region below breakdown, 2017 Int. Conf. Phen. Ionized Gases (ICPIG), July 9-14, 2017, Lisbon, Portugal.
    A comparison of streamer codes among different universities is performed. A test case with spatial domain of 1.25 x 1.25 cm is considered. Immobile positive charge is used to obtain electric field similar to the needle plane configuration, as some participants lacked modeling of curved geometries in their code. Electrons are simulated by drift diffusion formulation whereas the positive charge is modelled as ordinary differential equation (ODE) without any flux transport. All the participants used the same swarm parameters. The results are quantitatively compared and there is good match for the number densities, charges, streamer dimension etc.

9. Round robin test for streamer simulation codes, JPD, 2017, in manuscript

2 Generation and transport of electrical charges in hybrid insulation

Gas insulation failure under high voltage is preceded by streamer discharges, which carry enough charges to distort locally the background electric field. The insulation performance of gaseous system can be enhanced by introducing solid dielectric barriers or coatings [18]. Discharges and breakdown in gas-solid systems have been subjects of numerous investigations, see e.g. [19-24]. In many cases, breakdown voltages of hybrid gas-solid insulation were of interest and were examined experimentally. Computational studies mainly focused on the systems, where dielectric barrier(s) was (were) in contact with electrode(s), e.g. so-called dielectric barrier discharges (DBD) used for technological purposes [25-27] and dielectric coatings [28, 29]. Less attention has been given to the systems with a solid barrier which is not connected to the electrodes, and is inserted in a gas gap between the electrodes perpendicular to the direction of the discharge propagation. Despite numerous experimental studies of such systems [30-32], relevant simulations studies have not been reported yet.

In general, solid dielectric barrier inserted between the electrodes acts as an obstacle for a discharge reaching its surface and, based on experimental observations, it can develop along gas-solid interface provided that the electric field across the barrier is not strong enough to initiate discharges at its opposite side. Depending upon particular conditions, the discharge along the surface may decay or propagate fully and leave the solid surface before continuing in the gaseous media. This may lead to partial or complete breakdown of the hybrid insulation system. During this surface propagation process, electric charges are injected and transported inside the solid insulation due to the strong electric field. Thus, an analysis of the performance of a hybrid gas-solid system should include considerations of coupled charge generation and transport in both gas and solid media as well as on interfaces between them, even though time scales could be much different. The charging of barrier surface is due to sum total of all charge fluxes at the surface. According to the performed literature survey, no studies of this type, which account for all necessary details of involved physical processes, have been reported. Approaches for modeling charge generation and transport in solids are presented e.g. in [33-35] whereas descriptions of the models for gaseous media can be found elsewhere [36, 37].

In the present study, charge transport models developed for gas and solid materials are coupled accounting for continuity of charge carriers' fluxes at the gas-solid interface. The surface charge density is calculated accurately by combining the fluxes of all involved types of charged species. Disturbances in the local electric fields caused by accumulated space and surface charges are accounted for by solving the Poisson's equation for both the gas and the solid domains including the interface between them. Next, fundamentals of charge generation and transport in hybrid systems are presented.

2.1 Basics of electrical discharges in gas

When a voltage is applied between a pair of metallic parallel-plate electrodes immersed in air, a current is observed in the external circuit. By varying the applied voltage, the electric field strength between the electrodes can be changed and different processes in gas can be activated resulting in a certain current. Typical discharge voltage-current characteristic for electrodes providing uniform field distribution is shown in Figure 2.1 where different discharge stages are indicated. As seen, the current is extremely weak at low applied voltages and it is due to the drift of charged species existing in gas due to natural background sources (e.g., terrestrial and cosmic radiation, see [38]). This region of the V-I characteristic is linear and obeys Ohm's law. At higher voltages (and fields), all available carriers are participating in the charge transport and, due to their finite amount, the current reaches saturation. Note that in this stage, the number of free charges are not growing and there is always a balance between the charge generation and the loss processes. If the voltage increases further, the fraction of non-elastic collisions (in their total number) of electrons with neutral molecules increases leading to the presence of large number of excited species and at certain voltage level ionization due to electron impact becomes norm and the current starts growing. This kind of non-self-sustained discharge is called Townsend's discharge after the famous scientist who proposed a theory for this low current regime.

2.1.1 Townsend discharge and breakdown

On the rising part of the characteristic corresponding to the Townsend's discharge, the electrons gain sufficient energy between the collisions to cause impact ionization of the gas molecules. The intensity of the impact ionization is represented by Townsend's first ionization coefficient α [cm^{-1}], which is the number of electrons generated by one initial electron due to impact ionization per unit length of its path in the electric field. Starting with n_0 initial electrons, the total number of electrons after travelling a distance d is $n = n_0 e^{\alpha d}$. This exponential
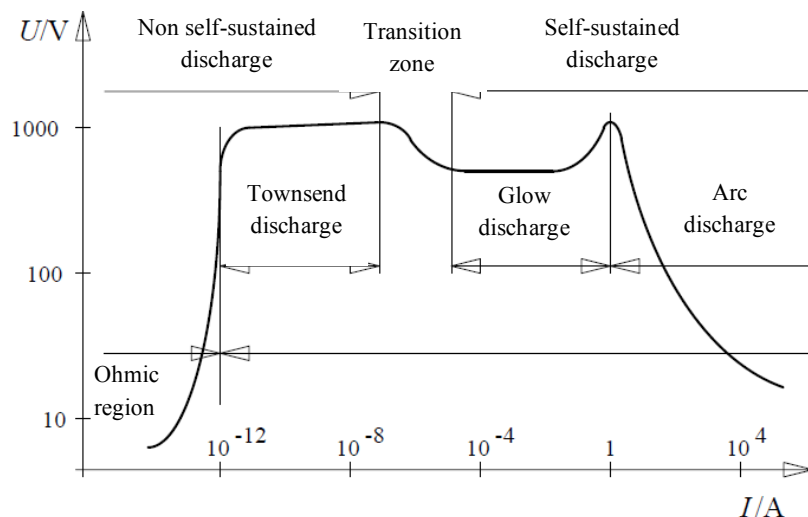
Figure 2.1: Sketch of a current-voltage characteristic of a discharge showing transition between different regimes. Note that voltage-current characteristic is mentioned in the text whereas here, the axes (voltage and current) are changed for convenience.

increase in electron numbers $e^{\alpha d}$ is due to the fact that each newly produced electron gains energy from the field and generates new electrons. This process is called an electron avalanche in the literature and is shown schematically in Figure 2.2 [1].

The ionization coefficient α is unique property of the gas and depends on electric field strength E and gas pressure p (or density $N = p/kT$, k is Boltzmann's constant, T is gas temperature) and usually is presented as a function of the pressure (density) reduced field E/p (or E/N):

$$\frac{\alpha}{p} = f\left(\frac{E}{p}\right) \tag{2.1}$$

Electronegative gases, as discussed above, are capable of capturing free electrons. The intensity of this process is characterized by attachment coefficient η [cm^{-1}], which is defined in a similar way as Townsend's coefficient but with regards to electron attachment. In practice, the intensity of electrons production in electronegative gases is described by so-called effective ionization coefficient $\bar{\alpha}$ defined as

$$\bar{\alpha} = \alpha - \eta \tag{2.2}$$

At sufficiently strong fields, the production of new electrons and thus positive ions in Townsend's discharge becomes regular and significant amount of ions may reach the cathode. Bombardment of cathode's surface by positive ions leads to a yield of secondary electrons from the metal. This process is characterized by Townsend's second coefficient γ, which is a number of electrons released per impact of a single positive ion. Accounting for the secondary electrons, their total number at distance d from the cathode is

$$n = n_0 \frac{e^{\bar{\alpha}d}}{1 - \gamma(e^{\bar{\alpha}d} - 1)} \tag{2.3}$$

The electron yield from the cathode compensates their losses and at certain voltage a transition from Townsend's to a self-sustained discharge takes place. This transition is associated with production of significant space charges and modifications of the electric field in the inter-electrode space in a way that the increased discharge current can be supported by much lower applied voltage. In Figure 2.1, this process is indicated as a transition zone and the highest voltage reached on Townsend's discharge branch corresponds to the breakdown voltage. On the right-hand side of the transition region, different types of self-sustained discharges occur which belong to classes of glow and arc discharges. These, however, are not subjects of the present study and are not considered further below.

The condition for the breakdown is derived from (2.3) assuming infinite increase in the total number of electrons taking place when the denominator is equal to zero:

$$\bar{\alpha}d = ln\left(\frac{1}{\gamma} + 1\right) \tag{2.4}$$

This expression is known as Townsend's breakdown condition and provides a basis for deriving the Paschen's law for the breakdown voltages. It states that the electrical breakdown of a gas gap with uniform electric field occurs at a certain voltage which is a function of the product of gas pressure and the electrode separation distance as shown in Figure 2.3 for air [1].
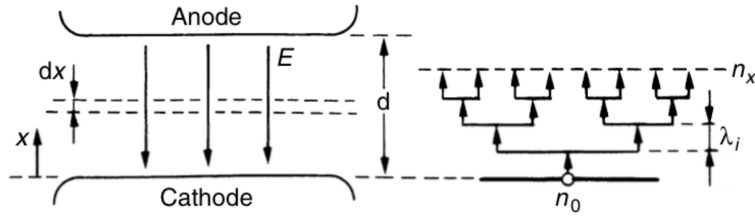
Figure 2.2: Electron multiplication process leading to electron avalanche, borrowed from [1].

The condition (2.4) can be extended to cases with slightly non-uniform field by taking $\int \bar{\alpha}\, d\, l$ along the electric field line l and comparing it with the magnitude of the right-hand side

$$\int_l \bar{\alpha}\, dl = k = \ln\left(\frac{1}{\gamma} + 1\right) \tag{2.5}$$

Further extension is possible for cases with strongly divergent fields, where even corona discharges may appear, e.g., in a needle-plane electrode arrangement. In such cases, condition (2.5) requires integration across just a part of the space between the electrodes, where ionization takes place, and provides so-called corona inception voltages. For such situations, the value of k to be used in (2.5) has been (and still it is) a subject of discussions, see e.g. [39]. Typically, the value of 9.15 provides a good fit with experimental data for fields ranging from uniform to non-uniform ones [18].

Townsend's theory predicts quite well the breakdown voltages at medium-low gas pressures, small distances and uniform-slightly non-uniform electric fields. In all the other cases the predicted breakdown values diverges from the actual breakdown. This is due to the fact that the Townsend discharge doesn't account for the electric field variation due to the free charges in the medium.

2.1.2 Streamer formation and propagation

At high gas pressures (atmospheric and higher), provided $pd > 10^3$ Torr·cm and sufficiently high voltages, the local space charges generated in electron avalanches are strong enough to produce their own field which masks the external applied field. This phenomenon can be observed in electrode configurations providing uniform as well as non-uniform field distributions. In the latter case, the ionization of gas starts in a high electric field region and leads to the formation of electron avalanches, which may attenuate on their way to the counter electrode. If an electron avalanche comprising Townsend's discharge is strong and electron generation rate at its tip is significant, the electric field is enhanced due to the localized space charge in the head and this field may cause a transition of the avalanche to a streamer. For this, the local electric field needs to become comparable with the initial background field and that happens when the number of charge carriers (electrons) in the avalanche head becomes larger than $\sim 10^8$ (for typical diameter of the head of 100 μm at atmospheric pressure this corresponds to the density $\sim 10^{14}$ cm^{-3} and degree of ionization of the gas $\sim 10^{-5}$). A streamer in air is observed as a thin bright channel, which is able to propagate even in the regions with low fields. Streamer propagation is supported by local processes at its head, where the field is extremely high and causes ionization of the gas. Thus, streamer development between electrodes can be seen as a propagation of ionization wave.
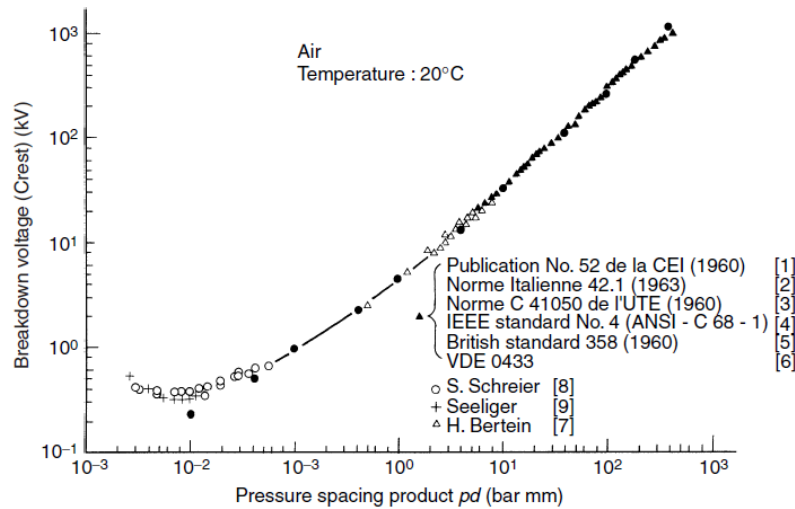
Figure 2.3: Paschen's curve for air, borrowed from [1].

According to the commonly accepted concepts, local generation of charged species at the streamer head is associated with the photo-ionization of the gas (in air). N_2 molecules are excited to higher states by electron impact (typically 1.2-12.65 eV). Some of these excited species come back to the ground state by releasing photons with energy exceeding the ionization potential of O_2 (12.06 eV). These photons causes the ionization of O_2. Photoionization leads to "smearing" of the streamer head and amplification of charge generation near to the streamer head. These processes expand the spatial signature of the moving charge head and, as a result, the photoionization maximum appears just in front of the charge edge. It is the source of electrons for the streamer front and leads to enhancement of local electric field due to the charge separation between the fast moving electrons and slowly moving ions (note that the mobility of the electrons is 2-3 order of magnitude higher than that of the ions thus they drift much faster in the gas [1]). The local field strength at the streamer head is typically in the range 50-200 kV/cm due to the small channel radius (10-50 micrometers in air at atmospheric pressure) and high density of the charge carriers, which may reach 10^{13}-10^{15} cm^{-3}. In this context, streamer development can be seen as propagation of a disturbance in electric field or ionization wave in the gap. One should distinguish between the streamer propagation speed, which is a phase velocity of the ionization wave, and speeds of the electrons or ions, which are defined by their mobilities and electric field strength and are essentially velocities of their drift in the field.

Typically, experimental investigations of the streamers are conducted by utilizing needle-plane, needle-needle or coaxial wire-cylinder configurations of the electrodes, which provide high level of control over streamer development by varying few parameters, like electrodes radiuses, etc. [40]. Voltage-current characteristic are usually recorded during the discharge process. In some studies, light emission during streamer development was also recorded with microsecond resolution and very recently in a nanosecond range [41]. Capturing light emission provides a simple way to measure the speed of streamer propagation by way of multiple exposures. The measured propagation speed of streamer head is in the range of 10^7-10^8 cm/s [42, 43] and it is dependent on many factors, in particular, electric field distribution between the electrodes.

Streamers can be classified according to the directions of propagation into the positive (cathode directed) and the negative (anode directed) electrodes. The former occurs typically in the vicinity of sharp anode (e.g. needle), where positive space charge appears after single strong or multiple avalanches. These space charges generates a field, which screens out the external field at the anode and produces a spike in front of the space charge cloud, where photoionization starts providing conditions for the streamer inception. In the case of negative streamers, avalanches can reach critical number of charge carriers on their way from the cathode to the anode and the streamer channel can grow due to secondary avalanches produced by the runaway electrons (thus, there is no need of photoionization). Further progression of streamers in the gas requires certain minimal field strength, which is called propagation field in the literature. Thus, the background electric field needed for the positive streamer is in the range of 4-6 kV/cm whereas for negative streamer it is in the range 10-20 kV/cm [1]. The difference in the propagation field is due to the various secondary mechanisms supporting discharge development as mentioned above.

If the field pattern is characterized by enhancements at both electrodes (e.g., needle-needle or sphere-sphere systems), the streamer propagation can be bidirectional. In such cases, streamer heads are created at locations of strong fields at both the anode and the cathode and discharge channels from both sides of the gap propagate towards each other and eventually meet in the bulk of the gas volume. An example of such situation is considered in chapter 5 as a study case.

2.2 Streamer modeling

Physical processes in non-thermal gas discharges are usually modeled utilizing kinetic, hydrodynamic or hybrid approaches [44-47]. The second one is the most popular for types of discharges dealt within the thesis and, therefore, it is presented in detail below.

2.2.1 Drift-diffusion equations for charge carriers

The general form of Boltzmann's equation for distribution function $f(\mathbf{v}, \mathbf{r})$ is written as

$$\frac{\mathrm{D}f}{\mathrm{D}t} = \mathrm{J}_{st}(f), \quad \text{where} \quad \frac{\mathrm{D}}{\mathrm{D}t} = \frac{\partial}{\partial t} + \mathbf{v}\frac{\partial}{\partial \mathbf{r}} + \mathbf{F}\frac{\partial}{\partial \mathbf{v}} \tag{2.6}$$

$f(\mathbf{v}, \mathbf{r})$ is the number of particles at a given position and velocity vector. Here variables $\mathbf{v}$ and $\mathbf{r}$ represent the velocity and position vector, respectively, and J_{st} is the collision integral [48]. According to (2.6), the total time variance of the distribution function is due to the sum of rates of its changes due to an external force $\mathbf{F}$, diffusion and collisions. The equation for charged species (e.g. electrons) can be written accounting for the external electrostatic force provided by the electric field.

Normally, the powers of velocity vector (0,1,2) are multiplied with the Boltzmann equation and integrated to achieve zeroth, first and second moment of the equation. The integration over the velocity space leads to the loss of velocity space distribution information. The continuity equation (drift-diffusion approximation) can be derived by taking the zeroth power of velocity vector and integrating after multiplying with each term of the Boltzmann equation. This assumption implies symmetry around the velocity vector space and only variation in the distribution function is due to the position vector [49].

$$\int \frac{\partial f}{\partial t} d^3v + \int v \nabla_r f d^3v + \frac{q}{m} \int [(\boldsymbol{E} + v \times \boldsymbol{B}) \nabla_v] f d^3v = \int \left(\frac{\partial f}{\partial t}\right)_{coll} d^3v \qquad (2.7)$$

Where $\boldsymbol{B}$ is magnetic flux density, which in the present application is zero due to the absence of external magnetic fields and the streamer current is much too small to produce significant B field. The elastic collisions only lead to changes in momentum and energy, but they do not change the number density of the particles. Inelastic collisions are considered as a source of particle generation and loss. This is important consideration for ionized gases, where the number density may change due to collisions; impact ionization, attachment, recombination etc. as described before. So, from the solution of Boltzmann's equation for particle distribution function, drift diffusion equation for charge continuity is derived considering the following relation between the distribution function and the number density $n(\boldsymbol{r}, t)$

$$n(\boldsymbol{r}, t) = \int f(\boldsymbol{r}, \boldsymbol{v}, t) \, \mathrm{d}^3v \qquad (2.8)$$

Within a hydrodynamic approximation, dynamic behavior of the charge carriers in gas is considered as a motion of corresponding fluids (electronic and ionic), which are characterized by volume densities of the carriers n [cm^{-3}] and are controlled by electrostatic forces. The latter define convective fluxes of charged species $n\mathbf{w}$ [cm^{-2}s^{-1}] associated with their drift velocities $\mathbf{w}$ [m/s]. In addition, diffusive fluxes may exist due to gradients of carriers densities ∇n. The concentrations of the charged particles may change locally due to different mechanisms of their generation and loss, rates of which R [cm^{-3}s^{-1}] are typically dependent on the intensity of the local electric field. All these result in time variations of the densities of electrons and ions that can be described by their respective mass conservation equations also known as continuity equations for the corresponding fluxes. In the case of air, the set of PDEs (eq. 2.9) can be written after considering the reduction of ionic species in gas to two generic types of ions (positive and negative).

Here, subscripts e, p and n indicate electrons, positive and negative ions, respectively; D stands for diffusion coefficient. The first term represents the rate of change of the number density over time. The second and third terms are divergence of the flux due to advection and diffusion of particles respectively. The velocity for advection is due to the electric field acting on the charged particles (along E field direction for positive species and opposite direction for negative species). The current density can be calculated from the flux of the charge particles.

$$\frac{\partial n_e}{\partial t} + \nabla \cdot (n_e \mathbf{w_e} - D_e \nabla n_e) = R_e$$

$$\frac{\partial n_p}{\partial t} + \nabla \cdot (n_p \mathbf{w_p} - D_p \nabla n_p) = R_p \qquad (2.9)$$

$$\frac{\partial n_n}{\partial t} + \nabla \cdot (n_n \mathbf{w_n} - D_n \nabla n_n) = R_n$$

The source terms in (2.9) incorporate rates of processes to be considered in the model. Typical set of reactions includes electron impact ionization and attachment, recombination of charge carriers as well as background ionization and photoionization of the gas. The resulting rates of the processes for the different charged particles can be expressed as

$$R_e = \alpha\, n_e |w_e| - \eta n_e |w_e| - \beta_{ep} n_e n_p + R_0 + R_{ph}$$

$$R_p = \alpha\, n_e |w_e| - \beta_{ep} n_e n_p - \beta_{pn} n_p n_n + R_0 + R_{ph} \tag{2.10}$$

$$R_n = \eta n_e |w_e| - \beta_{pn} n_p n_n \text{ and } R_p - R_e - R_n = 0$$

where β_{ep} and β_{pn} are coefficients of electron-ion and ion-ion recombination $[cm^3 s^{-1}]$, respectively; R_0 and R_{ph} are the rates of background and photo ionization, $[cm^{-3} s^{-1}]$, respectively. Note that the positive sign in (2.10) indicates sources of the charged species while the negative sign indicates rates of losses.

Since most of the parameters in (2.9) and (2.10) are dependent on the electric field $\mathbf{E}$, the drift diffusion equations are to be coupled with the Poisson's equation

$$\nabla \cdot (-\epsilon_0 \epsilon_r \nabla V) = e\, (n_p - n_e - n_n) \tag{2.11}$$

$$-\nabla V = \mathbf{E} \tag{2.12}$$

Here, ϵ_0 is the permittivity of the vacuum, ϵ_r is the relative permittivity, V is the electric potential and e is the electron charge. Note that the right-hand side of the Poisson's equation comprises the volume charge density, which varies in space occupied by the discharge and may lead to local field enhancements or weakening thus affecting different volumetric sources/sinks of the charged species and hence their fluxes. Thus, equations (2.9) - (2.12) are coupled via the field dependencies of the problem parameters.

2.3   Calculations of kinetic coefficients

Parameters and rate coefficients (sources and sinks) in the hydrodynamic models can be obtained from a solution of Boltzmann's equation for electron energy distribution function (EEDF) similar to the equation 2.6. The energy distribution function is defined by six dimensions in phase space (space vector $\mathbf{r}$ and velocity vector $\mathbf{v}$). In order to reduce the complexity, assumptions are usually made, in particular, using symmetry of the electron distribution in momentum/velocity space, the equation can be reduced to four dimensions including time co-ordinate. Further simplifications, e.g. by utilizing spherical harmonics expansion, yield the following equation for the isotropic part of the distribution function f_0 and anisotropic part f_1 [50]. This means that out of the three-position vector, the distribution function is only dependent on one space variable z:

$$\frac{\partial f_0}{\partial t} + \frac{\Upsilon}{3}\, \varepsilon^{1/2} \frac{\partial f_1}{\partial z} - \frac{\Upsilon}{3}\, \varepsilon^{-1/2} \frac{\partial f_1}{\partial \varepsilon} \varepsilon \mathbf{E} f_1 = C_0 \tag{2.13}$$

$$\frac{\partial f_1}{\partial t} + \Upsilon \varepsilon^{1/2} \frac{\partial f_0}{\partial z} - \mathbf{E} \Upsilon \varepsilon^{\frac{1}{2}} \frac{\partial f_0}{\partial \varepsilon} = -N \sigma_m \Upsilon \varepsilon^{1/2} f_1$$

Here, Υ is a constant defined as $(2e/m_e)^{1/2}$; C_0 is the collision generation rate for f_0; ε stands for the electron energy. It is further assumed that there is no time varying contribution to the isotropic part f_0, and thus can be reduced to F_0, which is obtained from

$$\frac{\partial}{\partial \varepsilon} \left(\widetilde{W} F_0 - \widetilde{D} \frac{\partial F_0}{\partial \varepsilon} \right) = \widetilde{S} \tag{2.14}$$

Where $\widetilde{W}$ represents the electron velocity associated with the negative energy flux (cooling by collisions with neutrals and electrons of lower energy); $\widetilde{D}$ stands for the heating by high energy

species. Note that $\widetilde{W}$ and $\widetilde{D}$ represent elastic collisions associated with the electron energy distribution function (EEDF) whereas $\widetilde{S}$ is the source assosciated with the inelastic collisions processes discussed earlier [50-52].

Knowing F_0, the electron density is obtained by integrating it over the velocity space that yields

$$n_e = 4\pi \int_0^\infty F_0 \, v^2 dv \tag{2.15}$$

In general, the mass conservation (drift-diffusion) equations (2.9) can be deduced from (2.14) by multiplying it with $\varepsilon^{1/2}$ and integrating over all the energies:

$$\frac{\partial n_e}{\partial t} + \frac{\partial\left(-\mu E n_e - \frac{\partial D_e n_e}{\partial z}\right)}{\partial z} = C_0 \tag{2.16}$$

Here, μ is the mobility and D is the diffusion coefficient described as follows

$$\mu_e N = \frac{\Upsilon}{3} \int_0^\infty \frac{\varepsilon}{\sigma_m} \frac{\partial F_0}{\partial \varepsilon} d\varepsilon \tag{2.17}$$

$$D_e N = \frac{\Upsilon}{3} \int_0^\infty \frac{\varepsilon}{\sigma_m} F_0 d\varepsilon \tag{2.18}$$

where σ_m is the effective cross-section for all the collision processes.

The coefficients needed for setting up the drift-diffusion equations for synthetic air (80% nitrogen and 20% oxygen) are obtained from the solution of Boltzmann's equation for the mixture. Thus, by knowing the electrons energy distribution function, effective rates of ionization, attachment, and recombination can be evaluated. In the present study, Boltzmann's equation is solved using two-term approximation (isotropic-anisotropic part, as explained above) for the regime in which a small fraction of collisions are inelastic. The solution is found by utilizing Galerkin method as implemented in COMSOL Multiphysics Plasma module [53]. The collisions considered in the calculations include those leading to excitation and ionization of molecules by electron impact and electron attachment [50]

$$\widetilde{S} = \left(\sum_k C_k \right) \tag{2.19}$$

Here, C_k indicates all types of collisions causing energy exchange as described in chapter 1, which are functions of electron energy and cross section. Since equation (2.14) is a one-dimensional partial differential equation of convective-diffusive type with respect to energy, it is solved by discretizing over electron energy with following boundary conditions.

$$F_0 = 0 \; at \; \varepsilon = \infty \tag{2.20}$$

$$\frac{\partial F_0}{\partial \varepsilon} = 0 \; at \; \varepsilon = 0 \tag{2.21}$$

In the calculations, the highest value of electrons energy is taken to be high enough that it encompasses all the reactions, e.g. $\varepsilon = 100$ eV.

The source terms in the drift-diffusion equations (2.9) are defined in terms of reactions rates and solution of Boltzmann's equation yields rate coefficients as function of electron energy for the collisions (2.19). Thus, the rate coefficient k_k for k_{th} collision process is defined by [52]

$$k_k = \gamma \int_0^\infty \varepsilon \, \sigma_k F_0 d\varepsilon \tag{2.22}$$

where σ_k is the corresponding cross-section. In the present calculations, the cross-section data for interactions of electrons with molecules of N_2 and O_2 were taken from databases [54] and [52]. Knowing the coefficient k_k, the reaction rate R_k is obtained as

$$R_k = k_k x_k N\, n_e \tag{2.23}$$

where x_k is the mole fraction of target species and N is the gas density. Considering (2.23) to be applied to electron impact ionization of neutral species (with corresponding cross-section), one may link Townsend's ionization coefficient to the rate coefficient by [50]

$$\frac{\alpha_k}{N} = \frac{k_k}{\mu_e E} \tag{2.24}$$

COMSOL Multiphysics allows for Maxwellian distribution solution for the Boltzmann equation under equilibrium condition. However, the distribution function deviates from the Maxwellian distribution for non-equilibrium condition and, hence, a solution of Boltzmann's equation is desired. The solution of EEDF distribution function by Boltzmann equation gives different reaction rates and transport coefficients for the charge continuity equation.

The outcome from the solution of EEDF is the rates of reactions as functions of a reduced electric field (ration E/N) for the mixture N_2:O_2 (80:20). To be used in equations (2.9)-(2.10), the reaction rates are converted into Townsend's ionization coefficient and attachment coefficient according to [50] eq. (2.24). To verify the results, they are compared with those obtained using popular Boltzmann equation solver BOLSIG+ [50, 54] in Figures 2.4-2.7. It can be seen that there is a very good match between both the sets of the results for pure gases as well as for the mixture. Threshold values of the reduced electric field can be identified for the field dependences of the ionization coefficients, above which the curves show an exponential increase. Note that the attachment rates of electrons to the molecules O_2 are calculated for two-body collisions only.

The results of the calculations of the ionization and attachment coefficients for the mixture are compared with the empirical results for air [55, 56] in Figures 2.8 and 2.9, respectively. The achieved agreement confirms the validity of the theoretical results, which were utilized in the simulations of discharges presented in the following chapters.

Transport coefficients needed for simulations of discharges were obtained from available empirical data. Thus, field dependences of the drift velocity [42, 43, 57, 58] and diffusion coefficient [42, 59] of electrons in air are often approximated as a power functions of the reduced field, which matches with the equations (2.17-2.18):

$$\mathbf{w_e} = 3.2\; \text{x} \frac{10^3 \left(\frac{|E|}{N}\right)^{0.8}\, \text{m}}{\text{s}} \quad \text{along Efield direction for the positive species and opposite for the}$$
negative species $\tag{2.25}$

$$D_e = 7 \times 10^{-2} + 8 \times \left(\frac{E}{N}\right)^{0.8}, \text{m}^2/\text{s} \tag{2.26}$$

Magnitudes of other parameters used in the model are presented in Table 2.1 [42, 43, 57-60]. Different approximations used by various authors for swarm parameters can be found elsewhere [13].

Table 2.1: Parameters used in the simulations

Parameter	Magnitude	Definition
μ_p m^2/Vs	2e-4	mobility of positive ions
D_p m^2/s	5.05e-6	diffusion coefficient of positive ions
μ_n m^2/Vs	2.2e-4	mobility of negative ions
D_n m^2/s	5.56e-6	diffusion coefficient of negative ions
β_{ep} m^3/s	5e-4	recombination rate of electron and positive ions
β_{pn} m^3/s	2.07e-12	recombination rate of positive and negative ions
R_0 1/m^{3}s	1.7e9	background ionization rate
k_{det} m^3/s	1e-18	electron detachment rate
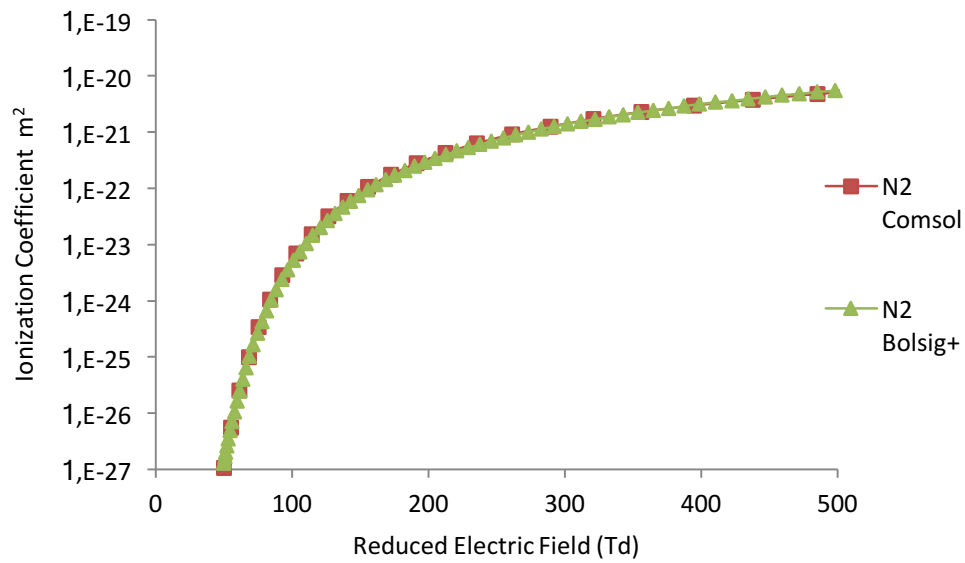
Figure 2.4: Ionization coefficient in N2 vs. reduced electric field
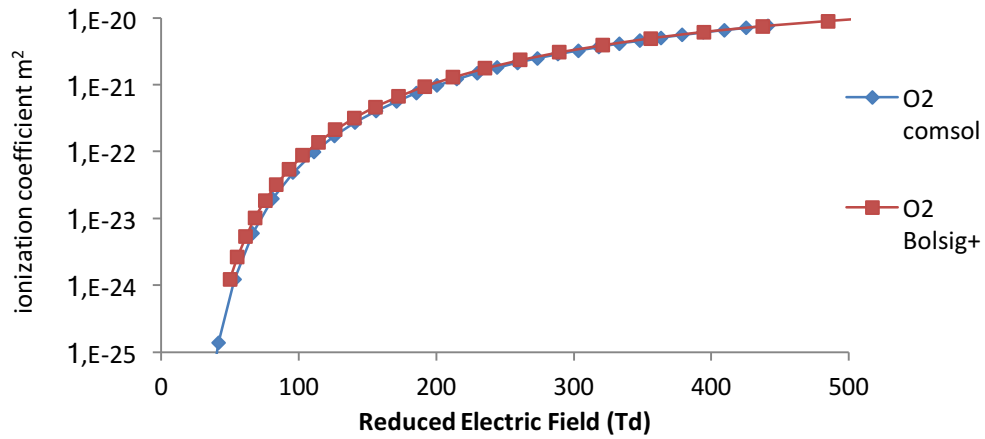
Figure 2.5: Ionization coefficient in O2 vs. reduced electric field
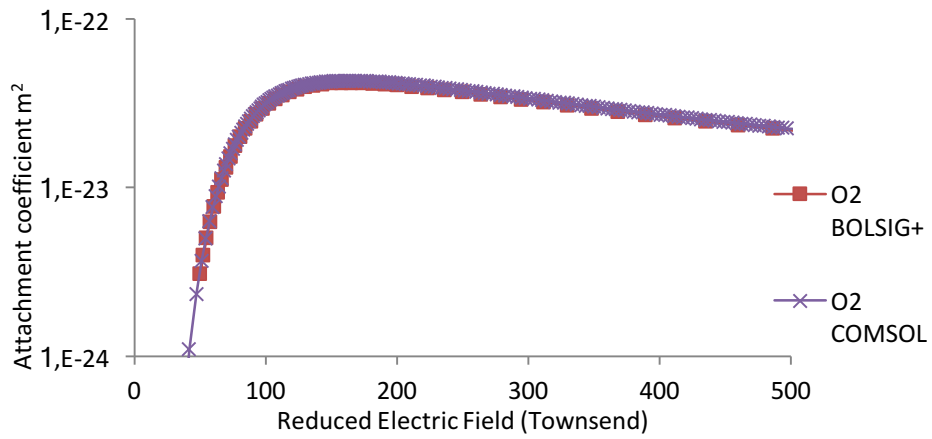
Figure 2.6: Attachment coefficient in O2 vs. reduced electric field
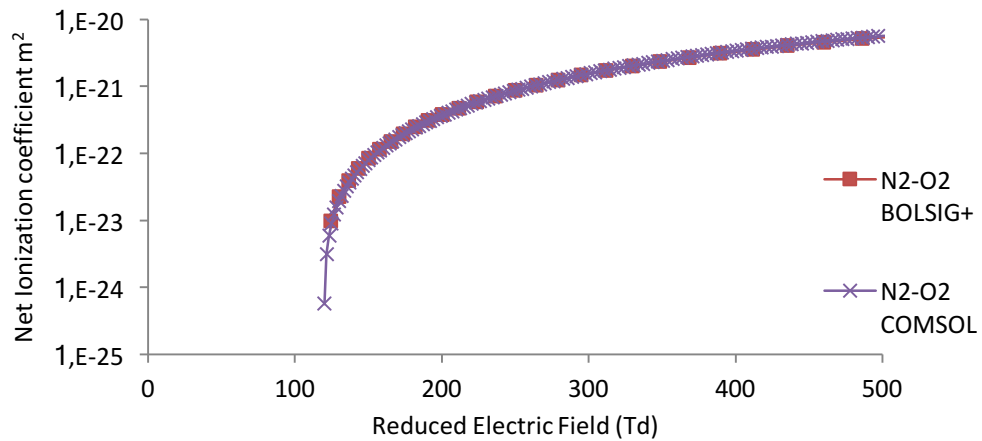
Figure 2.7: Net ionization coefficient of air vs. reduced electric field
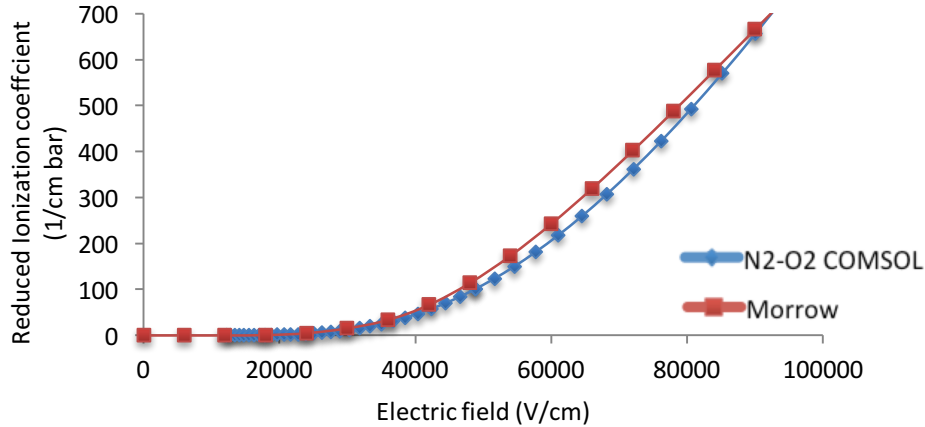
Figure 2.8: Ionization coefficient of air (calculated vs. empirical data from Morrow [60])
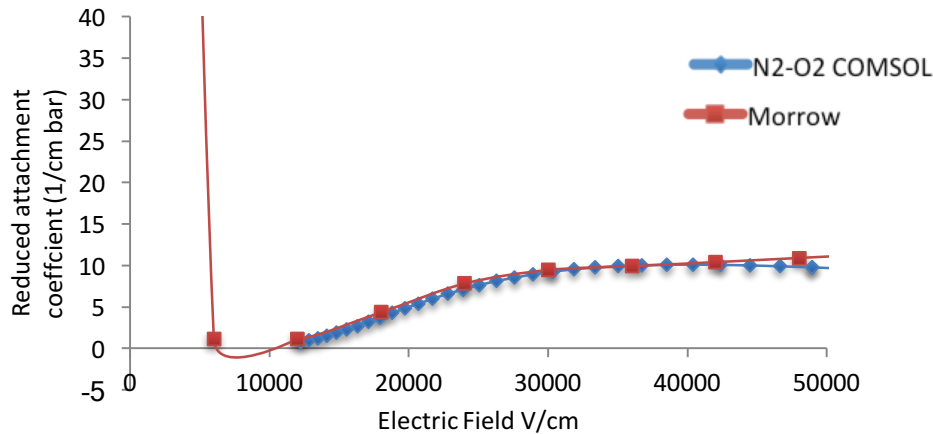
Figure 2.9: Attachment coefficient for air as a function of the Electric field compared with Morrow [60].

Note that the swarm parameters and rate coefficients described above are valid only when the reduced electric field E/N is relatively weak (<500 Townsends) allowing for distribution function to be considered as isotropic [61].

2.4 Photoionization

The additional source included in the drift diffusion equation is photo-ionization, which is a non-local process of generation of seed electrons in front of the streamer head during the streamer propagation. For simulations purposes, it is possible to replicate the effect of photoionization by introducing reasonably high background density of electrons that has been implemented in several studies, e.g. [62-64]. However, such approach is not physically meaningful and, therefore, models of photoionization in gas discharges in air have been introduced.

According to the existing theories [63, 65], photons in air appear due to the quenching of excited nitrogen molecules to the ground state and they transfer energy (1.2 -12.65) eV sufficient for the ionization of oxygen molecules with the ionization potential of 12.06 eV:

$$e^- + N_2 \rightarrow e^- + N_2^*$$

$$N_2^* \rightarrow N_2 + h\nu_{UV} \tag{2.27}$$

$$O_2 + h\nu_{UV} \rightarrow e^- + O_2^+$$
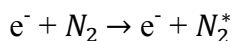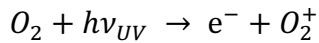
The wavelength interval considered for UV photons $h\nu_{UV}$ in air radiated by excited nitrogen molecules is $98 - 102.5$ nm.

Early streamer models were based on integral formulation of photoionization process [66]. The principle used was based on considering the local photoionization rate at a given point as a sum of contributions from all the photons born in the gas and travelling through it, which are being absorbed at this location with a certain probability. The latter is characterized by an absorption coefficient. It can be seen like ray tracing in which the individual UV rays are generated from each element to the observation point with certain attenuation based on the geometric length or the view factor.

The integral form of the ionization rate can be written as [64, 66]

$$R_{ph}(\mathbf{r}, t) = c \int_0^\infty d\nu \, \kappa \int_\Omega \Psi d\Omega \tag{2.28}$$

where $\Psi(\mathbf{r}, \mathbf{\Omega}, t)$ is radiation distribution function for a given frequency ν, position vector $\mathbf{r}$, direction $\mathbf{\Omega}$ (solid angle) [sr] and time t [s] ; κ [cm-1]is photoionization coefficient defined by the product of photoionization efficiency [62] and absorption coefficient; c is the speed of light.

Zhelzenayak et al [66] proposed an integration procedure over entire discharge volume for obtaining the photoionization source. The integration is to be applied to the product of photon generation rate $I(\mathbf{r})$ and function $g(R)$, which is a radiation absorption function. In the following, R [cm] denotes the magnitude of the difference between the observation position vector and a vector defining other position contributing to the photoionization. Since the number density of the excited molecules in gas is related to the impact ionization intensity, photon production rate $I(\mathbf{r})$ is assumed to be proportional to the ionization rate. Accounting for this, the rate of photoionization is written as

$$R_{ph}(r) = \iiint \frac{I(r)g(R)}{4\pi R^2} dV \tag{2.29}$$

This equation can be derived from the transport equation of radiation distribution function $\Psi(\mathbf{r}, \mathbf{\Omega}, \mathbf{t})$

$$\frac{\partial \Psi}{\partial t} + c\,\mathbf{\Omega}\,\nabla\,\Psi = \sum_{u,d} \frac{n_u \emptyset_{ud}}{4\pi\tau_{ud}} - \kappa_\nu\,c\,\Psi \tag{2.30}$$

where subscripts u and d represent energy levels of the excited species and summation is done over all u such that $d < u$; κ_ν is the absorption coefficient [cm-1] and $1/\tau_{ud}$ represents Einstein's coefficient for spontaneous transition [s-1]; n_u [cm-3] is the number density of excited species at level u; $\emptyset_{ud}$ is normalizing function.

Assuming instantaneous emission of photons, one can obtain R_{ph} [cm-3 s-1]

$$R_{ph}(r, t) = \iiint \frac{n_u(r't)\,\emptyset_u}{4\pi R^2\,c\,\tau_u} \exp(-\kappa_\nu R)\,dV' \tag{2.31}$$

The photon absorption coefficient within the considered frequency range is introduced as

$$\kappa_\nu = \kappa_1 \left(\frac{\kappa_2}{\kappa_1}\right)^{(\kappa_\nu - \kappa_1)/(\kappa_2 - \kappa_1)} \tag{2.32}$$

Here, κ_1 and κ_2 are the values corresponding to the minimum and maximum frequencies, respectively. The absorption coefficient is approximated in [66] as a function of partial pressure of oxygen p_{O_2} (Torr) in air

$$\kappa_1 = .035 p_{O_2} \text{ (Torr. cm)} \text{and } \kappa_2 = 2 \, p_{O_2} \text{ (Torr.cm)} \tag{2.33}$$

This yields the absorption function in the form

$$\frac{g(R)}{p_{O_2}} = \frac{\exp(-\kappa_1 R) - \exp(-\kappa_2 R)}{p_{O_2} R \ln \left(\frac{\kappa_2}{\kappa_1}\right)} \tag{2.34}$$

The solution of equation 2.31 is to be updated for each time step while solving the set of PDEs describing evolution of gas discharge plasma. This makes the solution time for the whole problem using this type of integral formulation to be unacceptably long. In addition, the demands to the hardware (in particular computer RAM) are extremely high since the integration is needed for each point in the discharge volume accounting for contributions from all the other points that results in a full matrix to be stored. Several strategies were formulated over the years to overcome the problem. Thus, Kulikovsky [62, 67, 68] proposed a system of rings as emitting source for a axisymmetric geometry and the contribution from each ring to the source point was calculated by the use of a geometric factor calculated once and stored. Other strategies included use of a fine grid near streamer head and coarse grid everywhere else in the discharge volume to reduce the integration efforts [64, 69].

The direct numerical solution for obtaining the photoionization rate employs Eddington method [70]. Another method developed by Lowke et al. [2] and Bourdon et al. [64], does not include direct numerical solution, but starts at equation (2.31) proposed by Zhelzenayak [66]. Further, the $g(R)/R$ function is replaced by a series of exponential functions. These yield integral terms R_{ph}^n

$$R_{ph}(\boldsymbol{r}) = \sum_n R_{ph}^n(\boldsymbol{r}) \tag{2.35}$$

$$R_{ph}^n(\boldsymbol{r}) = \iiint \frac{I(r\prime) A_n p_{O_2}{}^2 \exp(-\lambda_n p_{O_2} R)}{4\pi R} dV\prime \tag{2.36}$$

which are assumed to be solutions of Helmholtz equations

$$\nabla^2 R_{ph}^n(\mathbf{r}) - \left(\lambda_n p_{O_2}\right)^2 R_{ph}^n(\mathbf{r}) = -A_n p_{O_2}{}^2 I(\mathbf{r}) \tag{2.37}$$

In the present study, three terms are accounted for the summation (2.35). Hence, the resulting set Helmholtz equations to be solved is

$$\nabla^2 R_{ph}^1 - (\lambda_1 p_{O_2})^2 R_{ph}^1 = -A_1 p_{O_2}{}^2 I$$

$$\nabla^2 R_{ph}^2 - (\lambda_2 p_{O_2})^2 R_{ph}^2 = -A_2 p_{O_2}{}^2 I \tag{2.38}$$

$$\nabla^2 R_{ph}^3 - (\lambda_3 p_{O_2})^2 R_{ph}^3 = -A_3 p_{O_2}{}^2 I$$

Here, A_n and λ_n are fitting parameters taken from [64] (Table 2.2); I [cm-3 s-1] is the photon generation intensity proportional to the ionization rate. It has been proven in [64] that the three

Table 2.2: Fitting parameters for photoionization

n	A_n, (cm Torr)$^{-2}$	λ_n, (cm Torr)$^{-1}$
1	1.986e-4	.0553
2	.0051	.146
3	.4886	.89

term approximation provides better fit to the integral model than the two term approximation and yields closer match to the Eddington direct solutions [64, 70]. Thus, the photoionization rate is

$$R_{ph} = R_{ph}^1 + R_{ph}^2 + R_{ph}^3 \qquad (2.39)$$

2.5   Surface charging and charge transport in solid dielectrics

Insulation of GIS has to withstand operating stresses as well as multiple lightning impulse over-voltages, which are characterized by rise time of 1.2 microsecond. During type testing, when fifteen continuous pulses are applied successively, solid insulator surfaces become charged due to the generation and migration of charges under unidirectional electric fields. Different parameters affecting charge accumulation and migration on insulator surface like voltage, conductivity, permittivity etc. have been studied [30, 71]. It has been found that the surface charges are dynamic, their distributions varied with time and were dependent on the properties of both gas and solid materials as well as the interface between them. Thus, amount of deposited charges are affected by the rates of charge generation and transport in gas. At the same time, charge dynamics on the surface is controlled also by injection, bulk conduction and trapping in the solid. These processes together determine conduction (i.e. charge transport) normal and transverse to the insulator surface and any mathematical modeling should account for processes in both the media [71].

Charge transport under strong electric fields has been studied by means of computer simulations separately for solid and gas media, see e.g. [72] and [73], respectively. Attempts have been undertaken to link processes in gas and on gas-solid interface while treating the latter as blocking for the charge carriers and solid material as an ideal insulator [74, 75]. It is evident, however, that a consistent description of the interaction of streamers with solid insulating surfaces requires simultaneous consideration of charge transport in both the phases. Therefore, in the present study, computer simulations were conducted combining charge dynamics in a streamer discharge in atmospheric pressure air with charge transport in the bulk and on the surface of a physically floating solid dielectric barrier between the electrodes.

It is suggested that the charges generated by the discharges in the gas media may reach gas-solid interface and get accumulated on the surface. A fraction of these charges are injected into the bulk of the solid by Schottky's mechanism depending on the orientation of the electric field. Thus, electron injection takes place when E-field vector has a negative component directed towards the solid bulk volume, whereas the hole injection takes place if it is positively aligned. Thus, the current density J provided by the injected charges inside the solid bulk is [33]

$$J_{c,a} = AT^2 \exp\left(-\psi_{c,a}/kT\right)\exp\left(\tfrac{q}{kT}\sqrt{qE_{c,a}/4\pi\varepsilon_0\varepsilon_r}\right) \tag{2.40}$$

Here, subscripts c and a represents cathode and anode (hence, the alignment according to the field direction), respectively; Richardson's constant A is $1.2\cdot10^6$ A/(m²K²); T stands for temperature, K; ψ is injection barrier energy, eV; k is Boltzmann's constant, J/K.

The charge transport inside the solid insulator includes trapping/release to/from local states and recombination (mainly at recombination centers composed of deeply trapped charges). Uniform distribution of deep traps is considered across the bulk volume. The drift and diffusion inside the solid is approximated by (2.41) and (2.42) respectively for electrons and holes, represented by subscripts e and h:

$$\mu_{e,h} = \mu_{be,h}\exp\left(-\psi_{st\,e,h}/kT\right) \tag{2.41}$$

$$D_{e,h} = \left(\tfrac{kT}{q}\right)\mu_{e,h} \tag{2.42}$$

Here, μ represents band mobility, m²/Vs; ψ_{st} is the depth of shallow traps, eV.

The fluxes of charge species are defined as ('sign' represents the polarity of the charge)

$$\vec{q}_{e,h} = \text{sign}_{e,h}n_{e,h}\mu_{e,h}\vec{E} - D_{e,h}\nabla n_{e,h} \tag{2.43}$$

and transport equations for charge carriers densities n, m⁻³ are

$$\frac{\partial n_{e,h}}{\partial t} + \nabla\cdot\left(\vec{q}_{e,h}\right) = R_{e,h} \tag{2.44}$$

The source terms $R_{e,h}$ for electrons and holes account for their trapping, detrapping and recombination:

$$R_e = -R_{eh}n_en_h - R_{eht}n_en_{ht} - T_en_e\left(1 - \frac{n_{et}}{n_{0et}}\right) + \upsilon\exp\left(\frac{-\psi_{et}}{kT}\right)n_{et}\frac{n_{et}}{n_{0et}}$$

$$\tag{2.45}$$

$$R_h = -R_{eh}n_en_h - R_{eth}n_hn_{et} - T_hn_h\left(1 - \frac{n_{ht}}{n_{0ht}}\right) + \upsilon\exp\left(\frac{-\psi_{ht}}{kT}\right)n_{ht}\frac{n_{ht}}{n_{0ht}}$$

Here, n_{et} and n_{ht} are densities of trapped electrons and holes, m⁻³; n_{0et} and n_{0ht} are densities of deep traps (electrons and holes respectively), m⁻³; R_{eh}, R_{eht}, R_{eth} and R_{etht} are recombination coefficients represented by their subscripts, m³/s; T_e and T_h represents trapping coefficient s⁻¹; υ is attempt to escape frequency, s⁻¹; ψ_{et} and ψ_{ht} indicate barrier height (energy needed) for de-trapping of electrons and holes, eV, respectively.

Additionally, the following ordinary differential equations are used to introduce dynamics of filling/empting immobile deep traps (subscripts et and ht represents trapped electrons and holes, respectively):

Note that here, positive source indicates filling process while negative sign indicates release of charges from the traps.

All charges present in the solid domain define the distribution of the electric field which is found as a solution of the Poisson's equation for the solid media

$$\frac{dn_{et}}{dt} = T_e n_e \left(1 - \frac{n_{et}}{n_{0et}}\right) - R_{eth} n_{et} n_h - R_{etht} n_{et} n_{ht} - \upsilon \exp\left(\frac{-\psi_{et}}{kT}\right) n_{et} \frac{n_{et}}{n_{0et}}$$

(2.46)

$$\frac{dn_{ht}}{dt} = T_h n_h \left(1 - \frac{n_{ht}}{n_{0ht}}\right) - R_{eht} n_e n_{ht} - R_{etht} n_{et} n_{ht} - \upsilon \exp\left(\frac{-\psi_{ht}}{kT}\right) n_{ht} \frac{n_{ht}}{n_{0ht}}$$

$$(-\epsilon_0 \epsilon_r \, \Delta V) = q \, (n_h + n_{ht} - n_e - n_{et}) \tag{2.47}$$

The coupling of gaseous and solid phase charge carriers is introduced by considering accumulation of surface charges with the density σ_s (C/m^2) found as a solution of equation

$$-\left(\frac{d\sigma_s}{dt}\right) = j_b + j_g \tag{2.48}$$

which is essentially a current continuity equation incorporating different mechanism of charge transport. According to (2.48), the rate of change of surface charge density is sum of the densities of bulk conduction currents in solid phase j_b and gaseous phase j_g. These vector quantities are defined by outward fluxes of charged species in each domain and, hence, the negative sign in front of the rate of change of surface charge density represents its reduction over time.

In the model, the surface charge is included in the Poisson equation for the gas phase as an additional source represented by Dirac delta function δ_s:

$$-(\epsilon_0 \epsilon_r \, \Delta V) = q \left(-n_e - n_n + n_p\right) + q \left(\sigma_s \, \delta_s\right) \tag{2.49}$$

The function δ_s is defined for barrier surface, e.g., located at coordinates x=a and y=b as

$$\delta_s(x - a, y - b) = \delta_s(x - a)(y - b) = \{\infty \text{ for } x = a, y = b, 0 \text{ elsewhere}\} \tag{2.50}$$

$$\iint \delta_s(x - a, y - b) \, \sigma_s(x, y) \, dx \, dy = \sigma_s \text{ for all points on a, b} \tag{2.51}$$

This representation makes the delta function to take the value of surface charge density at the surface only and being equal to zero everywhere else. This is implemented by additional weak contribution source on the barrier surface in the software.

The set of model parameters used in the simulations correspond to polyethylene are provided in Table 2.3.

Table 2.3: Parameters used in the simulations of charge transport in solid material

Parameter	Value
$\mu_{e,h}$ Band mobilities, m^2/Vs, electrons / holes	10^{-14} / $2\cdot10^{-13}$
ψ_{st} Depths of shallow traps, eV	0.05
$R_{eht} = R_{eth}$ Recombination coefficients, m^3/s,	$6.4\cdot10^{-22}$
n_{0et}, n_{0ht} Densities of deep traps, m^{-3}, electrons / holes	$6.3\cdot10^{20}$
T_e, T_h Trapping coefficients, s^{-1}, electrons / holes	10^{-1} / $2\cdot10^{-1}$
ν Attempt-to-escape frequency, s^{-1}	$6\cdot10^{12}$
ψ_{et}, ψ_{ht} Barrier height for de-trapping, eV, electrons / holes	0.96 / 0.99
ψ Barrier height for injection, eV, electrons / holes	1.27 / 1.16
ε_r Material dielectric constant	2.3

3   Numerical Implementation

The drift-diffusion equations for fluxes of the charged species formulated in the previous chapter together with the Helmholtz and the Poisson equations for the photoionization rate and electric potential, respectively, are solved in COMSOL Multiphysics utilizing the mathematical module. This allowed for customizing the weak formulation so as to obtain stable numerical solution.

3.1   Logarithmic formulation of transport equations

As indicated in the previous chapter, the hydrodynamic approximation used to describe transport of charge carries in discharge plasma utilizes drift-diffusion equations with source/sinks terms determined by different microscopic processes. The PDEs are to be solved numerically due to strong couplings, non-linearity and involvement of field dependent coefficients. Numerical solution assumes that the equation is discretized on a computational mesh using certain procedure, e.g. utilizing finite elements (FE) method for which the original equation is transformed into so-called weak form that is essentially an integral form of the PDE.

Let us consider a convection-diffusion equation, where u is a scalar number density

$$\frac{\partial u}{\partial t} + \nabla \cdot (u\boldsymbol{\beta} - D\,\nabla u) = source \tag{3.1}$$

Assuming for simplicity one-dimensional case (x is the spatial co-ordinate), constant velocity $\boldsymbol{\beta}$ and isotropic diffusion coefficient D, expanding the brackets yields

$$\frac{\partial u}{\partial t} + \beta\nabla u - D\,\Delta u = source \tag{3.2}$$

A solution can be derived using, e.g., so-called method of characteristics based on known pattern of particles streamlines. The idea here is to reduce the PDE to ordinary differential equation (ODE) such that the scalar quantity along a streamline is dependent on only one space coordinate i.e. streamline curve length. The streamlines are defined by a family of curves $\boldsymbol{x}$ such that

$$\frac{dx_i}{ds} = \beta_i \tag{3.3}$$

where 's' is a parameter. This approach, however, does not always provide stable and positive solution for u due to the nature of (3.2) while applying it to charge transport in streamers. The second and the third terms in the equation are convective flux and diffusive flux, respectively. If the problem is dominated by diffusion, the FE formulation of (3.2) is stable [76]. In case when the diffusive flux is small as compared to the convective flux, (3.1) is essentially a PDE of hyperbolic type and its numerical solution obtained with conventional algorithms is inherently unstable exhibiting oscillations like those in Figure 3.1. The stability conditions are usually linked to so-called Peclet number for a given mesh size h which indicates relative
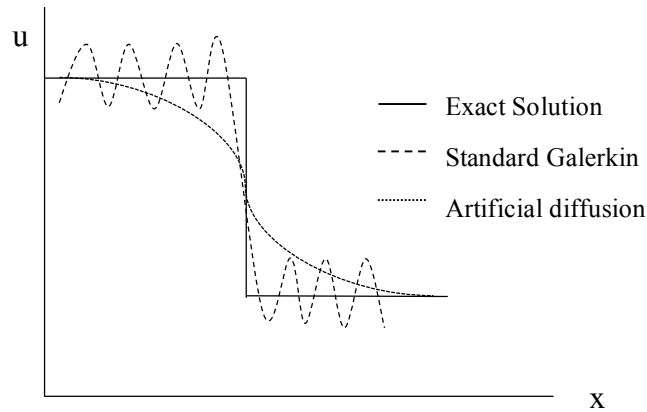
Figure 3.1: Solution of a steady state convection–diffusion equation at discontinuity

$$Pe = \frac{|\beta|h}{2\,D} \tag{3.4}$$

contributions of convective flux and diffusive fluxes. If Peclet number is greater than unity, that is typical for streamer propagation problem, oscillations in the solution appear. The higher is the value of *Pe* the stronger instability occurs, which may even lead to unphysical results such as negative concentrations of the charge carriers. Preventing these effects requires implementing special approaches since the positivity of the solution of (3.1) is not guaranteed by FE formulation. Various methods to tackle this problem have been proposed, e.g., introducing artificial source terms, which provide positive carrier density when it becomes too low. Also, neglecting the negative densities and replacing them with some small positive magnitudes is sometimes used. Such methods, however, are fully artificial and are not based on any physical background.

Resolving equations (2.9) for the densities of charged species, in particular electrons, is the most challenging part in the numerical solution of the streamer model. From general formulation of stability (3.4) [76], the FE discretization of (2.9) will provide stable solution when the electron number density transport is dominated by the diffusive flux. This is not normally the case as the drift velocity of electron and, hence, the convective flux is order of magnitudes higher than the diffusive flux. It can be stated that the electron Peclet number as defined by (3.5) is always be greater than the unity and thus the solution of (2.9) exhibit oscillations when finite element method is used [77].

For the considered drift-diffusion model, oscillation in the density solution yields a corrupted space charge distribution in (2.11) and thus distorted field pattern that, in turn, leads to self-reinforcing of the errors in the particles densities in (2.9) and so on. Furthermore, the oscillations may occur in regions where the rates of carriers′ losses exceed rates of their generation providing strong negative terms (2.10) that may result in numerical artefacts such as negative concentrations of the species.

A consistent way of avoiding described numerical artifacts in the solution is to formulate the original drift-diffusion equations in an equivalent logarithmic form so that the problem can be solved for the *log* of the number density [53]. Such formulation ensures that the concentration of species always remains positive without the need for an artificial source or density capping.

This also helps when the gradients in the solution are strong like in the case of streamer head, where the number density of electrons changes by many orders of magnitude over few mesh elements. The transformation is implemented by defining new variables $n_{el} = \log(n_e)$, $n_{pl} = \log(n_p)$, $n_{nl} = \log(n_n)$. Being introduced into the original equations (2.9), these yield

$$e^{n_{el}} \, \partial n_{el}/\partial t + \nabla \cdot (e^{n_{el}} \, (\mathbf{w}_e - \mathrm{D}_e \, \nabla n_{el})) \; = \; \mathrm{R}_{el}$$

$$e^{n_{pl}} \, \partial n_{pl}/\partial t + \nabla \cdot \left(e^{n_{pl}} \, (\mathbf{w}_p - \mathrm{D}_p \, \nabla n_{pl})\right) \; = \; \mathrm{R}_{pl} \qquad (3.5)$$

$$e^{n_{nl}} \, \partial n_{nl}/\partial t + \nabla \cdot (e^{n_{nl}} \, (\mathbf{w}_n - \mathrm{D}_n \, \nabla n_{nl})) \; = \; \mathrm{R}_{nl}$$

Note that in this case, isotropic diffusion coefficients are assumed. Also, the source terms on the right-hand sides need to be transformed as well by replacing the carriers' densities in (2.10) by their logarithmic counterparts. The same is valid for the boundary and the initial conditions. As seen from (3.5), the cost for such modification is the fact that the non-linearity of the problem becomes much stronger and needs to be taken into account when selecting and tuning a suitable solver for the matrix problem arising from FE discretization of the PDEs.

Although the logarithmic formulation of the charge transport equations (3.5) ensures positivity for the solutions, it does not resolve the issue of unphysical distortions (oscillations) in the profiles of the densities of transported species. A traditional way of damping them is to utilize some kind of numerical stabilization. The simplest approach is to use the first one, i.e., an extra value D_{iso} directly added to the diffusion coefficient so that the Peclet number

$$Pe = \frac{wh}{2\,(D+D_{iso})} \qquad (3.6)$$

becomes less than unity. While doing so, the original problem definition has been changed and hence the method is often referred to as 'inconsistent stabilization'. The method is simple and robust, but sharp gradients in the solution gets smeared out. To minimize this effect, the selected amount of artificial diffusion should guarantee that the resulted equation remains consistent with the original formulation. Such consistent stabilization can be implemented utilizing so-called streamline diffusion [76] that selectively introduces diffusion only along the streamline direction. Moreover, the original Galerkin FE formulation can be modified by introducing a trial function dependent on the flow direction and requiring that the new trial function yields the same solution as for the original equation [76]. This type of numerical stabilization for certain trial function is known as streamline upwind Petrov-Galerkin method (SUPG) and it is explained below in details. It can be further improved by introducing so-called shock capturing technique that requires modifying the test function such that there is the solution of the scalar quantity(dependent variable) inside the trial function.

In software package used in this work, both consistent and inconsistent types of stabilization are provided in various modules for application oriented problems (Physics modules like transport of diluted species etc.) but not for general form of PDEs. Therefore, the model was implemented utilizing the general mathematical module due to the need of introducing the logarithmic formulation (3.5) and thus the inbuilt stabilization tools were not accessible. Thus, a consistent SUPG stabilization was introduced manually through a weak representation of the

charge carriers transport equations (2.9). This implementation was verified by using several commonly utilized numerical test cases.

3.2   Petrov-Galerkin stabilized logarithmic formulation

For the sake of clarity, a general convection-diffusion PDE, similar to that in (2.9), is defined for a scalar quantity u. To make the case even more complex, pure convection with the velocity $\mathbf{w}$ is considered, as it makes the solution unstable due to the lack of diffusion:

$$\partial u / \partial t + \nabla \cdot (u\mathbf{w}) = S \tag{3.7}$$

As shown below, positivity of the solution is achieved by introducing a variable $ul = \log{(u)}$ that yields

$$e^{ul} \frac{\partial ul}{\partial t} + \nabla \cdot (e^{ul}\mathbf{w}) = S \tag{3.8}$$

The source term S needs to be modified accordingly if it is non-linear and dependent on u.

Solving (3.8) by FE method implies splitting the domain Ω (within which the problem is defined) in a number of non-overlapping elements by introducing a computational mesh. A numerical solution $\widehat{ul}$ is found as an approximation to the exact one and is constructed as a linear combination of unknown local solutions at the mesh nodes $\widetilde{ul}$ multiplied by so-called basis (also known as interpolation or shape) functions N, i.e., $\widehat{ul} = \sum_{i=1}^{M} \widetilde{ul}_i N_i$ (here M stands for the number of mesh nodes). The latter are defined as smooth functions (continuous within an element and at least once differentiable) equal to unity at node i and vanishing at all other nodes. Being introduced into the original equation, the approximate solution yields a residual that needs to be minimized. Such procedure can be implemented by utilizing weighted residual method, which implies transferring the terms in (3.8) to one side, multiplying them by a weight (also called trial or test) function V_m and integrating over the domain. It is obvious that for the numerical solution equal to the exact one, the residual approaches zero:

$$\int_{\Omega} V_m \left[e^{\widetilde{ul}} \frac{\partial \widetilde{ul}}{\partial t} + \nabla \cdot \left(e^{\widetilde{ul}}\mathbf{w} \right) - S \right] d\Omega = 0 \tag{3.9}$$

From (3.9), a weak form of the problem can be derived which is further transformed into a discrete (matrix) form utilizing the piecewise polynomial representation of $\widehat{ul}$ above. Finally, the discrete problem is solved by applying methods of linear algebra yielding nodal values $\widetilde{ul}$ and, thus, interpolation is required to find the solution in the entire domain in between the nodes [77].

Various choices can be made for the weight function in (3.9). Thus the most popular one is to select V_m from the same class as the basis functions, in particular, to adopt $V_m = N$ that is essentially Galerkin formulation of FEM. This approach, however, is known to provide oscillating solutions for the hyperbolic (convection dominated) PDEs, as mentioned above and is demonstrated in the next section. A consistent SUPG stabilization can be introduced by choosing $V_m \neq N$ (that leads to so-called Petrov-Galerkin method) and modifying the test function by a streamline upwind perturbation of kind [78]

$$V_m = V + \delta \nabla \cdot \left(e^{\widetilde{ul}}\mathbf{w} \right) V \tag{3.10}$$

where δ is the stabilization parameter and $V = N$ is the Galerkin test function. By introducing (3.10) into (3.9), weak term stabilizing the solution of (3.8) can be identified as:

$$\int_{\Omega} \delta \, \nabla \cdot \left(e^{\widetilde{u_l}} \mathbf{w} \right) V \left[e^{\widetilde{u_l}} \frac{\partial \widetilde{u_l}}{\partial t} + \nabla \cdot \left(e^{\widetilde{u_l}} \mathbf{w} \right) - S \right] d\Omega = 0 \qquad (3.11)$$

This expression is added as a weak domain contribution for the test problem (3.8).

3.3 Numerical tests

To examine the effect of SUPG stabilization (3.11) on numerical solution of equation (3.7) represented in the logarithmic form (3.8), numerical tests were conducted for conditions reflecting the fact that the streamer development is associated with the propagation of sharp fronts of carriers´ densities. The analysis focuses first of all on the stability of the solution process and eligibility of the results.

3.3.1 1D tests

The common conditions of one-dimensional tests were as follows. The problem was defined on the interval $x \in (0 - 1)$ on which a uniform mesh consisting of 100 elements was imposed. Most of the calculations were conducted using first order linear elements (if otherwise not stated directly). The tests comprised convection of a unit step of u

(i) with a constant velocity w and zero source term S [79],

(ii) with a constant velocity and non-linear stiff source term [80], and

(iii) with variable velocity and zero source term [81].

In the tests, the velocity was set to $w = 10$ except for the last case conditions, which are introduced later. Abrupt changes of $u(x)$ in the initial profiles at $t = 0$ (front or tail) occupied single mesh element. Time steps were calculated implicitly by utilizing backward differentiation formula (BDF) of high order (up to 5) and were limited by the value $\Delta t_{max} = 2 \cdot 10^{-4}$s. The latter yielded low Courant numbers (below 0.2) allowing for obtaining also non-stabilized solutions for comparison purposes. Note that the use of the high order BDF for time stepping is crucial since first order algorithm (backward Euler) severely damps high frequency components and leads to a diffusive solution [82].

The results of the first test are shown in Figure 3.2. As seen, the non-stabilized solution exhibits strong oscillations reaching to their maxima ~40% of the initial magnitude. It is notable that even in this case the positivity of u is preserved due to the logarithmic formulation (3.8) of the problem. The weak contribution (3.11) provides stabilizing diffusion in a consistent way leading to a smooth solution with overshoots ~5% appearing at the propagating front (shown by stars). These can be attributed to the low order shape function used (linear elements). Increasing the element order leads to attenuation of the overshooting as demonstrated by the solid lines representing the profiles obtained with the second order elements (quadratic). To achieve this result, some tuning of the stabilization parameter δ was required. Thus, the calculations with linear elements were done using its "optimal" value $\delta_{opt} = h_{elem}/2w$ [77], where $h_{elem} = 1/100$ is the mesh element size, while for quadratic elements this value was multiplied by a factor 10. In general, identifying proper magnitude of δ is essentially a subject

of special analysis since it depends on many factors such as amount of physical diffusion in the system, dimensionality of the problem, order of elements used for discretization of (3.8), etc. [77]. Such analysis, however, is out of the scope of the present study.

For the second test, a rectangular unit density profile of width 0.4 was introduced in the middle of the computational region at $t = 0$ and it was transported through the domain with periodic boundary conditions. The latter were implemented in a sense that the flux leaving the region at $x = 1$ appeared at the origin at $x = 0$.

Thus, the duration of a period was $1/w = 0.1$. The obtained results are shown in Figure 3.3. Similarly, to the previous case, one may observe that the non-stabilized solution suffers from strong oscillations which, however, are less significant on the tail of the profile (left edge). Introduction of weak stabilizing term (3.11) yields positive and smooth profiles, which are just slightly diffusive at the front and tail of the pulse, where strong gradients of u exist, and are characterized by maximum overshoot ~8% at the tail (recall that the shown solutions were obtained with the first order elements).

This case was further utilized to study the effect of a non-linear source term $S(u)$ in (3.7) that is essential for the streamer problem since the right-hand sides of equations (2.9) depend on their respective concentrations (2.10) making the equations non-linear (note that the field dependencies of the rates coefficients in (2.10) make the entire system (2.9) - (2.11) non-linear). To implement the test, the source term was represented in the form suggested in [83]

$$S(u) = -\mu\, u\, (u - 1)(u - 1/2) \tag{3.12}$$

which is written as

$$S(ul) = -\mu \exp(ul)\, (\exp(ul) - 1)(\exp(ul) - 1/2) \tag{3.13}$$

using logarithmic formulation. Factor μ can be interpreted as a constant reaction rate and being multiplied with the time step Δt determines the stiffness of the PDE [83] (the larger the product $\mu \Delta t$, the stiffer is the system). One may notice that the structure of the source term (3.12) is such that it is equal to zero in the region outside of the rectangular profile (due to the first term $u = 0$), inside it (second term $(u-1) = 0$) and at points where $u = 1/2$.

It is significant only around discontinuities and changes its sign from negative at $u < 1/2$ to positive at $u > 1/2$ with the magnitude being symmetric around this point. The latter feature provides physical conservation of the transported quantity and thus allows for identifying possible numerical artifacts in the solution.

The results of the calculations performed with second order elements (used to represent the discontinuities more accurately) are shown in Figure 3.4. As seen, the solution for the case with less stiff term $S(u)$ (Figure 3.4 a) is very close to the exact one (initial profile) and the front of the profile is well reproduced. However, oscillations with the magnitude in the interval $\pm 8\%$ appear ahead of the propagating tail of the pulse. One may also notice weak outrunning of the tail, which becomes stronger if the stiffness of the system is enhanced. It is clearly seen in Figure 3.4 b. This numerical phenomenon of wrong propagation speeds observed for stiff PDEs is well known (for details see e.g. [83]). In the present test, it appeared only on the tail of

the profile and thus is expected to be insignificant for the streamer problem where discontinuities are present mainly at the propagating plasma front.

The next test was performed assuming zero source term and stationary but spatially varying velocity in (3.7), represented as a function of the coordinate

$$u(x) = 1 + 9\sin^8(\pi x) \tag{3.15}$$

providing a peak value $u = 10$ at $x = 0.5$ and the magnitude $u = 1$ at the ends of the domain as shown in Figure 3.5 by dotted line. Periodic boundary conditions were used and the time of the period was $T_p = \int_0^1 dx/u(x)$.
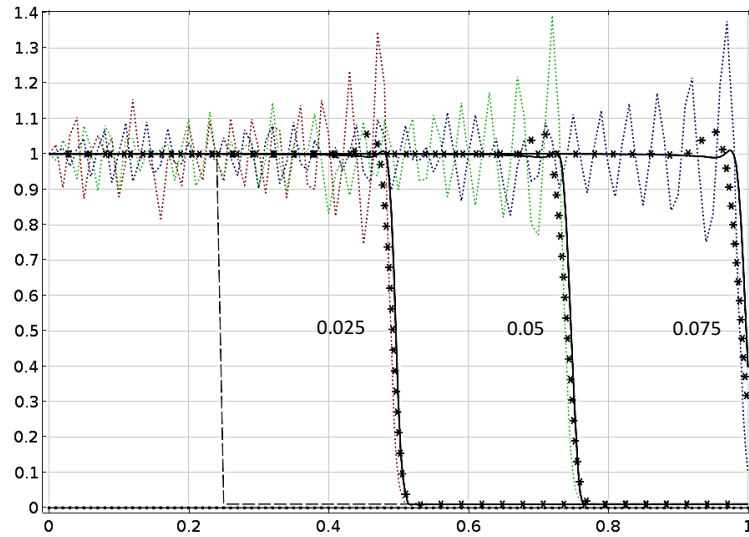
Figure 3.2 Advection of a unit step profile (shown by dashed line at t = 0). Dotted lines are non-stabilized solutions, stars and solid lines indicate profiles obtained with SUPG. Numbers show the output times and dots at the bottom represent mesh nodes.
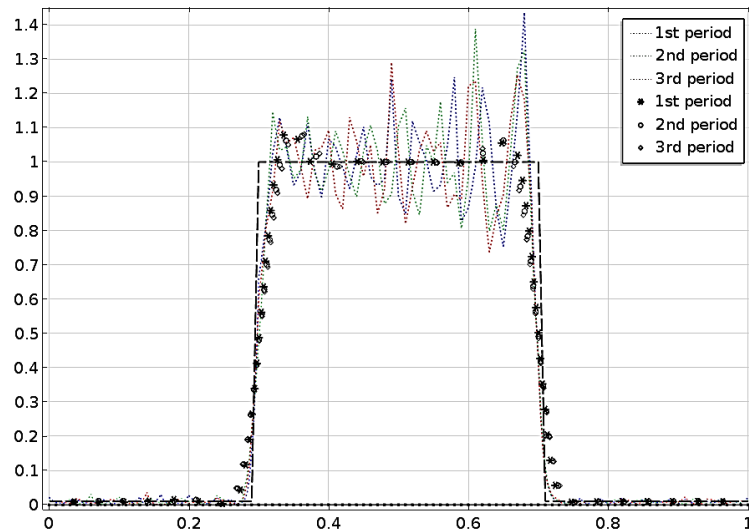
Figure 3.3 Advection of unit rectangular profile (shown by dashed line). Dotted lines are non-stabilized solutions and symbols indicate results obtained with SUPG stabilization with $\delta = \delta_{opt}$. The number of periods is shown in the legend.

Since no exact solution of the problem is known, a reference one was calculated by utilizing standard FEM with extremely fine mesh consisting of 5000 linear elements (no solution could be obtained with courser mesh). As seen in Figure 3.5, weak SUPG stabilization worked well in this case providing satisfactory reproduction of the profile as well as propagating front (compare stars and solid line). At the same time, slightly smeared tail of the pulse can be recognized. Note that it is hard to expect that the sharp peak in the profile for $t = 0.4 \cdot T_p$ can be properly resolved due to the strong difference in mesh resolutions (respective elements sizes were 1/5000 and 1/100). The solution for the full period (circles) is quite close to the initial profile but some delay of the front can be observed.

(a)   (b)
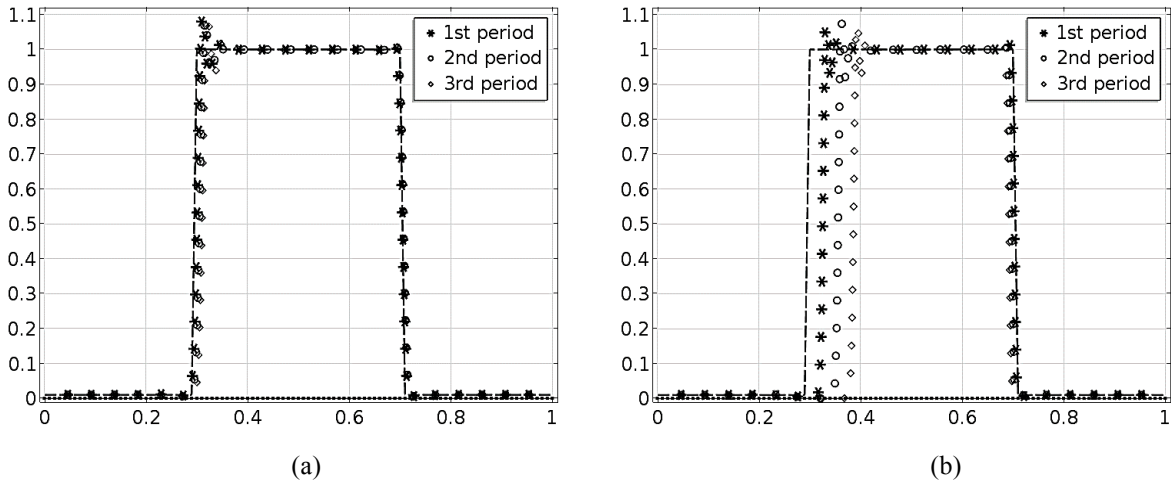
Figure 3.4 Advection of unit rectangular profile (dashed line) with constant velocity and non-linear source term (3.15) with factor μ = 100 (a) and 1000 (b). Symbols indicate stabilized solutions obtained with δ = 4δ$_{opt}$ for the number of periods indicated in the legend.
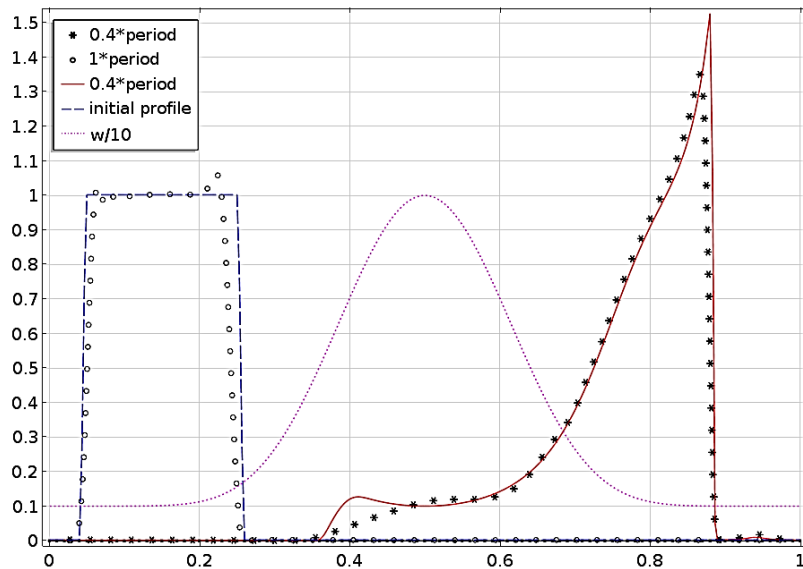
Figure 3.5. Advection of unit rectangular profile (dashed line) with variable velocity (dotted line). Solid line represents the solution at time 0.4*T$_p$ obtained by Galerkin FEM on refined mesh. Symbols (circles and stars) indicate results obtained with SUPG. Calculations were performed with linear elements.

Overall, the test demonstrated that the SUPG method provided strong stabilizing effect which yields superior results as compared to the other methods [80].

3.3.2. 2D tests

The first two-dimensional test comprises of uniform convection of a rectangular unit pulse and essentially presented a generalization of the one performed at lower spatial dimension. Thus, equation (3.9) was defined in a unit square domain with homogeneous Dirichlet conditions on boundaries at $x = 0$ and $y = 0$ while outflow flux was specified on boundaries at $x = 1$ and $y = 1$. The x- and y-components of the velocity were set to 1 which defines the transport along the streamlines parallel to the diagonal $x = y$. Structured (rectangular) computational mesh was used with 128 elements in each direction.

The initial profile and the expected (exact) solution are shown in Figures 3.6 a and 3.6 b, respectively. Note that each edge of the unit pulse occupies single mesh element similarly to 1d case. For the numerical solution, second order BDF was used since the lower order BDF (even being more robust) damps high frequency components in the solution making it more diffusive. The time step was limited by the value 10^{-3} providing generalized Courant number equal to 0.512. The non-stabilized solution obtained with linear elements is shown in Figure 3.6 c (one should mention here that the use of higher order elements hindered convergence of the non-stabilized problem). The unstabilized result is clearly not acceptable due to the strong oscillations and overshoots which at their maximum exceeded the initial magnitude by more than ~2.5 times. Introducing SUPG damped the oscillations and allowed the use of second order elements enhancing the accuracy. The stabilized solution is shown in Figure 3.6 d. As seen, the steepness of the initial profile is well preserved and the computed solution is just slightly diffusive (compare with Figure 3.6 b) despite of the fact that the Courant number is relatively high. The obtained result is in general similar to that in [79] computed by other methods. However, it could be achieved with much less efforts, i.e., simply by introducing weak expression (3.11) to the problem.

Another two-dimensional numerical test comprised of rotation of a cylinder with a slot in a non-uniform velocity field $w = (-y, x)$. Despite of the fact that such a problem does not directly reflect features of a developing streamer, the test is a challenging benchmark for numerical algorithms and was considered in a number of studies, see e.g. [79] and references therein. Thus, the problem was defined in a square domain $(-1,1) \times (-1,1)$, where $u = 0$ except the region limited by $(R < 1/3$ and $(|x| > 0.05$ or $y > 0.5))$, within which $u = 1$ (here, $R = ((x^2 + (y - 1/3)^2)^{1/2})$, as seen in Figure 3.7 a. The rotation took place in counterclockwise direction about the center of the domain, i.e. the origin of co-ordinates. The test was run utilizing structured mesh 128×128 and second order BDF for the time stepping. Since the magnitude of the velocity was varying in space (zero at the center and ~0.7 at the rear of the cylinder), the generalized Courant number was also varying, remaining below the upper limit ~0.12. In this test, it was not possible to obtain non-stabilized solution due to the poor convergence. Solutions of the problem obtained with linear elements and SUPG stabilization with $\delta = 0.25\delta_{opt}$ are presented in Figures 3.7 b and 3.7 c. As seen, the rear of the cylinder and the slot are reproduced fairly well after rotation by 180º (Figure 3.7 b). After full rotation, the edges of the object

become diffusive, but the slot is still well recognized (Figure 3.7 c). Overall, the result of the test is positive and demonstrates capabilities of the SUPG stabilization.

To conclude this section, one should stress again that the presented numerical tests were conducted for pure convective problem (3.8) and introduction of physical diffusion (as in equations (2.9)) yieldes significant improvements in the solutions in terms of stability and ability of capturing discontinuities.

(a)

(b)

(c)

(d)
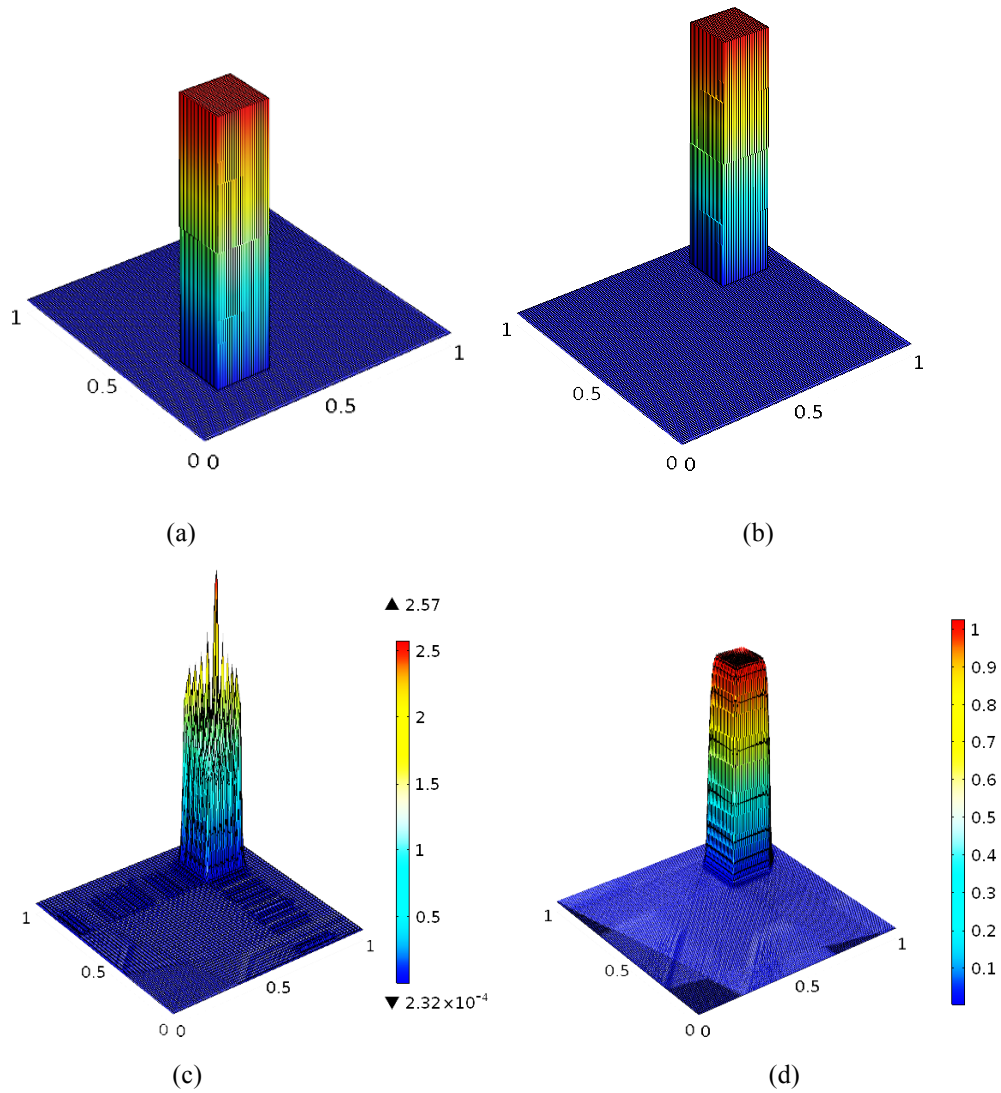
Figure 3.6. Advection of a unit rectangular profile (a) in a unit square domain with constant velocity. Solutions: exact (b), non-stabilized (c), stabilized with SUPG ($\delta = 0.05\delta_{opt}$) (d).

(a)   (b)   c)
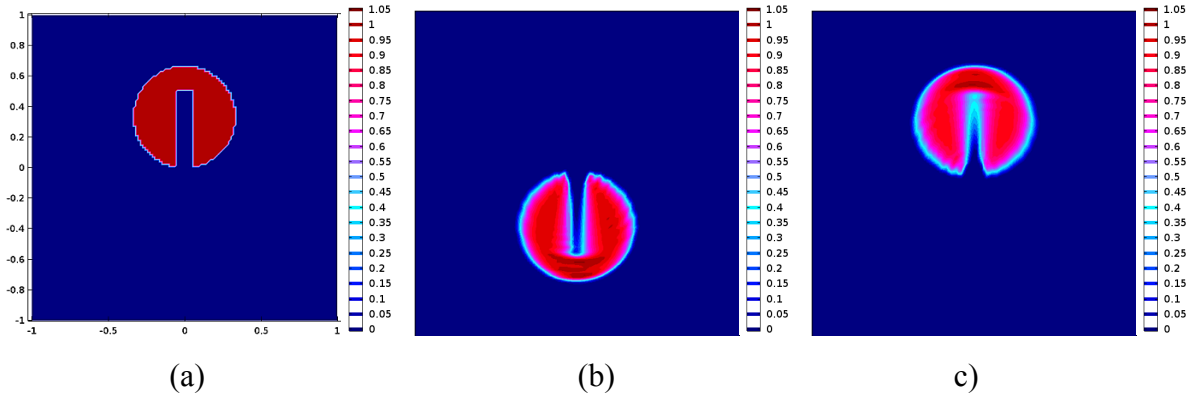
Figure 3.7 Rotation of a cylinder with slot ((a) and (d)) with variable velocity around the center of the domain. Solutions obtained with SUPG stabilization: rotation for 180° (b) and 360° ((c)).

3.4 Adaptive Mesh Refinement

The considered drift-diffusion problem consists of three transport equations with highly non-linear sources and coefficients. Solution of them is stabilized by utilizing consistent SUPG method. These equations are coupled with Poisson equation and three Helmholtz equations. Taking into account that resolving the streamer head properly required mesh resolution (0.1-10) μm, FE discretization in micron scale for the centimetre scale spatial domain for all these equations yields a huge number of unknowns resulting in extremely long computational time. To reduce it, a smart meshing technique can be utilized. Firstly, one may notice that the high resolution is required only locally (streamer head) while for the main part of the discharge volume a coarse mesh can be used. In such cases, a technique called adaptive mesh refinement (AMR) is usually employed [84]. When using AMR, the mesh is refined only in the areas where the gradient of a certain quantity of interest is high. To realize this technique, a coarse mesh is generated first throughout the domain such that a solution is achieved through various stabilization techniques. The local L2-norm error in gradients of the primary variable of all the elements is then calculated using the residuals [82]. The AMR criteria for equations (2.7) can be chosen as

$$High\ Gradient\ (error)\ V = \sqrt{\left[\left(\frac{\partial V}{\partial y}\right)^2 + \left(\frac{\partial V}{\partial y}\right)^2 + \left(\frac{\partial V}{\partial z}\right)^2\right]} \qquad (3.15)$$

$$High\ Gradient\ (error)\ ne = \sqrt{\left[\left(\frac{\partial ne}{\partial y}\right)^2 + \left(\frac{\partial ne}{\partial y}\right)^2 + \left(\frac{\partial ne}{\partial z}\right)^2\right]} \qquad (3.16)$$

As a sharp gradient of the field appears at the tip of streamer head (due to space charges) and low strength everywhere else in the domain, the AMR routine is active only at the tip. The mesh is refined in the elements with the higher L2-norm (3.15). The results from the previous mesh are mapped onto the new mesh and the new mesh is used to calculate the solution for the next time step. The error norm check is repeated until the defined number of refinements is reached for each time step. This allows introducing a coarse mesh in almost the entire domain and provide very fine mesh wherever it is needed thus reducing significantly the size of the problem and simulation time. Sometimes error norm can be defined for other quantities, e.g., the quantity whose magnitude changes very fast. One of the quantity could be photoionization source which

is a function of number density and electric field and is limited to the tip of streamer. The adaptive mesh refinement of photoionization variable at the streamer tip is used in all the test cases in next chapters. The mesh is refined for each 0.05 ns, so that the streamer head remains within the fine mesh region. The adaptive mesh refinement is critical for the fast calculation when the simulation model has similar dimension as seen in real geometry application for e.g. conductor separation in gas insulated switchgears.

4 Streamers in air in needle-plane arrangement

The developed approach was utilized for simulations of streamers in air in two different geometrical arrangements, namely, between needle and plane electrodes, and between edges of parallel disc electrodes. In the former, a single axisymmetric discharge channel was considered whereas in the latter one, a simultaneous development of two channels heading towards each other was analyzed. The results of the simulations are presented below for the needle-plane electrodes and for the parallel-disc electrodes in chapter 5.

4.1 Comparison with earlier performed simulations

A hyperbolic needle-plane electrode system separated by 1 cm was adopted following [17] as shown in Fig. 4.1. The geometry was represented in 2d axial co-ordinates with the symmetry axis coinciding with that of the needle. The discharge was initiated in dry atmospheric air at room temperature by applying a step voltage of 13 kV to the needle electrode while the plane was grounded. Model coefficients and parameters presented in chapter 2 were utilized. Boundary conditions for the charge carriers implied their zero flux on the electrodes with the same sign of the potential as the polarity of the transported charge while outgoing convective fluxes were specified in the opposite cases. One should mention that in contrast to the reference study, no special means were provided to initiate the streamer since the process proceeded naturally due to the provided rates for the background ionization and detachment of the electrons from the negative ions (Table 2.1), which play essential role in early stages of the discharge development.
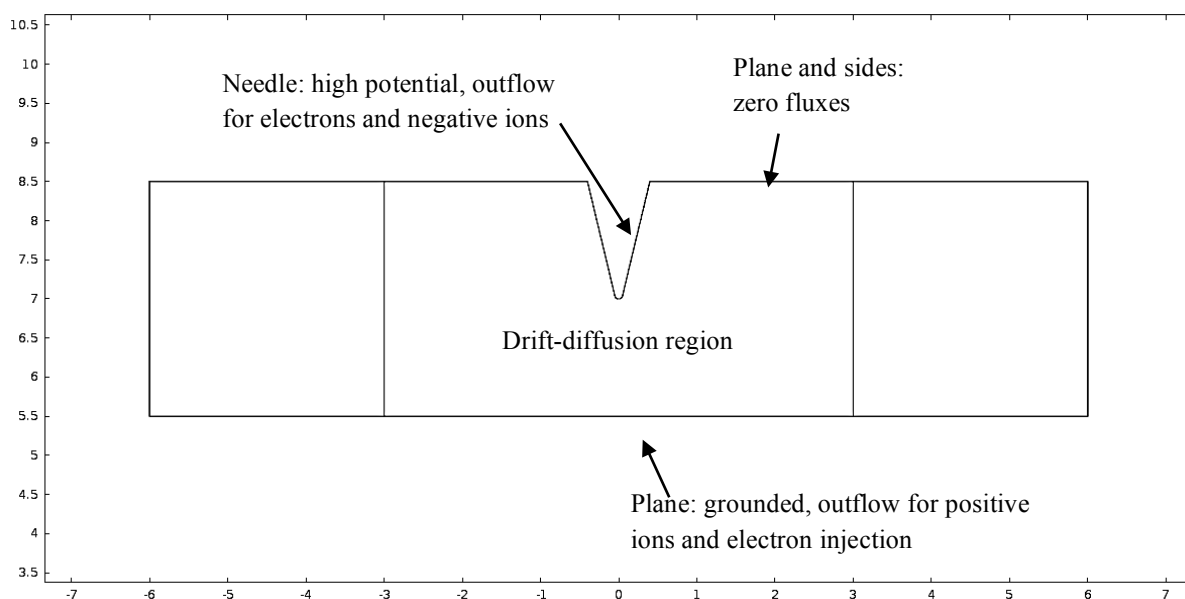
Figure 4.1: Details of the simulation model. Note: the side subdomain is used to extend the central domain for electric field calculations only.

The simulation model for this case utilizes 2d axisymmetric representation of the reference calculation domain and the drift-diffusion equations in logarithmic form are transformed to the cylindrical coordinate system. The SUPG for the consistent stabilization is applied by introducing a weak form contribution for the logarithmic formulation of the transport equations as stated in the previous chapter. Photoionization is implemented by utilizing three-term Helmholtz approximation of the integral model. Helmholtz equations are provided with zero boundary conditions according to [63]. All the equations are symmetric about the central axis, which is represented as Neumann boundary for all the scalar dependent variables.

To summarize the boundary conditions for the different PDE's for the domain in Figure 4.1:

- Dirichlet boundary conditions are provided for the Poisson's equation with the potential of 13 kV applied to the needle and the plane is grounded. The external boundaries are set to zero normal flux boundary condition for Voltage flux.

- The drift diffusion equations are provided with outflow or zero flux boundary conditions on the electrode's boundaries depending on the drift direction. Zero flux boundary conditions are applied on the external boundary and zero radial flux on the symmetry axis. Electron emission from the cathode (bottom line in the figure) is specified as an injected flux of the electrons proportional to the flux of ions scaled with the Townsend's second coefficient.

The simulations were conducted utilizing unstructured strongly inhomogeneous (in radial and axial direction) computational mesh with element sizes ranging from 50 um at the symmetry axis (where actual streamer propagation takes place) to 1000 um and larger at the external boundaries (radial coordinate of 1 cm and higher). In order to capture the sharp gradients of the scalar quantities being transported, adaptive mesh refinement was used and the mesh was updated based on the sharp gradients around the electric field at the tip of the streamer every 0.05 nanosecond.

A direct solver is used with variable high order (up to 2nd) BDF for implicit time stepping. The solution process involved two segregated groups of equations, which were iteratively solved one after another to reach the convergence. Poisson's equation together with the transport equations formed the first segregated group while the second one was composed of Helmholtz equations. Due to the strong non-linearities involved, Newton-Raphson solver with constant damping was used such that the Jacobian was updated at every iteration. The matrix solution was achieved through the direct solver, which allowed for parallel (shared memory) computations.

The calculated dynamic patterns of the electron density and the electric field in the progressing streamer are presented in Figure 4.2 and 4.3, respectively. As seen, the inception stage is completed during the first five nanoseconds when a region with high concentration of space charges is formed close to the needle tip. The electric field induced in the gas volume becomes strong enough to generate new portions of space charges thus providing continuous growth of the discharge channel (the process is linked to the development of secondary electron avalanches initiated from the photoelectrons, details can be found elsewhere [85]). As can be observed, high field region associated with the streamer head travels in inter-electrode space as an ionization wave converting neutral gas to a partially conductive state. According to the simulations, such self-supporting propagation lasts for ~20 ns until streamer crosses the

| 5 ns | 11 ns | 14 ns | 16 ns | 18 ns | 19.27 ns |
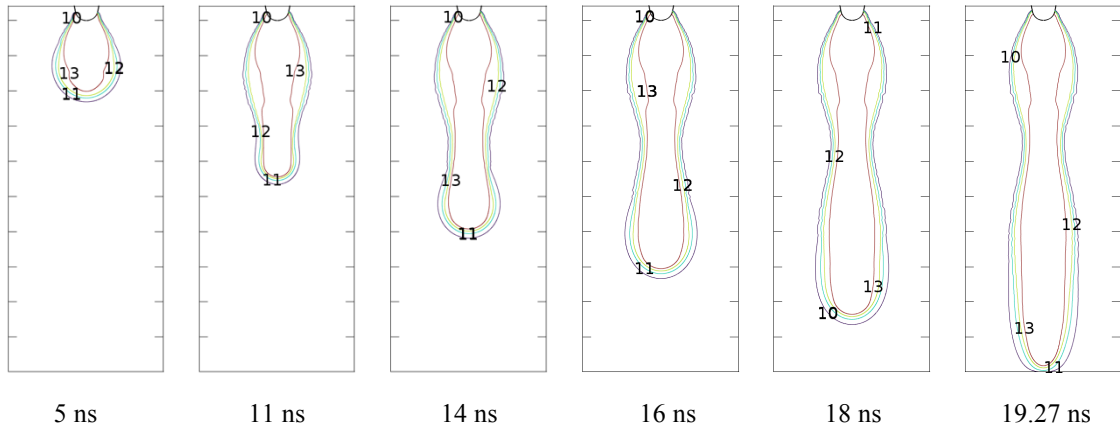
Figure 4.2 Profiles of electron densities (numbers indicate log10 of the density in cm^{-3}). The bottom line corresponds to the surface of the grounded plane; the dashes on the vertical and horizontal axes are 0.1 cm and 0.2 cm, respectively.

| 5 ns | 11 ns | 14 ns | 16 ns | 18 ns | 19.27 ns |
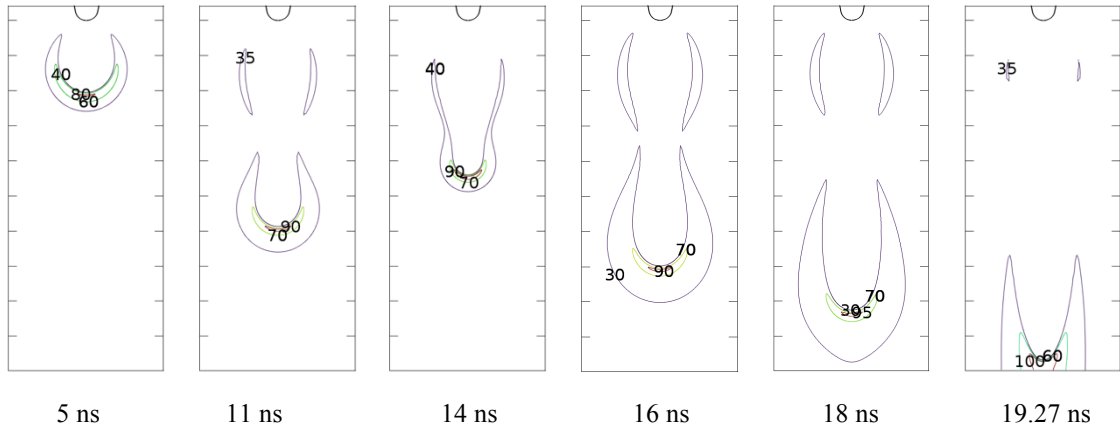
Figure 4.3. Profiles of electric field strength (numbers show levels in kV/cm) at different instants. The bottom line corresponds to the surface of the grounded plane; the dashes on the vertical and horizontal axes are 0.1 cm and 0.2 cm respectively.

inter-electrode space, yielding the average streamer velocity of ~50 cm/us. This parameter, as well as the apparent radius of the discharge channel (~150 um), agrees well with the experimental data [86].

It is important to stress that the photoionization plays a crucial role making the streamer capable to propagate in air. It becomes especially critical when the field strength along the propagation path is relatively weak. In the present case, the electric field along the axis is strongly inhomogeneous and it is higher than the critical field for ionization only in a small volume next to the needle tip whereas it is as low as ~10 kV/cm in other locations. The photoionization provides seed electrons at the tip of streamer for it to move ahead. The electrons generated by the photoionization leave the streamer head quickly and leftover positive ions strengthen the electric field in front of it. In order to simulate streamer propagation in very weakly ionized gas (background ionization in atmosphere with 10^3 free electron / cm^3), photoionization mechanism for extra electron generation is crucial, otherwise unrealistically high background density of free electron is needed.

More detailed structures of the electron density and fields on the axis of the discharge are shown in Figure 4.4 and 4.5, respectively. One can observe discontinuities in the profiles of the electron densities associated with their strong gradients and sharp peaks of the electric field strength. Both physical features are well reproduced in the computed characteristics of charge species transport. One may notice also the smoothness (absence of oscillations) of the solutions. These observations reveal the efficiency of the proposed weak logarithmic formulation stabilized with SUPG, as discussed in the previous sections.

As for a direct comparison of the calculated streamer properties with the results presented in the reference work [17], it is hard to expect a perfect match due to a number of reasons. First of all, essentially diverse approaches used for implementing such fundamental processes like photoionization (narrow radiating rings were considered in [17] instead of full discharge volume), making the calculated yield of secondary electrons in front of streamer's head to be significantly different in the two models. Also, taking into account the differences in the model parameters (drift velocities, ionization and attachment coefficients, etc.), it becomes obvious that only qualitative comparison of the results can be performed. In this context, it is notable that the main features discussed earlier in relation to the Figures 4.2 – 4.5 can be observed on their counterparts in [17] (Figures 2 and 3 therein). Moreover, the highest level of electron density ~10^{13} cm^{-3} reached in the propagating streamer is similar in both the studies. The present simulation yielded higher maximum electric field at the streamer head reaching ~180 kV/cm during the final bridging phase. The difference associated with the maximum electric field at the streamer head between the two studies is less than 5 kV/cm (Figure 4.5 is to be compared with Figure 4 in [17]). This leads to slightly different propagation time to cross the gap (~20 ns against ~23 ns in the reference simulations). The maximum of field magnitude along the axis is plotted against the streamer length in Figure 4.6. The streamer maximum field stays around 100 kV/cm during the propagation [87]. Nevertheless, the results of the present calculations are considered as acceptable and are in line with the known characteristics of the streamer discharges.
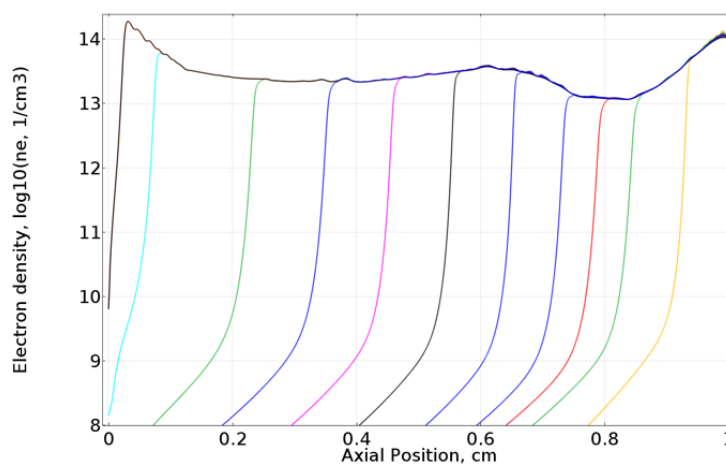
Figure 4.4. Electron density profiles along symmetry axis. Axial position is accounted from the plane electrode (bottom in Figure 4.2), so the propagation is from the right to the left. The first curves on the right correspond to time 1 ns, the step is 2 ns.
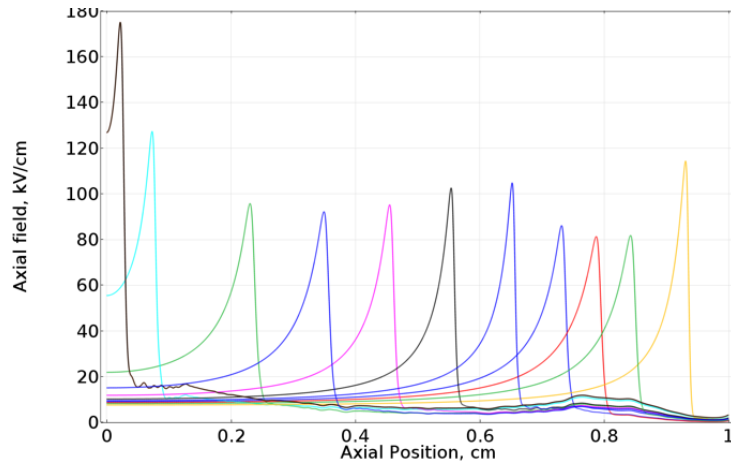
Figure 4.5. Electric field profiles along symmetry axis. Axial position is accounted from the plane electrode (bottom in Figure 4.2), so the propagation is from the right to the left. The first curves on the right correspond to time 1 ns, the step is 2 ns.
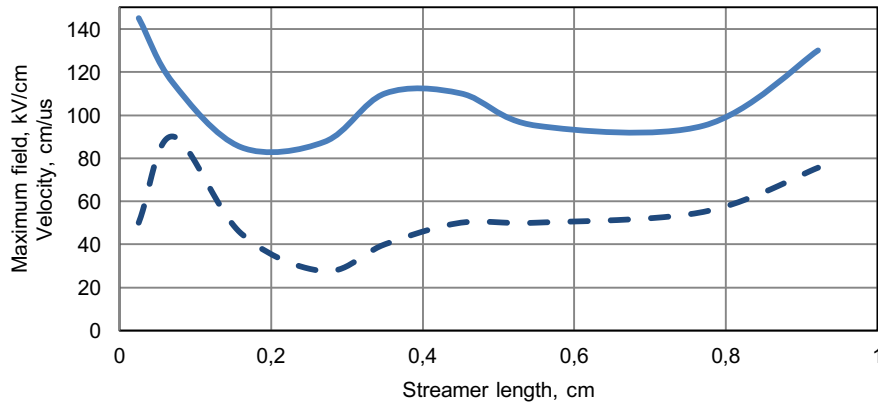
Figure 4.6. Field strength associated with streamer head (solid line) and its velocity (dashed line). The results are deduced from Figure 4.5.

The developed computational approach was further tested focusing on the stability of the calculations. For this, simulations of streamer similar to the presented above were conducted for longer inter-electrode distance of 3 cm and applied voltage of 40 kV. Such conditions physically correspond to overstressing of the system well above the breakdown level, thus enhancing field dependences of model parameters and stiffness of the PDEs (2.7) - (2.10). Implementation of streamer propagation model in COMSOL Multiphysics for similar conditions has been attempted earlier [42]. That study utilized standard transport module with non-logarithmic formulation and with isotropic diffusion and several other methods to overcome the numerical challenges discussed before; introducing auxiliary source terms, manual mesh refinement, etc. All these problems are dealt with in the present work and, therefore, it was of interest to repeat the simulations presented in [42] with the new method. The boundary conditions used were kept as indicated in the Figure 4.1 for previous model as well as the source terms in the drift-diffusion PDEs (terms, which were artificially introduced for stabilization purposes in [42] were not used). The contribution from the diffusion of ions was included. Note that the new model utilized the logarithmic formulation of the transport

equations, SUPG consistent stabilizations and three-term Helmholtz approximation for the photoionization (two-terms representation was used in [42]) that enhances the photoionization model as the fit provided better agreement with the integration formulation [64].

The computed electron density and field strength patterns are shown in Figure 4.7-4.8, respectively. Overall, they inherit features presented in Figure 4.2-4.3 for shorter streamer, e.g., the development of the spherical electron cloud at the anode (needle) tip and channel expansion along the gap with very little radial growth. The streamer needs about 25 ns to cross the gap that corresponds to the average velocity of $1.2 \cdot 10^8$ cm/s, which is consistent with the data reported in the literature [1, 41, 43, 88]. A specific property related to the applied overvoltage that provided stronger initial fields and thus shortened inception time, is a higher level of concentration of electrons, which reached $\sim 10^{14}$ cm^{-3}. This makes the propagating density profile to be close to a cylindrical shape with the field pattern as an envelope, Figure 4.8, instead of being a crone-like as in the previous case, Figure 4.3. Note that due to the higher charge density, the ionization threshold (field strength $\sim$30 kV/cm) is reached/exceeded not only at the streamer head, but also along the sides of the channel. This as well additional photo-electrons generated in its vicinity, make the discharge to expand in radial direction. These features can be compared with the results of the reference work [42] shown in Figure 4.9. One should mention that the so-called moving mesh frame technique was utilized in [42], where a frame with a very fine mesh (resolution $\sim$5 micrometer) was placed around the streamer head while a relatively rough mesh was used in the rest of the domain. When the discharge front was about to leave the region of the fine mesh during propagation, the simulations were interrupted, the frame with the fine mesh was brought in front of the head, the solution was mapped into the new global mesh and the calculations were continued. This approach produced uncompensated fluxes of charged species each time when re-meshing and mapping of the solutions on an updated computational mesh was done.

| 1 ns | 10 ns | 15 ns | 20 ns | 25.63 ns |
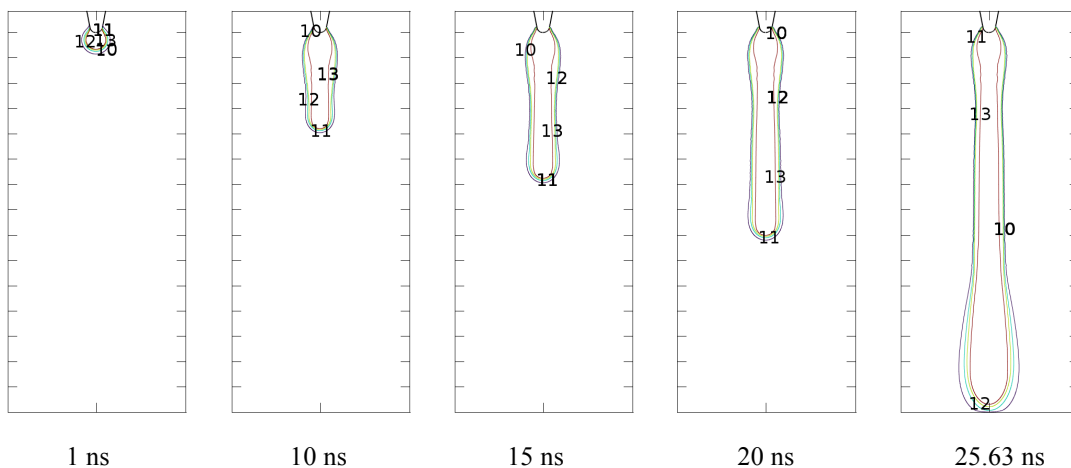
Figure 4.7. Profiles of electron densities (numbers indicate log10 of the density in cm^{-3}) at different instants. The bottom line corresponds to the surface of the grounded plane; the step on the vertical and horizontal axes are 0.2 cm and 0.5 cm respectively.
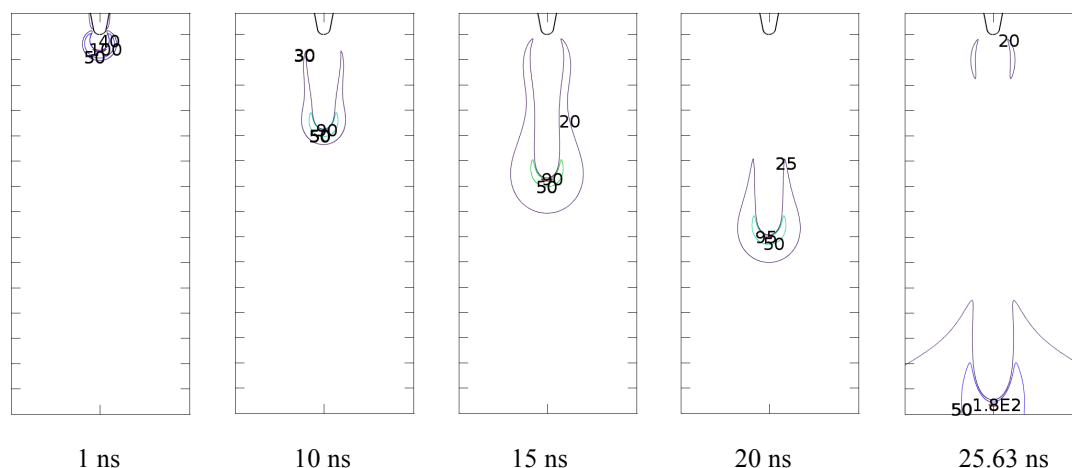
Figure 4.8. Profiles of electric field strength (numbers show levels in kV/cm) at different instants. The bottom line corresponds to the surface of the grounded plane; the step on the vertical and horizontal axes are 0.2 cm and 0.5 cm respectively.
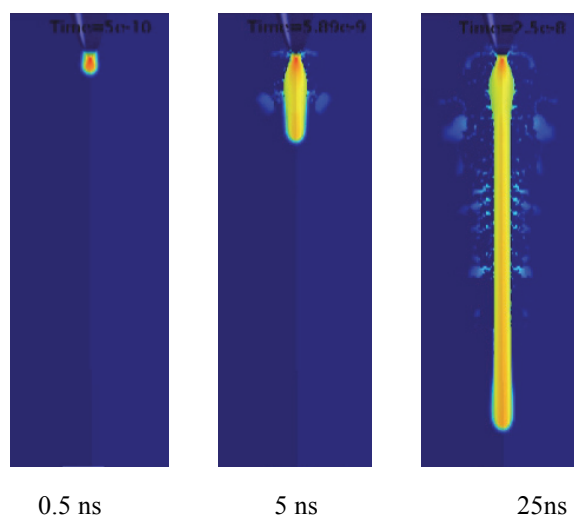
Figure 4.9: Profiles of log of electron density obtained in the reference model [42].

This effect is seen in Figure 4.9 in the form of radially directed electron jets. Despite of the presence of such numerical artefacts, the number densities in the jets are rather low and thus obtained characteristics of streamers are quite reasonable and close to those obtained in the present study, in particular, magnitudes of the densities of charge carriers and corresponding fields, propagation velocities, transported charges, etc. However, the shapes of the streamer channel are quite different. In the reference simulation [42], formation of a cylindrical channel is achieved with practically constant radial dimension during entire propagation as seen in Figure 4.9 (if the artifacts are ignored). The new model yields a discharge channel, propagation of which towards the plane electrode is associated with a radial expansion as in Figure 4.7. This behavior is more realistic and such channel profile matches results of other publications [69].

The calculated distributions of the electron concentration and field strength along the symmetry axis for long discharge are shown in Figures 4.10 and 4.11, respectively. As in the previous case, the profiles are reasonably smooth and reproduce all the essential features in the solution including strong gradients of the densities and associated sharp peaks of the field. The peak magnitude of ~100 kV/cm can be noticed for the duration of streamer propagation and it rises

to ~180 kV/cm when the streamer reaches the cathode. These values are comparable with the literature data available for streamers in air [13, 89]. The calculated electron density profiles are also similar to those obtained in [42] (reproduced in Figure 4.12) Thus, the peak magnitudes of electron density ~10^{14} cm^{-3} are comparable as well as the sharp gradients at the streamer head. It is also notable that the average streamer velocity obtained with the new model is close to ~1 mm/ns obtained in [42]. As stated above, small differences can be due to the higher electric field in the new model and different photoionization models used.
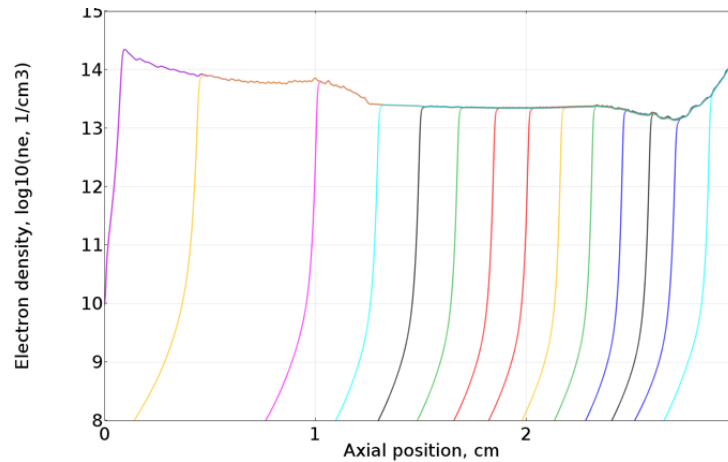
Figure 4.10.   Electron density (log$_{10}$, cm^{-3}) profiles along symmetry axis. Axial position is accounted from the plane electrode, so the propagation is from the right to the left. The first curve on the right correspond to time 1 ns, the step is 2 ns.
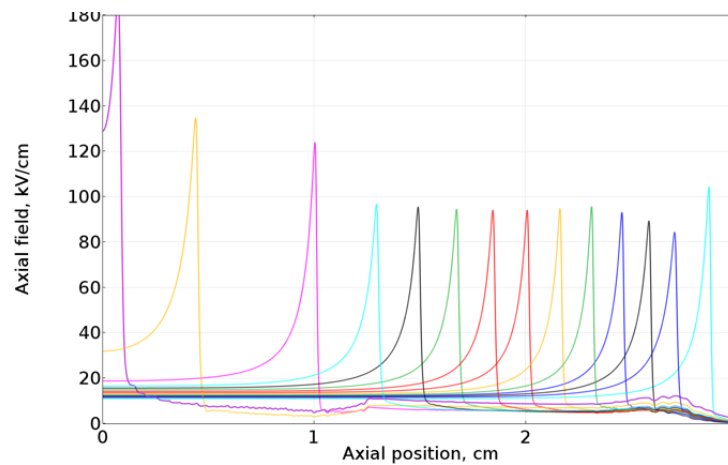
Figure 4.11. Electric field profiles along symmetry axis. Axial position is accounted from the plane electrode. The first curves on the right correspond to time 1 ns, the step is 2 ns.
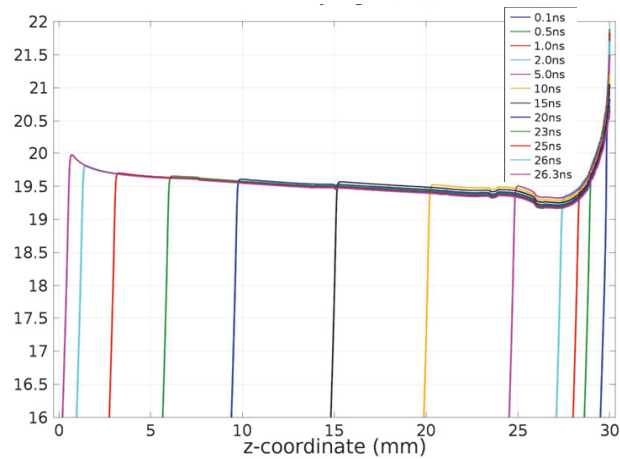
Figure 4.12: Electron density log_{10} (m^{-3}) along the axis at different instants in the reference model [42].
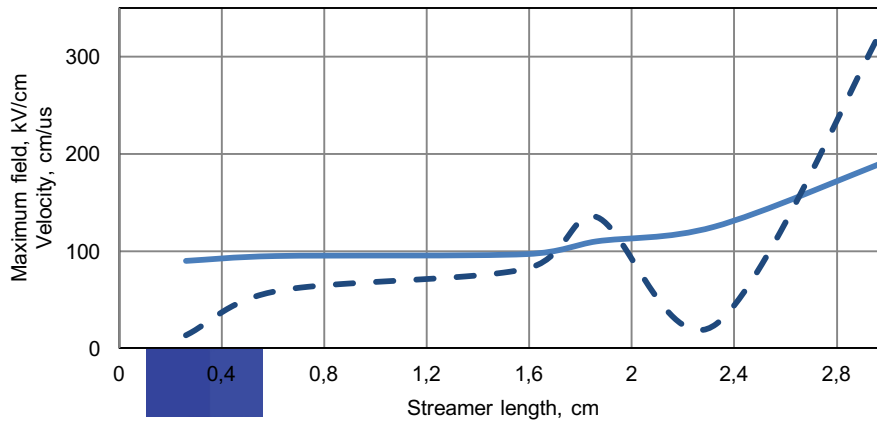
Figure 4.13. Field strength associated with the streamer head (solid line) and its velocity (dashed line).

The maximum field during the streamer propagation and derived velocities are plotted in Figure 4.13 and can be compared with the corresponding time dependences for the short discharge in Figure 4.6. As seen, the increased field levels at the streamer head provide higher local velocities that is consistent with the basic physical considerations and experimental results, see e.g. [90] and references therein.

5   Streamers between edges of disc electrodes in air

Simulations of streamer discharges are typically implemented in symmetrical electrode arrangements such as point-plane, needle-plane, coaxial cylinders, etc., which, however, are far from being representative of practical GIS designs. For instance, in medium voltage gas insulated switchgears, there are many locations with sharp edges and curved surfaces in conductors that, when being exposed to high voltages, may provide conditions for the inception of the streamers. The simple systems always suggest a common path for the discharges and breakdowns along the shortest distance between the electrodes coinciding with the geometrical symmetry axis. This is seldom the case in real situations. In this section, streamer development between the edges of two flat circular discs is analyzed.

This study case focuses on a discharge between disc-shaped electrodes (55 mm in diameter) with rounded edges (radius of 0.5 mm) separated by a distance of 50 mm as shown in the sketch of the domain in Figure 5.1. The system was energized by a positive step voltage of 100 kV applied to the top electrode while the other one was grounded. Boundary conditions for the drift-diffusion equations (2.7) - (2.10) were implemented specifying outward particles fluxes when charged species were moving towards electrode's surface whereas zero flux boundary conditions were used when the charge carriers were drifting into gas volume away from the boundary and on all other boundaries (i.e., no charge injection on either boundary). The treatment of boundary conditions for photoionization is based on Dirichlet formulation with zero values on all boundaries [63] .Uniform initial charge densities are applied similar to the previous models. The AMR based on photoionization source is used as discussed before to resolve the streamer head.
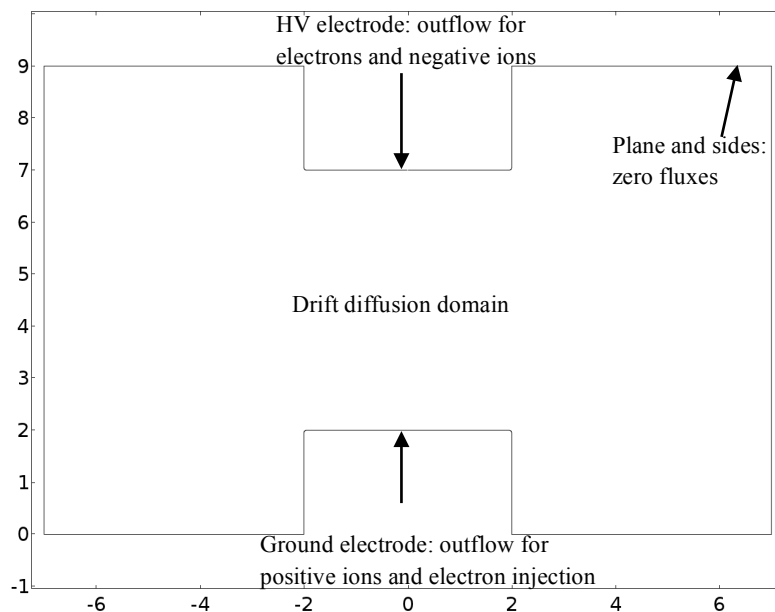
Figure 5.1: Computational domain for flat discs model.

The principle difference of the present case from the ones in the previous chapter is that the discharge propagation direction was considered to be non-axial itself, but being initiated in a rotationally symmetric system. By utilizing this global symmetry of the electrodes, the geometry was reduced to two dimensions. One should note that in reality, the problem is three-dimensional since the discharge is typically initiated at a location of the strongest field and propagates in a filamentary form. In the simulations, it is assumed that the probabilities of discharge inception are equal at each point on the edges of the electrodes and the discharge appeared in the form of a thin plasma sheet.

The calculated electron density and field patterns at various stages of the process are shown in Figures 5.2 and 5.3, respectively. As seen, streamer inception takes place in the region with the strongest electric field at the curved surface of the energized (top) electrode (see time frame 1 ns). At that time, the ionization threshold is exceeded at the edge of the grounded (bottom) electrode too and second streamer is initiated. During following few nanoseconds, both channels expand and start growing towards each other following the electrostatic field lines. One can notice on the plots showing corresponding field patterns in Figure 5.3 that the streamers heads are properly resolved and the peak electric field magnitudes are well above ~80 kV/cm.

According to the commonly used terminology, the streamer that develops from the top electrode can be considered as a positive streamer (cathode directed) and the other one is negative (anode directed). It is notable that the streamers shown in Figures 5.2-5.3 have different appearance: the positive channel is narrower and elongates faster while the negative one is more diffusive and slower. The corresponding electron densities in the discharges are also different, being higher for the positive streamer. As seen from the plots, both channels propagate along their respective field lines during the first ~30 ns. As their heads approach each other, the trajectories start deviating from the field lines due to the electrostatic interaction of the channels, as seen in the frame for 30 ns. The streamers finally meet at ~34 ns forming a continuous channel bridging the gap between the electrodes.

Profiles of electrons density and field strength along the axes of propagating discharges are shown in Figures 5.4 and 5.5, respectively. As seen, the levels of concentrations are lower for the negative streamer due to its more diffusive character (may be related to the fact that the secondary photoelectrons are pushed away from the channel rather than being attracted to it as in the case of positive streamer). Because of this, the field associated with the negative propagating front is weaker than in case of the positive discharge and the average propagation velocity is also lower (~5.7 cm/us and ~9 cm/us for the negative and positive fronts, respectively).

Merging the discharges at 34 ns results in formation of a path along which a spark leading to a complete breakdown may occur depending upon the properties of the external circuit. The deviation of this path from the electrostatic field line may result in significant errors when trying to apply well-known empirical streamer breakdown criteria for the evaluations of the breakdown voltages. Note that this problem inherently occurs in most practical cases, where the streamer propagation does not take place along the shortest geometric distance between the electrodes. The latter is typical for axisymmetric arrangements like point-plane or needle-plane, which are rather rare in practice. In the cases when the solid insulating elements are incorporated

into gas, uncertainties in choosing the breakdown path are even more significant [91] and can be cleared by conducting simulations based on the presented approach.
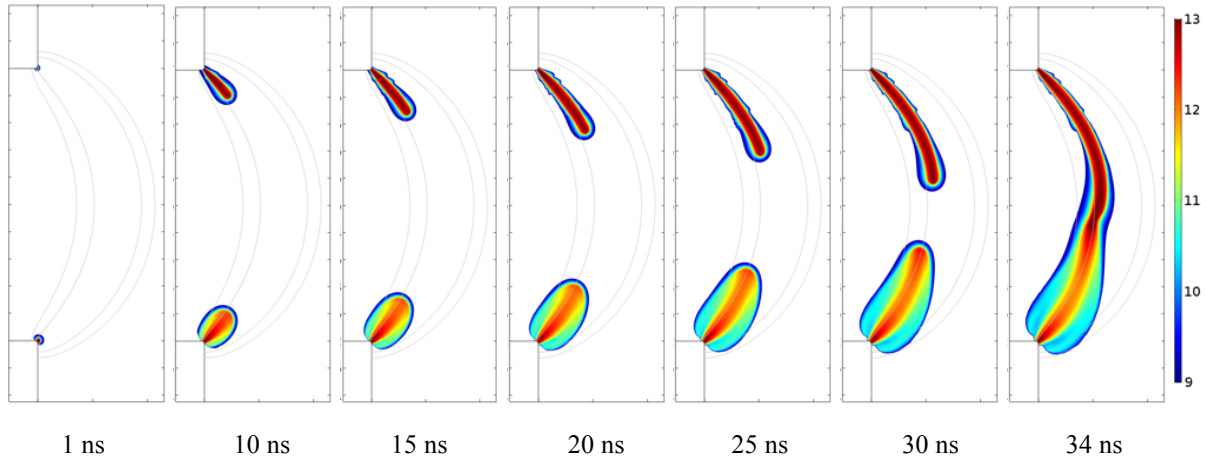
Figure 5.2 Profiles of electrons densities (the legend show log10 of the density in cm⁻³) at different instants. Steps between frame labels: 0.5 cm in vertical (axial) and 1 cm in horizontal (radial) directions. The frames show a part of the domain only focusing on edges of the electrodes (linked by electrostatic field lines).
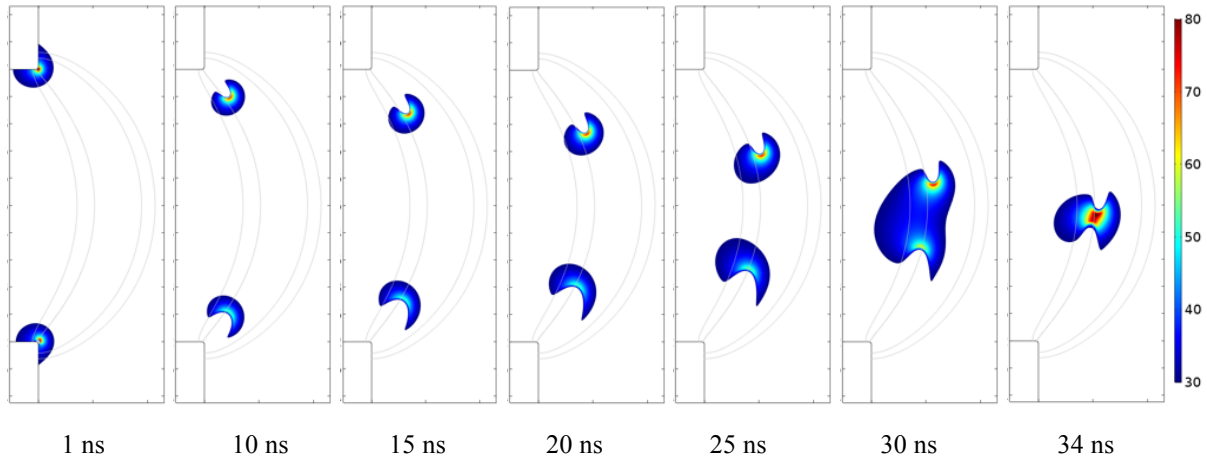
Figure 5.3 Profiles of electric field strength (the legend show levels in kV/cm) at different instants. Step between frame labels: 0.5 cm in vertical (axial) and 1 cm in horizontal (radial) directions. The frames show a part of the domain focusing on edges of the electrodes (linked by electrostatic field lines).
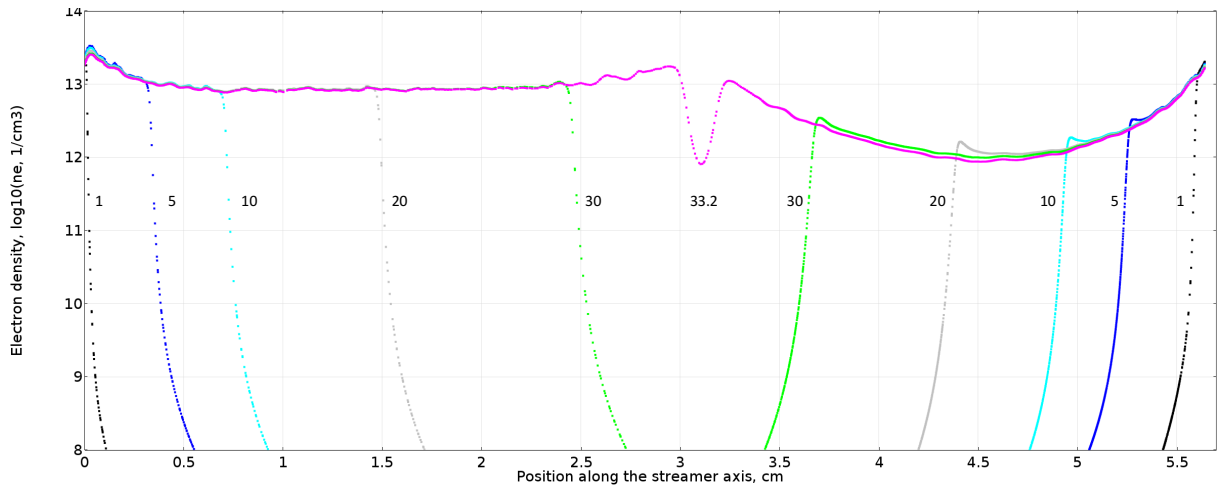
Figure 5.4 Electron density profiles for negative (right) and positive (left) discharges propagating along respective electrostatic field line. Labels on the vertical axes show log10 of the density in cm^{-3}. Numbers at the curves indicate time in ns.
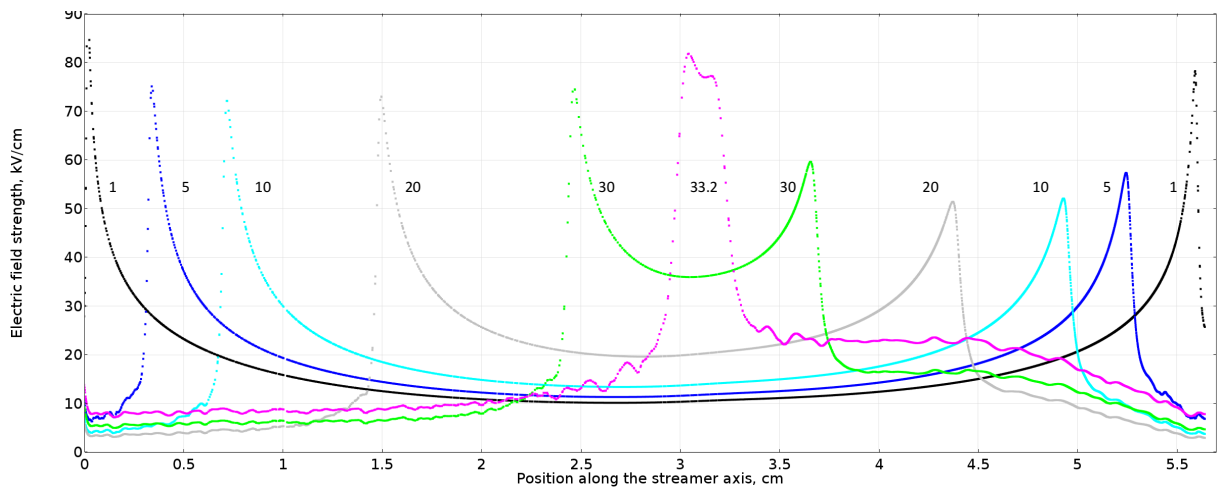
Figure 5.5 Field distributions along propagating negative (right) and positive (left) discharges. Numbers at the curves indicate time in ns.

6   Simulations of streamer branching

It is well known that the development of a streamer, especially at high gas pressure, for long distances and under over-voltages, is associated with its branching into multiple channels. An example of the visual appearance of such a discharge is shown in the photographs in Figure 6.1, which are borrowed from [92]. Reasons for this phenomenon are not absolutely clear, but several theories have been proposed, which consider inherent instabilities at the streamer head due to the probabilistic nature of the gas particles, influence of inhomogeneities in gas, localized charge centers, etc. [93].

Early attempts to simulate the process were based on simple 2-d models with fixed conductivity of the streamer channel [94]. Later on, streamer branching was introduced in single channel models [95]. Effects of the deterministic charge distributions on the streamer development were also modeled [96]. There are serious shortcomings in the simulation approaches used. First of all, branching is essentially a 3d phenomenon and can't be properly treated with 2d models. The 'Laplacian instability' hypothesis [95] is essentially being proposed for the 2d-axisymmetric model. It is assumed that the localized charge density at the streamer tip leads to multiple local electron avalanches and, hence, the branching. No special treatment has been done in the drift-diffusion equations for the development of these instabilities. It has been further interpreted as numerical artifacts by some peers [97]. Another probabilistic model based on the fixed conductivity of streamer channel interprets its growth in fixed steps. A critical electric field is defined on the streamer tip and it grows by fixed amount in the 'probabilistic' direction based on a defined 'fluctuation' [98]. This allows for the streamer to 'branch' in small region by allowing it to grow in the direction, which is not the original electric field direction. This scheme though allows for branching, but it is due to the artificial numerical treatment. The 3d branching of streamers has been attempted in simulations for liquid dielectrics based on random charge centers in the volume [96]. It has been concluded that the branching happens when the moving streamer head "sees" these charge centers and splits due to the electrostatic force interaction.
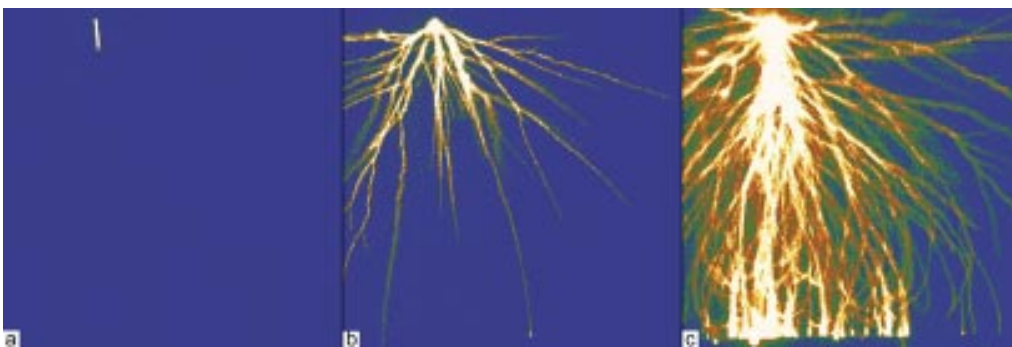
Figure 6.1: Time integrated images of streamers, borrowed from [92] *in 25 mm point-to-plane gap in ambient air at (a) 6 kV, (b) 12.5 kV, and (c) 25 kV.*
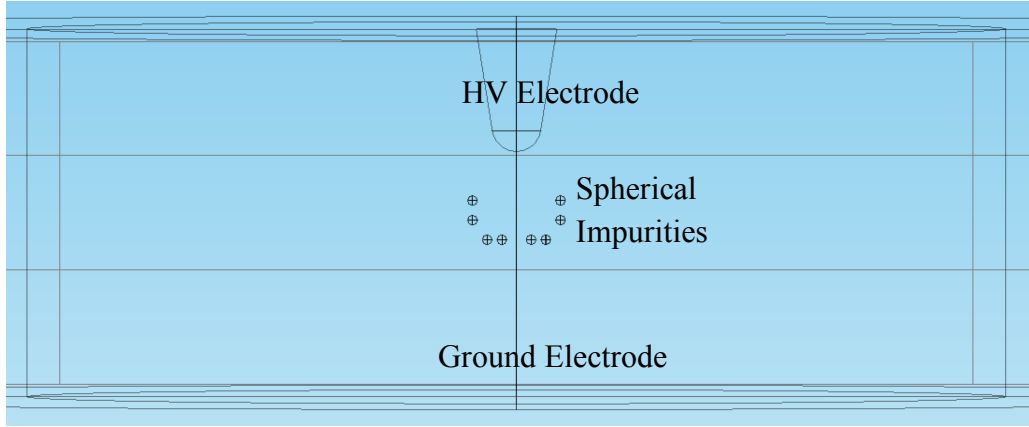
Figure 6.2: 3d simulation domain for streamer branching

The stochastic models are not based on any study of the local perturbations and the magnitudes of the distributed charges are general unknown. Based on the approach proposed for liquid dielectrics [96], an attempt of full 3d simulations of streamer branching was undertaken in the present study. In the analysis, charge accumulation centers are introduced as dielectric inhomogeneities in the medium appearing due to the suspended particulate (dust particles, clusters, etc.) providing local field enhancements in the gas volume and the amount of accumulated charges are derived from the inherent discharge processes without introducing any of the artificial approximations.

The simulations were performed in 3d domain formed by the needle and plane electrodes immersed in air at atmospheric pressure and separated by a distance of 1 mm as shown in Figure 6.2. The needle tip radius is 0.05 cm. A ramped potential of 2 kV is applied to the needle electrode and the other electrode is grounded The model implementation is similar to the previously considered study cases including adaptive mesh refinement, numerical stabilization and extended domain for the calculation of electric fields. Isotropic diffusion is used in this case to stabilize the solution. Charge accumulation centers are introduced as small spherical solid domains (.002 cm) located at some distance away from the path of single channel streamer discharge. Surfaces of these spherical domains allow for the charge accumulation that is modeled by the discontinuities in the local displacement fields

$$-\mathrm{n.}\,(\boldsymbol{D_1} - \boldsymbol{D_2}) = \rho_s \tag{6.1}$$

Here, $\boldsymbol{D_{1,2}}$ are vectors of the electric displacement field in air and solid inclusion, respectively; $\mathbf{n}$ is the unit normal vector; ρ_s is the surface charge density. The latter is calculated from the normal incoming flux of the volume charges

$$\frac{d\rho_s}{dt} = \sum_n J_n \tag{6.2}$$

where J_n is the corresponding normal current density calculated as $\mathbf{n}.(n_e\mathbf{W_e}+n_p\mathbf{W_p}+n_n\mathbf{W_n})$, where $\mathbf{n}$ is surface normal.
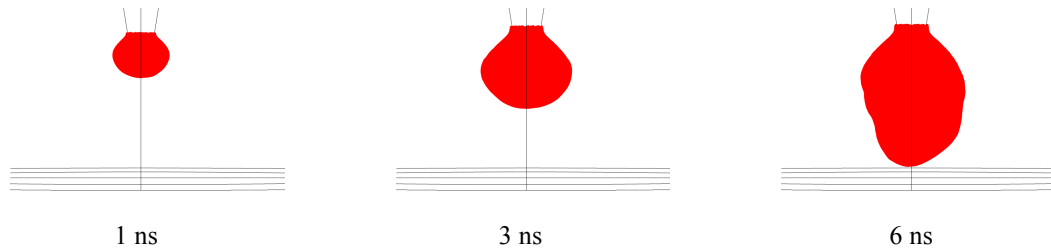
Figure 6.3: Electron density iso-surface (10^{12} cm^{-3}) at different instants after voltage application.
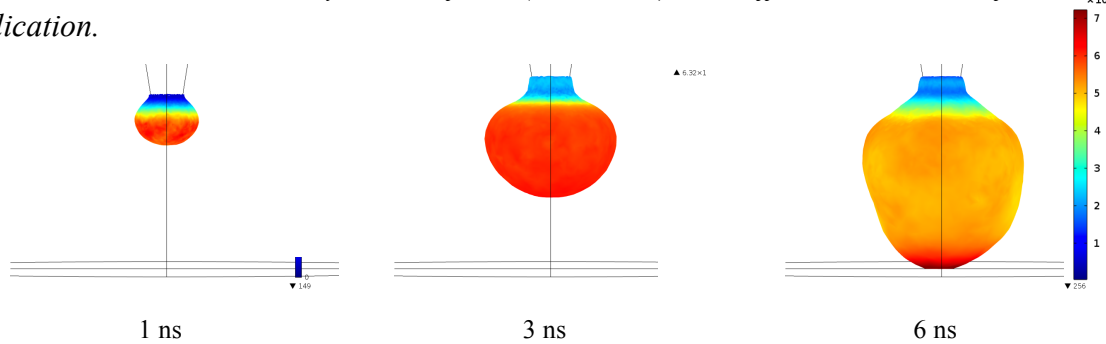
Figure 6.4: Electric field strength iso-surface at different instants.

In order to have a controlled setup and to detect any numerical artifacts, the simulation was first run without including the inhomogeneities. The boundary conditions were the same as described before for the 2d-models, but applied on the respective surfaces. Additionally, isotropic diffusion was used to stabilize the solution. The streamer inception in the form of growing electron density iso-surface of 10^{12} cm^{-3} over time is shown in Figure 6.3 (note that the maximum electron density is in the order of 10^{14} cm^{-3}). As seen, the simulations yield a single streamer channel developing from the needle to the plane electrode.

The iso-surface of the electric field is plotted over time in Figure 6.4. The peak electric field is in the range of 70 kV/cm, which is comparable with values reported in elsewhere [99]. Thus, the results obtained for pure air confirm that the dependent variables are properly resolved in the 3d simulations so that any instability due to the numerical discretization is avoided.

With the introduction of the dielectric inhomogeneities, the streamer moves away from the centrally defined base channel as seen in Figure 6.5. This is due to the fact that the electric field magnitude is enhanced in the gas next to the inclusions that leads to enhanced local generation of the charges. The charge movement and accumulation causes a local potential to be seen by the primary single channel discharge and the ionizing front is split into multiple branches. This can be seen clearly with the iso-surface plot of electron density in Figure 6.5. The bridging of the gap by streamer branches can be seen in the plot of the electric field iso-surfaces in Figure 6.6. The splitting of the streamer channel also has an influence on the propagating velocity that is reduced as compared to that of the single channel discharge. It is important to stress here that the position of the inhomogeneities plays a crucial role in the phenomenon and they have to be located close to the streamer channel to split it, as being placed far away, they have just little influence on the local electric field distribution.

It is notable that the results of the simulations of the streamer branching are sensitive to errors in the simulation model. Thus, it was observed during the simulations that with a small streamer head and, correspondingly, smaller photoionization region in front of the streamer, the splitting

of the channel (or deviation from the main path) is observed even without introducing charge accumulation centers if the mesh is not refined enough to resolve the head. Hence, the adaptive mesh refinement strategy is extremely important for the efficient modeling.

| 1 ns | 3 ns | 6.4 ns |

Figure 6.5 : Log$_{10}$ of electron density(cm^{-3}).

| 1 ns | 3 ns | 6.4 ns |

Figure 6.6: Electric field strength (V/cm).

7 Simulation of streamers in a hybrid gas-solid system

Numerical simulations were performed in hybrid gas-solid system for needle-plane electrode geometries of different dimensions. The generic sketch of the computational domain with boundary conditions is shown in Figure 7.1. As seen, the voltage is applied between the needle and plane electrodes. Boundary conditions for the gas domain at the electrodes include outflow flux conditions for the impinging species and zero flux for the flow in the opposite direction. The lateral boundaries are assigned to have zero flux boundary condition. As for the solid insulator the fluxes of electrons and holes are defined by (2.43). At the gas-solid interface, the flux balance equation (2.48) is solved. Dirichlet boundary condition for Poisson equation includes the potential as described in Chapter 2 for the electrodes. Neumann condition for the potential is applied on the external surfaces.

The following cases are considered in the simulations:

1. A needle-plane arrangement with the needle radius of 50 micrometers and separation between the electrodes - 10 mm. A physically floating dielectric barrier of thickness 1 mm is placed 5 mm away from the needle. A stepped positive voltage of 30 kV is applied to the needle electrode, and the plate electrode is grounded. The symmetry of such an arrangement is used to reduce the model size. This model corresponds to the experimental setup in [87], but it is assumed that the barrier is made of polyethylene (as charge transport parameters are available in the literature).

2. A needle-plane electrode system as presented in [100]. The electrode radius is 3.5 mm and the separation is 60 mm. A barrier of 5 mm thickness and diameter of 80 mm is placed at 20 mm away from the needle electrode. A voltage of 120 kV, higher with respect to the experimental setup, is applied to reduce the calculation time. This is a typical case of a large inter-electrode separation which is used to demonstrate a possibility for a fast-numerical solution by the proposed approach.

3. This case is an extension of case 2 with the inter-electrode distance increased up to 80 mm. The rest of the geometry and other conditions remains the same. The potential of 150 kV is applied to the needle electrode.

The resulting set of coupled equations are solved in COMSOL Multiphysics software using custom logarithmic formulation. Time stepping is done by using implicit formulation based on the backward differential formula. The segregation of the variables are done into three groups. They are iteratively solved until a convergence is reached with updated Jacobean in each iteration. The simulations were conducted utilizing unstructured strongly inhomogeneous (in radial direction) computational mesh with element sizes ranging from 10 microns at the symmetry axis and barrier surface (where actual streamer propagation takes place) to 200 microns and larger at the remaining geometry. Additionally, adaptive mesh refinement is performed (for cases 2 and 3 as described below) on the streamer head once it clears the top
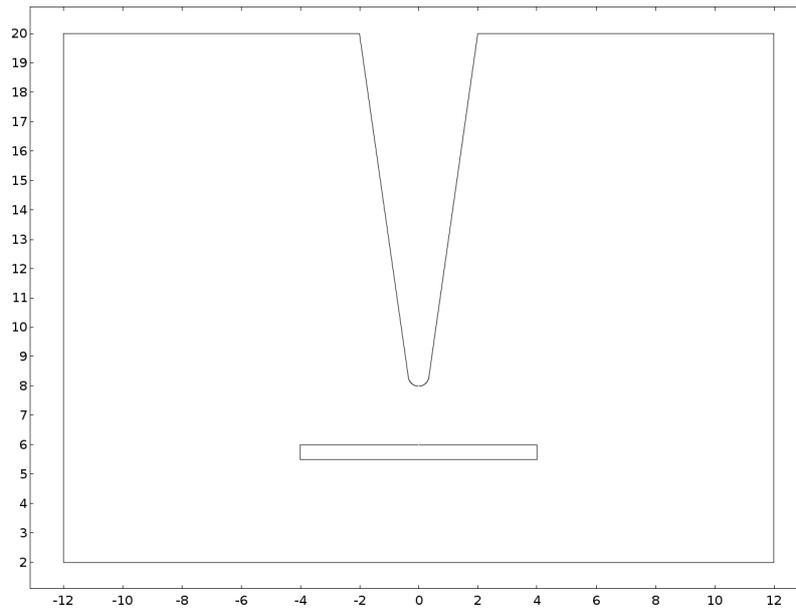
Figure 7.1 The computational domain for hybrid gas-solid insulation system

barrier surface for the rest of the simulation. This reduces the number of elements needed for the whole simulation and at the same time resolves the strong gradients in the electric field, number densities and source terms.

Case 1.

The contours of the electron density in Figure 7.2 demonstrate discharge initiation and development over time. It can be seen that initially the electron cloud is formed at the needle tip and it expands radially. Later, it develops in axial direction and reaches the barrier surface at ~0.5 ns. Soon afterwards, the discharge starts propagating along the top barrier surface with the peak electron number density ~10^{13} cm^{-3} at its front. At the same time, the applied high voltage induces supercritical electric field in the gas gap beneath the barrier (between its bottom surface and plane electrode), which being superimposed with the field created by charges deposited on the top surface (Figure 7.3, frame for $t = 1$ ns), provides conditions for the discharge inception in the bottom gas gap. As a result, discharges on both sides of the barrier develop: one expanding radially on the barrier upper surface and the other expanding from the bottom surface towards the plane electrode (observe profiles in Figures 7.2 and 7.3). The average propagation speed for the surface discharge is evaluated as ~3.7 mm/ns that is close to the value recorded in the experiments [87].

Propagation of the discharge along the surface of the barrier can be treated as a stationary wave travelling on the gas-solid interface. This is seen more prominently on the plot presenting time variations of the net surface charge density on the barrier surface in Figure 7.4. Note that the peak values are in the range of ~20 nC/cm^2. This value matches quite well to the results reported in [24]. Note that the electric field profiles associated with the moving charge are plotted in Figure 7.5. In the plot, the field in the barrier is shown as being negative just for the representation purposes, otherwise it is positive in magnitude. One may notice in the graph that the peak associated with the discharge front in the gas phase is ahead of the corresponding peak on the solid side of the interface. The reason for this is not clear and require further analysis.
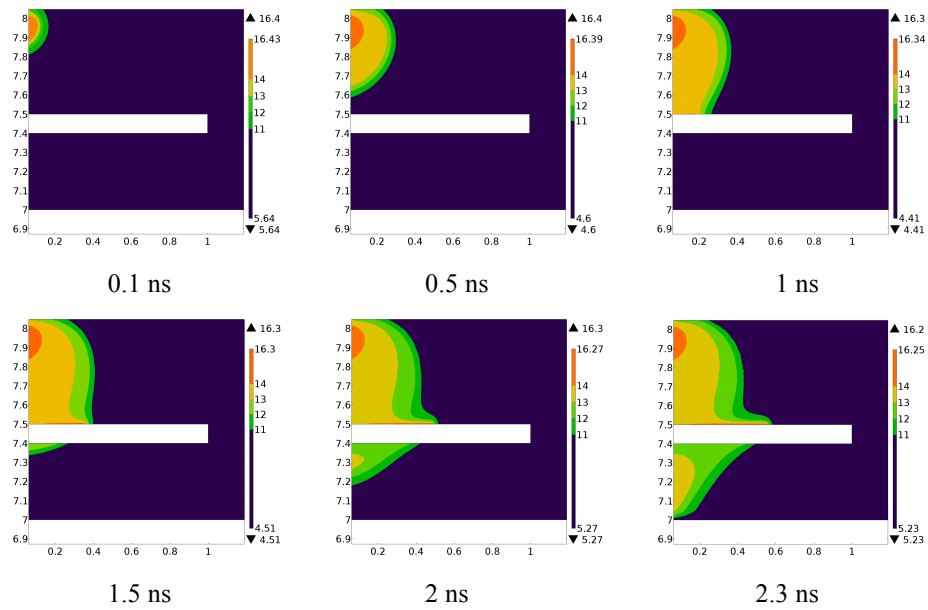
Figure 7.2 Electron density contours (cm^{-3}, log$_{10}$) at different time after voltage application.
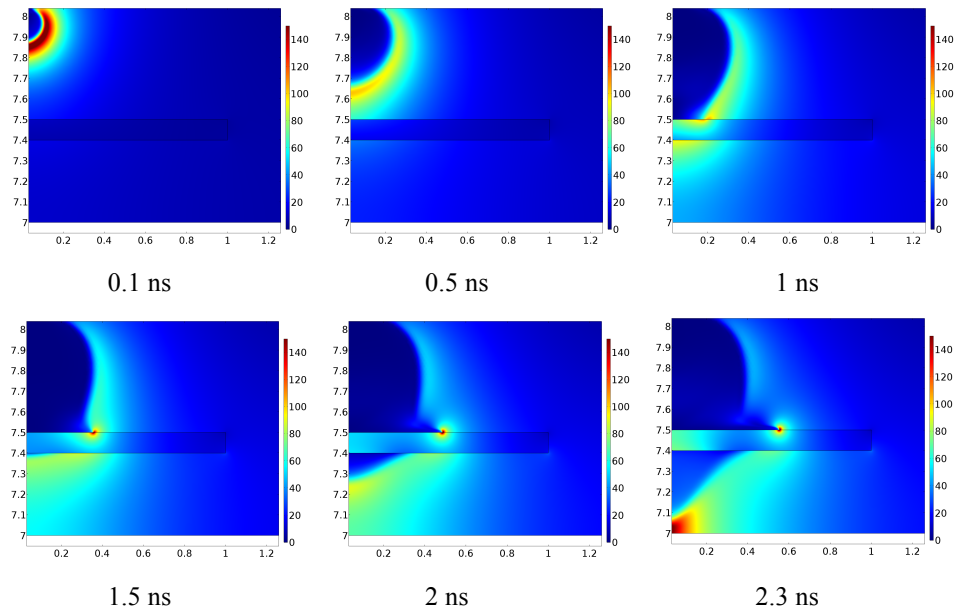
Figure 7.3 Electric field strength (kV/cm) at different time after voltage application.

Case 2.

Streamer initiation and propagation is similar to the previous case with initial radial expansion and later axial elongation. As seen in Figure 7.6, the discharge reaches the barrier surface at ~3 ns and a surface streamer is formed. Note that in contrast to the case 1, no secondary discharge is developed in the gas gap beneath the barrier due to rather low induced field. The discharge formed on the top surface propagates along the gas-solid interface with the electron density at the streamer front ~10^{14} cm^{-3} as seen in the frames for 6 ns and 9 ns. At the latter instant, it reaches the edge of the barrier and departs from it. By that time, the average velocity of propagation along the surface reaches ~6 mm/ns.
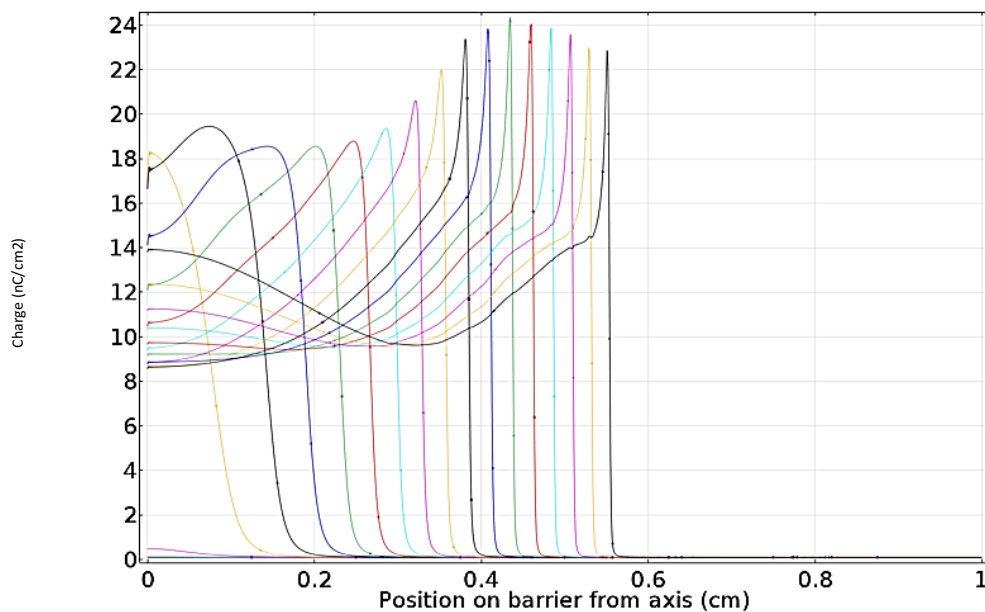
Figure 7.4 Surface charge (nC/cm²) on barrier surface, time ranges from 0.3 ns (leftmost profile) to 2.3 ns (rightmost profile) with the step of 0.1 ns.
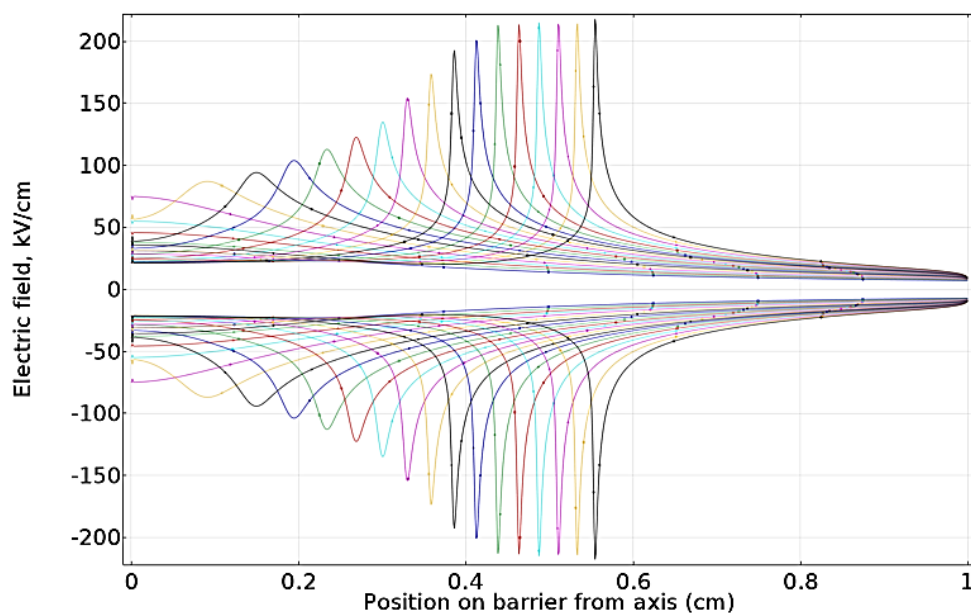
Figure 7.5 Electric field strength (kV/cm) on air-solid interface. The upper part is for air, the lower part is for solid phase (note that the field magnitude in the solid is also positive). Time ranges from 0.3 ns (leftmost profile) to 2.3 ns (rightmost profile) with the step of 0.1 ns.

Further, once the streamer leaves the barrier surface, it continues to develop in the gas following electrostatic field lines towards the grounded plane electrode, which is reached at ~21.5 ns. The average velocity of the propagation in the air alone can be estimated as ~3 mm/ns, i.e. being two times smaller as that on the gas-solid interface.

The corresponding time variations of the electric field are shown in Figure 7.7. It is interesting that the field profiles map the path between the electrodes taken by the discharge in the considered hybrid gas-solid insulation system.
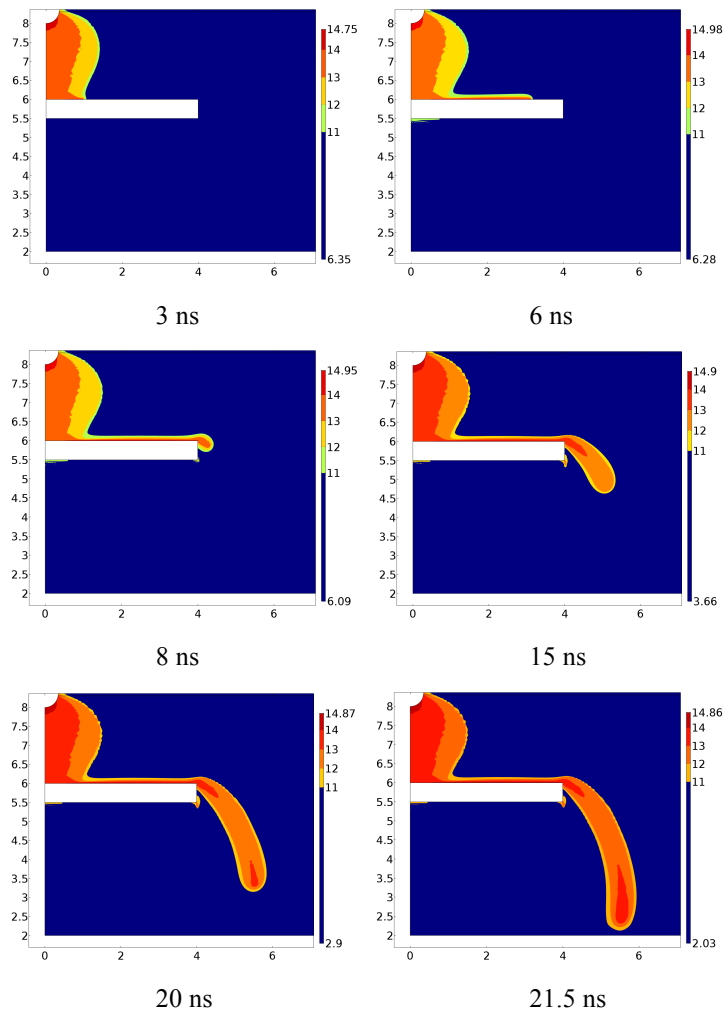
Figure 7.6 Electron density contours (cm^{-3}, log$_{10}$) at different time after voltage application.

Such information is particularly useful for practical purposes and can be applied for rough estimations of breakdown voltages with the streamer criteria [18]. The discharge path in Figure 7.7 is similar to the nanosecond imaging obtained in [100].

The distributions of the net charge and corresponding fields on the gas-solid interface are presented in Figure 7.8. As seen, the peaks of the surface charge density at the streamer head reaches ~45 nC/cm^2 (almost double as for the case 1, Figure 7.4) and that of the field strength are ~160 kV/cm. The latter is comparable with the case 1 (Figure 7.5). Also, the shift of the peaks in the air and the solid phases can be noticed.

Case 3.

The discharge development stages are similar to those in the previous case. The propagation time is increased up to 28 ns due to the larger inter-electrode distance. To track streamer head on the longer path, the adaptive mesh refinement was utilized and the computation mesh at the discharge front can be seen in Figure 7.9. The mesh is refined for each 0.05 ns, so that the streamer head is resolved properly at all the time during propagation. The adaptive mesh refinement is critical for the fast calculation when the simulation model has similar dimension as seen in the real geometry application for e.g. conductor separation in gas insulated

switchgears. The simulated streamer path can be seen in the plots of the electron number density and the electric fields in Figure 7.10.
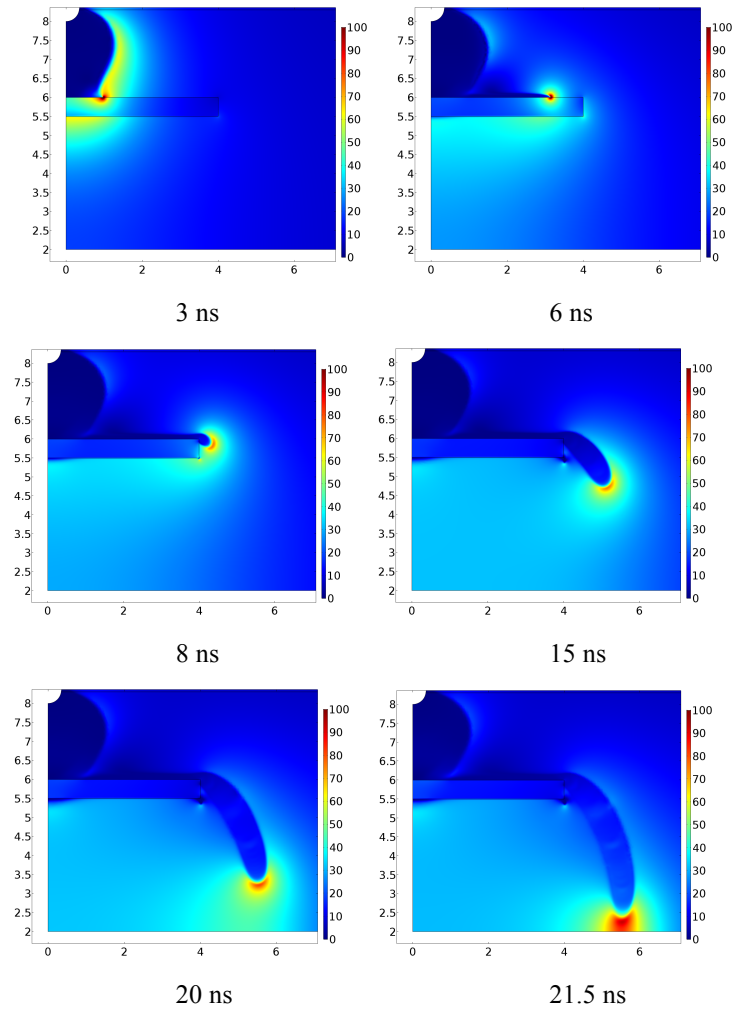
Figure 7.7 Electric field profiles (kV/cm) at different time after voltage application.
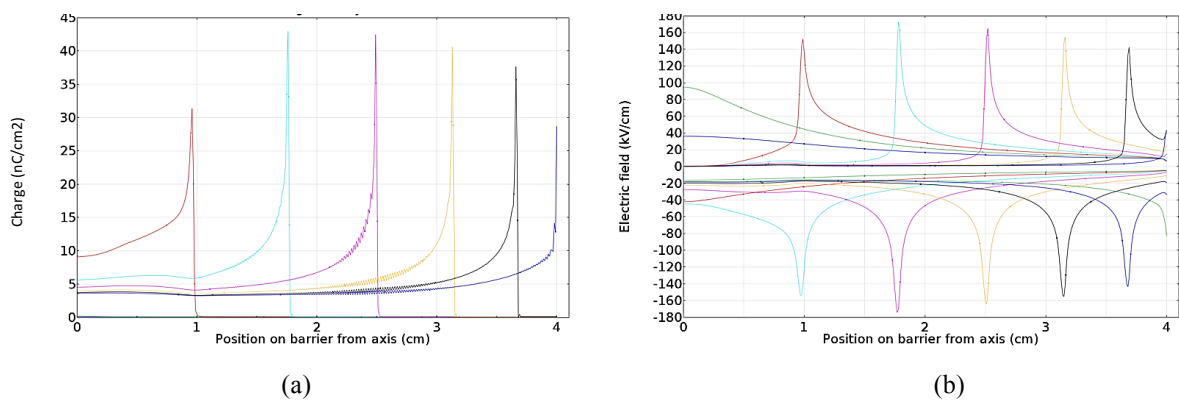
Figure 7.8 Surface charge (a) on barrier surface and electric field strength (b) on both sides of the interface (as in Figure 7.5). Time ranges from 1 ns (leftmost profiles) to 8 ns (rightmost profiles) with the step of 1 ns.
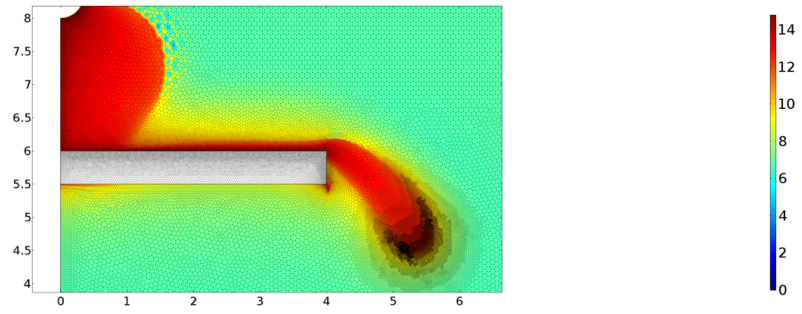
Figure 7.9. Electron density (cm^{-3}, log$_{10}$) at 15 ns, note adaptive mesh at the streamer head.

(a)   (b)
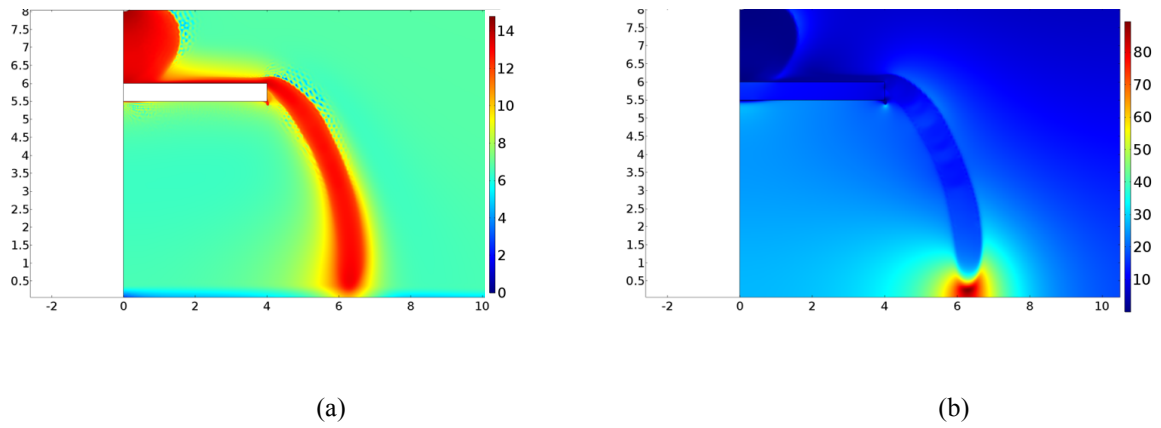
Figure 7.10. Electron density (cm^{-3}, log$_{10}$) (a) and electric field strength (kV/cm) (b) at 28 ns.

8   Conclusion

An efficient computational framework has been developed to analyse the charged species transport in hybrid air-solid insulation influenced by strong electric fields. The developed models are based on a set of coupled non-linear partial and ordinary differential equations comprising in the most general case

- time dependent drift-diffusion equations for fluxes of charge carriers (electrons and ions in gas, electrons and holes in solid) yielding dynamics of space charges;

- Poisson's equation for electric potential allowing for obtaining electric field distributions in gas and solid phases affected by the space charges;

- three Helmholtz equations for calculating the non-local photoionization rate;

- equations describing filling/empting traps in the bulk of the solid dielectric, and

- ordinary differential equation representing the dynamics of the surface charge accumulation/release on the gas-solid interfaces.

The densities of the charge carriers which are dependent variables varies by 15 order of magnitudes and that too, over couple of elements during the streamer propagation. There is a strong advection from the mobility of the electrons and hence the standard Galerkin scheme is unstable. In addition to that there is a strong negative source present due to the attachment of the electrons which may make densities negative as numerically there is no limit keeping the densities positive. In order to make the numerical scheme stable a class of function known as streamline upwind Petrov-Galerkin (SUPG) is introduced. These consistent form of stabilization in contrast to the inconsistent stabilization (Appendix 1), ensures that the mathematical nature of the original PDE's has not been changed. It also removes the oscillation associated with the discontinuities or sharp gradient in the advection dominated flow.

COMSOL Multiphysics has inbuilt stabilization in the 'Transport module', which is based on the Galerkin least square method (GLS). It is shown that the GLS is more diffusive than the SUPG in the literature, as a result it dampens the front of the streamer head resulting in lower E-fields. Therefore, SUPG stabilization is preferred and implemented by custom code in the COMSOL mathematics module. The problem of negative densities due to the large negative source is handled by a logarithmic formulation. Generally negative densities are observed next to a sharp streamer front in the form of damped oscillations. Logarithmic formulation ensures that the densities always stay positive. The logarithmic formulation is available in COMSOL plasma module but it lacks any form of stabilization and the whole implementation is limited to certain form of plasma lacking a way to implement streamer drift diffusion method. It includes the solution of EEDF for rate constants and additional energy equation, as a result the number of equations increases and hence the computation time. The E-field based drift diffusion formulation results in faster solution times for the problem domain of interest. This thesis

presents a logarithmically stabilized numerical scheme which is not published before and is not available in any commercial software.

Rates of reactions taking place in gas discharge plasma (input coefficients for the drift-diffusion equations) have been derived by the numerical solution of a Boltzmann equation for electrons energy distribution function in N_2:O_2 (80:20) mixture after introducing the two-term approximation. The rate coefficients calculated are converted into Townsend coefficients and compared against the existing codes (BOLSIG+). There is a good match to the existing codes. This allows for the implementation of any other gas from the experimental cross section data with control of energies up to which the two term approximation needs to be solved. This fits with the thesis goal of a complete framework for the streamer discharge simulation.

The inter-electrode dimension of interest is in the range of 50 mm (GIS insulation) for practical geometries. The electron source at the tip of the electrode is submicron in dimension. The resolution of 100 x 100 mm axisymmetric model in microns results in millions of elements which needs a server cluster for solving. To increase the efficiency of the calculation and to reduce the computational time, adaptive mesh refinement (AMR) was introduced into the model. The whole of the domain is resolved at millimeter spatial scale and only the electron source moving with the streamer is resolved at a submicron level. This results in only 10s of thousands of elements to be solved for the coupled PDEs, as increasing a single node results in seven more degree of freedom (DOF) to be solved. The previous model at the research group lacked AMR which is implemented in this thesis. This resulted in reduction of the solution time from few weeks to less than a day for all the test cases presented in the thesis.

In addition, many of the other self-made codes lacks implicit time stepping method. As a result the time stepping is limited by the CFL condition so that the Courant number has to be less than 1. In streamer discharge the time stepping is limited by the submicron resolution of the streamer head. Therefore, the explicit time stepping schemes takes months for a solution. The thesis implements higher order implicit time stepping so that the time steps are not limited by the spatial discretization.

The developed numerical scheme is rigorously checked against the standard test cases of advection and non-linear sources. These includes 1d test cases with constant velocity and zero source term, constant velocity and non-linear source and variable velocity. It is shown that the overshoots and undershoot associated with the stepped profile propagation in Galerkin formulation is removed by the SUPG stabilization. The test is done for linear and higher order elements, so as to present the feasibility of higher resolution solution which is lacking with the other discretization schemes. Similarly unit rectangular profile transport with nonlinear source shows complete removal of oscillations from a stabilized solution. The variable speed case resembles mathematically the streamer propagation in 1d and here there is a better match of the transported profile than the other publications.

The mathematical test is continued to include 2d test cases. The unit rectangular profile is advected in a plane diagonally. The unstabilized solution results in the dependent variable value reaching two times the unit value and having lots of oscillations. The stabilized solution is able to advect the profile without any of these issues. The last 2d case is rotation of the slotted cylinder in a 2d plane. Here too the stabilized solution works well with minimum of the

diffusion. The checking and verification of the logarithmic stabilized algorithm for 1d and 2d test cases presented a sound foundation to continue with the streamer discharge simulation in the next chapters.

Such developed computational framework has been utilized for several study cases to simulate the development of streamer discharges in air in different 2d geometrical arrangements as well as to model streamer branching in full 3d representation. Additionally, gas-solid insulation involving surface charge accumulation is also presented.

The needle-plane arrangement is the starting point for the streamer propagation in inhomogeneous electric field in the thesis. Initially the simulation is performed against the widely published test case and the result in the thesis shows highly resolved E-field with higher magnitude in comparison to it. This case is important because it shows the propagation of the streamer in undercritcal electric field. The streamer initiation happens in small region next to the needle electrode where electric field is higher than the critical electric field to cause the ionization. Initially the ionization grows spherically and bring the electric field value lower at the needle from the initial applied field. This is more like increasing the effective needle radius. The streamer propagates towards the ground if the field at the tip of streamer can be maintained above the ionization value. The background field in majority of the gap can be lower than that of the ionization field. The streamer bridging the gap results in a plasma channel with high conductivity. If the voltage is increased further, this may result in much more charge generation and resulting transformation of streamer into a thermal arc (leader), which is widely accepted as complete electrical breakdown. The thermal arc simulation is outside the scope of the thesis and typically involves single species model based on thermodynamic properties of the plasma at high temperature. It is important to mention that typically there is a statistical time lag after the application of Voltage for a free electron to come under the influence of electric field and ionize the neutral. In the presented simulations there are uniform background electrons, which results in positive source for the streamer to initiate. The applied voltage and initial electron density defines the duration of streamer initiation and hence statistical time lag is neglected in the simulations. Additionally there is a dependence of the streamer initiation to the slope of the applied voltage. Since the streamer propagation time is in nanoseconds and the typical Lightning Impulse voltage is in microseconds for a GIS type test, a DC voltage is considered for all the simulations, neglecting the effect of the Voltage slope.

The streamer is shown to propagate in a longer inter electrode gap of 30 mm under initial higher electric field. The propagation time is reduced at the higher initial electric field in comparison to the previous case (20 ns for 10 mm vs 25 ns for 30mm). The streamer channel is much narrower in longer test case with respect to the shorter streamer test cases. But the streamer tip field stays around 100kV/cm for all the needle-plane test cases during the propagation period. There is an increase of the streamer tip field seen near to the electrodes to higher value than the propagation tip field in all the test cases. The streamer propagation field also depends on the photoionization model used. The photoionization model provides additional electrons at the streamer head. The unintended consequence of it is smearing of the streamer head and resulting in lower electric field. In the absence of the photoionization source, test case performed but not included in the thesis, the propagation electric field at the streamer tip is higher ~150 kV/cm. This gives insight of old streamer propagation simulation having higher electric fields due to

the absence of the photoionization model. The qualitative comparison of the experimental streamer dimension from the radiation measurement to that of the performed simulation results in a good match for the value of theb streamer radius and the propagation speed.

The next investigation was guided by the typical geometries seen inside a GIS which includes flat busbars with rounded edges resulting in a streamer propagation not along the axis of the geometry. The streamer initiates from both the electrodes due to the local high ionization field. The positive streamer is seen to be narrower than the negative streamer and both deviates from the curved initial background field due to the electrostatic interaction at the middle. This is a novel simulation presented in the thesis as most of the previous publications involves needle-plane or plate-plate configuration.

The more complex simulation involves 3d modeling and a hypothesis for the streamer branching. It is proposed that the charge centers are present in the domain which allows charge accumulation. The model of the branching was introduced through the inhomogeneities in the gas, modeled as solid dielectric micro-particles. Charge accumulation on the solid surfaces inherently leads to local field enhancements, thus initiating splitting of the streamer channel and the formation of the branches. The model was carefully checked against the non-physical artifacts and numerical instabilities so as to avoid non-physical reasons for the streamer branching. Arbitrary values of charge is avoided at these centers and it is proposed that the charge accumulation is the result of the different permittivity of these spheres. This results in streamer branching for full 3-d geometry. Any 2d symmetry is not simulated for branching as it is inherently a 3d phenomenon lacking any circular symmetry. This is an improvement over the previous publications which consists of arbitrary charge centers in liquid dielectrics in the absence of photoionization.

The permittivity based 3d model was futher developed into hybrid gas-solid insulation simulation for a barrier normal to the electrodes. The barrier is used in GIS to increase the electrical breakdown withstandability of an interelctrode gap. The barriers are not touching any of the electrodes and hence this simulation is different from the dielectric barrier discharge (DBD). There are various hypothesis for the streamer propagation path in the presence of a barrier. It is shown in the simulation and later verified by experiments that the streamer propagation path is different from the previous hypothesis. There has been lot of experimental investigation for barrier discharge but this is the first simulation result for the same. The dynamics of charge accumulation on the gas-solid interface was quantified. It forms the background for the empirical streamer criteria method to estimate the gap withstandability which is outside the scope of the thesis.

It can be concluded that the developed simulation framework creates a tool for analyzing the complex systems and practically oriented tasks. The conducted study provides knowledge needed for developing design rules for the hybrid high voltage insulation, in particular, for the environmentally friendly SF_6-free gas-insulated systems.

9   Future work

Non-thermal discharges in air were studied in the present project utilizing the developed computational framework. The simulations were performed for the streamer discharges in different 2d geometries and later a more complex 3d model of streamer branching was introduced. The hybrid insulation system (solid-gas) was also validated successfully.

The next step could be to develop the model for the leader (arc) transition in the present framework. It involves additional equation for the number density of the neutrals. The joule heating of the plasma channel should be introduced to account for changes in the number density of the discharge. Together with higher temperature and change in the number density, the reaction and the transport coefficients are expected to change as they are functions of neutral particle density and temperature, which affect the electron cross-sections. External circuit needs to be added to the numerical model so as to provide voltage control in order to achieve a stable leader propagation. The model can be enhanced further by including a transition to the magnetohydrodynamic single fluid model after certain temperature and conductivity are achieved inside the channel. This will also involve change in radiation model to more computationally efficient formulation like the net emission coefficient. This way one single framework will cover a range from non-thermal plasma to high current electric arcs.

Another direction of study is related to the growing need to characterize the Fluoroketones and Fluoronitriles gases, which are marketed as environmentally friendly replacements for the SF_6 -gas. The reaction coefficients and the transport coefficients in this media can be calculated within the developed framework once the electron cross-section data are available from the experiments.

A parallel extension of the charge accumulation model could be to analyse the effect of mist on the streamer propagation as reported in [101]. It is seen that there is an enhancement of the breakdown voltage in the presence of mist particles. The developed framework can be used to check for the physical processes leading to such an enhancement in details. It is reported that the size of the droplets is the leading parameter for such an enhancement. Detailed quantitative analysis of the charge accumulation on the surface will enhance further understanding of the phenomena. The partial discharge is another topic which can be simulated for the voids in the present computational framework. Even though the void dimensions are small, multiple voids and their interaction can be simulated with the optimized method presented in the thesis.

Chapter 9 Future work

10 **Appendix**

Simulations of streamer discharge in air using isotropic diffusion

The logarithmic weak formulation of PDE governing streamer propagation is stabilized by Petrov-Galerkin contribution as presented in chapter 4. Additionally, adaptive mesh refinement is used to resolve the gradients at the tip of streamer together with isotropic diffusion. The previous model utilizes consistent stabilization in which the nature of PDE's was not changed and mathematically they remain the same even if Petrov-Galerkin contribution is added, but here additional diffusion was added during the simulation.

In order to increase the complexity of the problem slowly during the research project, initially small geometries were simulated. This provided a fast check on the solution progress and allowed for changes if the things went wrong. Isotropic diffusion was initially used to stabilize the solution of the PDEs. This should make the gradients of the charge carriers' densities less steep due to an additional diffusion term.

Most popular stabilization techniques are based on introducing a certain amount of artificial diffusion into the PDE that can be classified as isotropic diffusion. The simplest approach is to use, i.e., an extra value D_{iso} directly added to the diffusion coefficient so that the Peclet number becomes less than unity

$$\text{Pe} = \frac{wh}{2\,(D+D_{iso})} \tag{10.1}$$

While doing so, the original problem is affected and the method is often referred to as inconsistent stabilization. The method is simple and robust, but sharp gradients in the solution gets smeared out. To minimize this effect, the selected amount of artificial diffusion should guarantee that the resulted equation remains close to the original formulation.

To test the approach, streamer propagation in atmospheric pressure air between the needle and the plane electrodes separated by a distance of 5 mm is considered in 2d axisymmetric model as shown in Figure 10.1. Similarly to [42], a step voltage of 15 kV with rise time of 0.1 ns was applied between the electrodes. This model has been attempted earlier in [42]. In that study, several methods were utilized to overcome the numerical challenges discussed earlier e.g. by introducing additional auxiliary source terms, etc. This has allowed for simulating streamer propagation in air in short (5 mm) gaps in a needle-plane system that yielded reasonable agreement with the experimental results. Note that the length of the streamer is used in an electrostatic sense, meaning the strength of its interaction with the electrodes (it is stronger for a short streamer).

The boundary conditions used are indicated in the figure 10.1. Note that in the model the domain for solving Poisson's equation is extended. The physical source terms in the drift-diffusion PDEs are the same as in the reference model [42] while those, which were artificially introduced for stabilization purposes are removed in the present model. The contribution from the diffusion of ions is also neglected due to the short duration of the discharge event in the old model. Note that the new model utilizes the logarithmic formulation of the transport equations
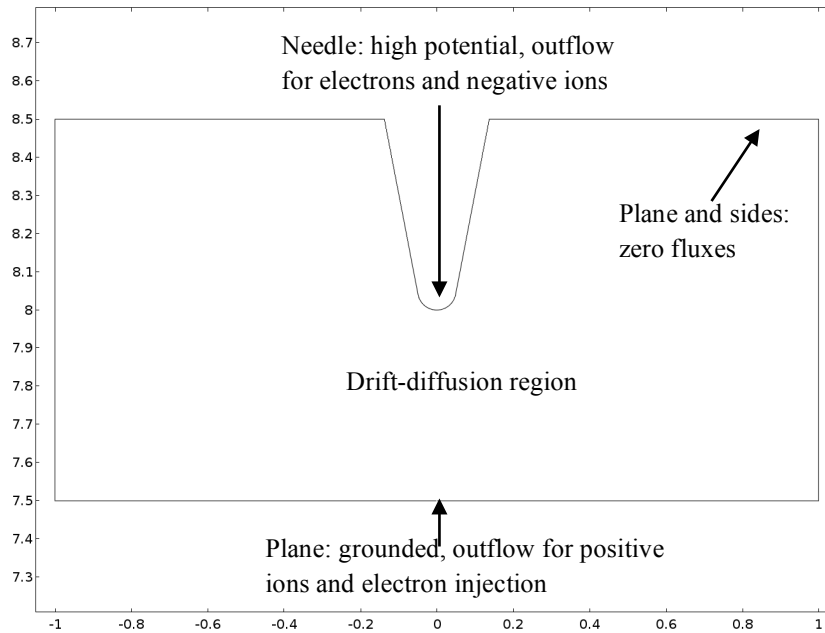
Figure 10.1: Geometry and boundary conditions used in the model.

In addition, three-term Helmholtz approximation is introduced instead of the two-terms used in [42] which enhances the photoionization model.

Calculated time variations of the electron density patterns are shown in Figures 10.2. The distributions of the densities along the symmetry axis are provided in Figure 10.3 together with the profiles obtained in the reference study. By comparing the profiles, one may notice that the calculated magnitudes of the densities are similar and the growth rate of the streamer are close in both the studies. Also, the steep gradients of the concentration at the front are well resolved. The time needed to bridge the gap in the reference model is 2.15 ns whereas in the present model it is 2.3 ns. Note that the Gaussian charge spot used as the initial condition for the streamer inception in the earlier model was not used in the new simulations. Instead, the process started from uniformly distributed charges carriers due to the background ionization. After voltage application, the local electric field causes the electrons to quickly get absorbed at the anode leaving aside the positive charges causing initiation of the streamer formation. This process needs about 0.2 ns to develop and produces a spike in the current measured during the experiments [55] [23]. At this stage, the electron density grows as a sphere surrounding the tip of the needle electrode (anode). Later on, the electronic cloud expands towards the plane (cathode) due to the generation of the electrons in the streamer head and after few nanoseconds the streamer bridges the entire inter-electrode space. The calculated diameter of the plasma channel during the streamer propagation is comparable in both the cases.

The calculated electric field patterns, Figure 10.4, demonstrate propagation of a high field region at the streamer tip, which is often referred to as an ionization wave in the literature. The distributions of the field strength along the axis of the streamer channel obtained with the different models (shown in Figures 10.5) are comparable. However, the maximum field strength and velocity are slightly different. Thus one may notice that the maximum field calculated in the present study is higher than that obtained in the previous work that may be related to the

different treatment of the photoionization term in the two models which is in general more accurate in the present work [64].
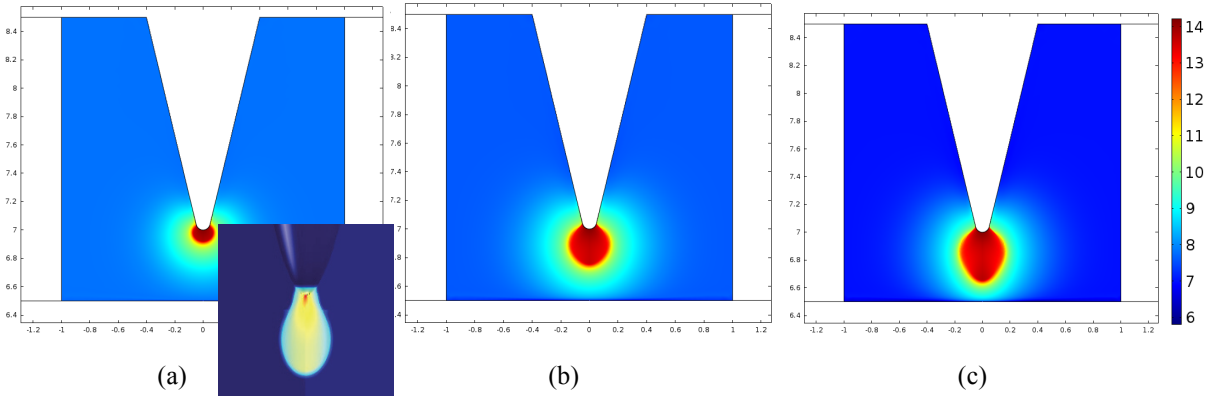
Figure 10.2: Log of electron number density (cm^{-3}) at 0.5 ns (a), 1.5 ns (b) and 2 ns (c)
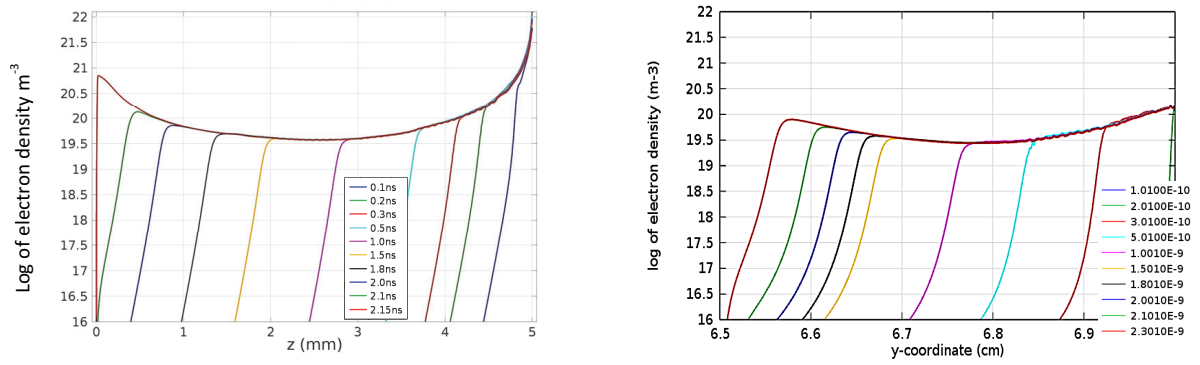
Figure 10.3: Electron density distribution (m^{-3}) along the ~~calculated~~ *by the reference model [42] (left) and by the developed model (right)*
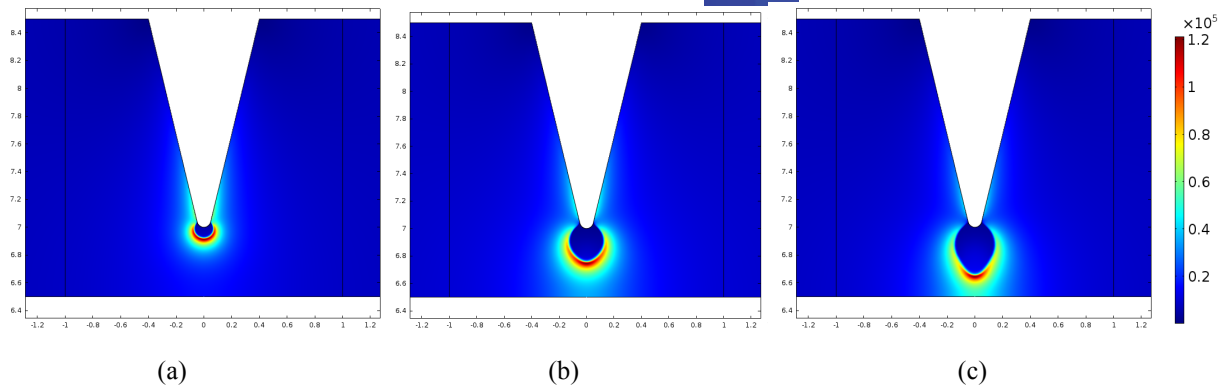
Figure 10.4: Evolution of the electric field (V/cm) at 0.5 ns (a), 1.5 ns (b) and 2 ns (c).
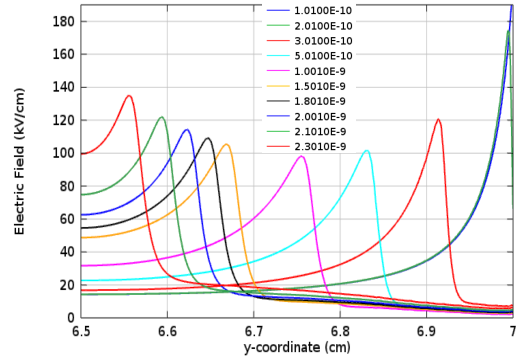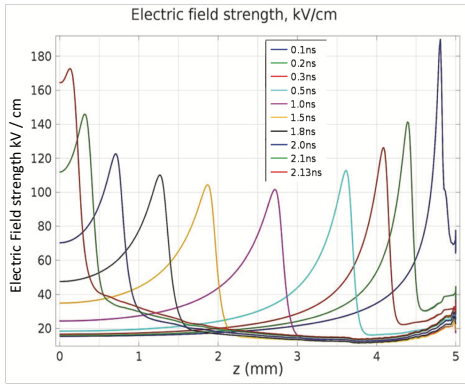
Figure 10.5. Electric field distribution along the streamer axis obtained from the reference model [42] (left) and in the present study (right).

References

[1]   E. Kuffel, W. S. Zaengl, and J. Kuffel, *High voltage engineering : Fundamentals*, 2nd ed. Oxford ; Boston: Butterworth-Heinemann, 2000.

[2]   J. J. Lowke and R. Morrow, "Theory of electric-corona including the role of plasma chemistry," *Pure and Applied Chemistry,* vol. 66, pp. 1287-1294, 1994.

[3]   N. L. Aleksandrov and E. M. Bazelyan, "Simulation of long-streamer propagation in air at atmospheric pressure," *Journal of Physics D: Applied Physics,* vol. 29, pp. 740-752, 1996.

[4]   M. S. Benilov and G. V. Naidis, "Modeling of low-current discharges in atmospheric-pressure air taking account of non-equilibrium effects," *Journal of Physics D: Applied Physics,* vol. 36, pp. 1834-1841, 2003.

[5]   A A. Haddad and D. F. Warne, *Advances in high voltage engineering.* London: Institution of Electrical Engineers, 2004.

[6]   F. Grangé, J. Loiseau, and N. Spyrou, "Random distribution of background charge density for numerical simulation of discharge inception," *International Symposium on High Pressure Low Temperature Plasma Chemistry, HAKONE V,* 1996.

[7]   M. Akyuz, L. Gao, V. Cooray, and A. Larsson, "Streamer current in a three-electrode system," *IEEE Transactions on Dielectrics and Electrical Insulation,* vol. 8, pp. 665-672, 2001.

[8]   N. L. Allen and M. Boutlendj, "Study of the electric-fields required for streamer propagation in humid air," *IEEE Proceedings of Science Measurement and Technology,* vol. 138, pp. 37-43, 1991.

[9]   M. Akyuz, M. Rahman, A. Larsson, V. Cooray, and A. Franke, "Characteristics of laser-triggered electric discharges in air," *IEEE Transactions on Dielectrics and Electrical Insulation,* vol. 12, pp. 1060-1070, 2005.

[10]   V. March, M. Arrayas, J. L. Trueba, J. Montanya, D. Romero, G. Sola*, et al.*, "Features of electrical discharges in air triggered by laser," *Journal of Electrostatics,* vol. 67, pp. 301-306, 2009.

[11]   X. B. Meng, H. W. Mei, C. L. Chen, L. M. Wang, Z. C. Guan, and J. Zhou, "Characteristics of streamer propagation along the insulation surface: influence of dielectric material," *IEEE Transactions on Dielectrics and Electrical Insulation,* vol. 22, pp. 1193-1203, 2015.

[12]   B. H. Tan, N. L. Allen, and H. Rodrigo, "Progression of positive corona on cylindrical insulating surfaces. Part I: Influence of dielectric material," *IEEE Transactions on Dielectrics and Electrical Insulation,* vol. 14, pp. 111-118, 2007.

[13]   G. E. Georghiou, A. P. Papadakis, R. Morrow, and A. C. Metaxas, "Numerical modeling of atmospheric pressure gas discharges leading to plasma production," *Journal of Physics D: Applied Physics,* vol. 38, pp. R303-R328, 2005.

[14]   J. P. Boris and D. L. Book, "Flux-corrected transport I SHASTA, a fluid transport algorithm that works," *Journal of Computational Physics,* vol. 11, pp. 38-69, 1973.

[15]   D. L. Book, J. P. Boris, and K. Hain, "Flux-Corrected Transport II - generalizations of method," *Journal of Computational Physics,* vol. 18, pp. 248-283, 1975.

[16] S. T. Zalesak, "Fully multidimensional flux-corrected transport algorithms for fluids," *Journal of Computational Physics,* vol. 31, pp. 335-362, 1979.

[17] A. A. Kulikovsky, "Positive streamer in a weak field in air: A moving avalanche to streamer transition," *Physical Review E,* vol. 57, pp. 7066-7074, 1998.

[18] M. Ramesh, S. Singh, Y. V. Serdyuk, S. M. Gubanski, and S. Kumara, "Application of streamer criteria for calculations of flashover voltages of gaseous insulation with solid dielectric barrier," presented at the *Proceedings 18th International Symposium High Voltage Engineering*, 2013.

[19] V. V. Timatkov, G. J. Pietsch, A. B. Saveliev, M. V. Sokolova, and A. G. Temnikov, "Influence of solid dielectric on the impulse discharge behaviour in a needle-to-plane air gap," *Journal of Physics D-Applied Physics,* vol. 38, pp. 877-886, Mar 2005.

[20] S. M. Lebedev, O. S. Gefle, and Y. P. Pokholkov, "The barrier effect in dielectrics: The role of interfaces in the breakdown of inhomogeneous dielectrics," *IEEE Transactions on Dielectrics and Electrical Insulation,* vol. 12, pp. 537-555, Jun 2005.

[21] I. Kitani, K. Edahiro, and K. Arii, "Spark breakdown in air/PP-film composite with point-sphere electrode system," *IEEE Transactions on Electrical Insulation,* vol. 25, pp. 393-398, Apr 1990.

[22] M. Li, L. J. Mats, T. Bengtsson, and M. Darveniza, "Barrier effects in a rod rod air gap under DC voltage," *Gaseous Dielectrics VII,* pp. 169-176, 1994.

[23] H. E. Remde, "Voltage-current characteristics during propagation of a surge breakdown of a point-to-plate gap with insulating barrier," *IEEE Transactions on Power Apparatus and Systems,* vol. 91, pp. 271, 1972.

[24] Y. V. Yurgelenas and H. E. Wagner, "A computational model of a barrier discharge in air at atmospheric pressure: the role of residual surface charges in microdischarge formation," *Journal of Physics D-Applied Physics,* vol. 39, pp. 4031-4043, 2006.

[25] U. Kogelschatz, "Dielectric-barrier discharges: Their history, discharge physics, and industrial applications," *Plasma Chemistry and Plasma Processing,* vol. 23, pp. 1-46, Mar 2003.

[26] V. I. Gibalov and G. J. Pietsch, "The development of dielectric barrier discharges in gas gaps and on surfaces," *Journal of Physics D-Applied Physics,* vol. 33, pp. 2618-2636, 2000.

[27] U. Kogelschatz, B. Eliasson, and W. Egli, "From ozone generators to flat television screens: history and future potential of dielectric-barrier discharges," *Pure and Applied Chemistry,* vol. 71, pp. 1819-1828, Oct 1999.

[28] M. Sjoberg, Y. V. Serdyuk, S. M. Gubanski, and M. A. S. Leijon, "Experimental study and numerical modeling of a dielectric barrier discharge in hybrid air-dielectric insulation," *Journal of Electrostatics,* vol. 59, pp. 87-113, Sep 2003.

[29] Y. V. Serdyuk and S. M. Gubanski, "Computer modeling of interaction of gas discharge plasma with solid dielectric barriers," *IEEE Transactions on Dielectrics and Electrical Insulation,* vol. 12, pp. 725-735, Aug 2005.

[30] J. A. Giacometti and O. N. Oliveira, "Corona charging of polymers," *IEEE Transactions on Electrical Insulation,* vol. 27, pp. 924-943, Oct 1992.

[31] F. Messerer, M. Finkel, and W. Boeck, "Surface charge accumulation on HVDC GIS Spacer," *Conference record of the 2002 IEEE International Symposium on Electrical Insulation,* pp. 421-425, 2002.

[32] T. Nitta and K. Nakanishi, "Charge accumulation on insulating spacers for HVDC GIS," *Ieee Transactions on Electrical Insulation,* vol. 26, pp. 418-427, Jun 1991.

[33] J. M. Alison, J. V. Champion, S. J. Dodd, and G. C. Stevens, "Dynamic bipolar charge recombination model for electroluminescence in polymer-based insulation during electrical tree initiation," *Journal of Physics D-Applied Physics,* vol. 28, pp. 1693-1701, Aug 1995.

[34] S. Le Roy, G. Teyssedre, C. Laurent, G. C. Montanari, and F. Palmieri, "Description of charge transport in polyethylene using a fluid model with a constant mobility: fitting model and experiments," *Journal of Physics D-Applied Physics,* vol. 39, pp. 1427-1436, Apr 2006.

[35] K. Wu and L. A. Dissado, "Model for electrical tree initiation in epoxy resin," *IEEE Transactions on Dielectrics and Electrical Insulation,* vol. 12, pp. 655-668, Aug 2005.

[36] S. Singh, "Adaptive numerical simulation of streamer propagation in atmospheric air," *Proceedings of the COMSOL Conference in Rotterdam,* 2013.

[37] S. Singh, Y. V. Serdyuk, and R. Summer, "Streamer branching in air: physical model and simulations in Fully 3D Spatial Domain," *2015 IEEE 11th International Conference on the Properties and Applications of Dielectric Materials,* pp. 220-223, 2015.

[38] S. Pancheshnyi, "Role of electronegative gas admixtures in streamer start, propagation and branching phenomena," *Plasma Sources Science and Technology,* vol. 14, 2005.

[39] W. S. Zaengl and K. Petcharaks, "Application of streamer breakdown criterion for inhomogeneous fields in dry air and SF6," in *Gaseous Dielectrics VII,* pp. 153-159, 1994.

[40] H. M. Ryan, D. Lightle, and D. Milne, "Factors influencing dielectric performance of SF6 insulated GIS," *IEEE transactions on Power Apparatus and Systems,* vol. PAS-104, pp. 1526-1535, 1985..

[41] A. Starikovskiy, A. Nikipelov, and A. Rakitin, "Streamer breakdown development in undercritical electric field," *IEEE Transactions on Plasma Science,* vol. 39, pp. 2606-2607, 2011.

[42] Y. V. Serdyuk, "Propagation of cathode-directed streamer discharges in air," *Proceedings of the COMSOL Conference , Rotterdam,* 2013.

[43] Y. V. Serdyuk, *Numerical simulations of non-thermal electrical discharges in air*: Lightning Electromagnetics , IET power and energy series, pp. 87-138, 2012.

[44] E. Worts and S. D. Kovaleski, "Theoretical investigation of a UV laser triggered spark gap," in *Pulsed Power Conference, IEEE*, pp. 623-626, 2005.

[45] C. Thoma, D. R. Welch, D. V. Rose, W. R. Zimmerman, C. L. Miller, R. E. Clark*, et al.*, "Fully kinetic particle-in-cell simulations of triggered three-electrode gas switches," in *19th IEEE Pulsed Power Conference*, pp. 1-6, 2013.

[46] M. Chung and E. Kunhardt, "Monte Carlo simulation of streamer propagation with E-E and E-E-ion collision," in *30th International Conference on Plasma Science*, 2003.

[47]   C. Li, J. Teunissen, M. Nool, W. Hundsdorfer, and U. Ebert, "A comparison of 3D particle, fluid and hybrid simulations for negative streamers," *Plasma Sources Science and Technology,* vol. 21, 2012.

[48]   B. V. Alexeev, *Generalized Boltzmann physical kinetics*, 1st ed.: Elsevier, 2004.

[49]   U. S. Inan and M. Gołkowski, *Principles of plasma physics for engineers and scientists*. Cambridge ; New York: Cambridge University Press, 2011.

[50]   G. J. M. Hagelaar and L. C. Pitchford, "Solving the Boltzmann equation to obtain electron transport coefficients and rate coefficients for fluid models," *Plasma Sources Science and Technology,* vol. 14, pp. 722-733, 2005.

[51]   L. Pitchford and A. Phelps, "Comparative calculations of electron-swarm properties in N2 at moderate E/N values," *Physical Review A,* vol. 25, pp. 540-554, 1982.

[52]   A. Phelps and L. Pitchford, "Anisotropic scattering of electrons by N2 and its effect on electron transport," *Physical Review A,* vol. 31, pp. 2932-2949, 1985.

[53]   "COMSOL Plasma Module User Manual," vol. Version 4.4-5.3, 2013-2017.

[54]   "Phelps database, http://www.lxcat.net/, retrieved on January 10, 2013."

[55]   R. Morrow, "Properties of streamers and streamer channels in SF6," *Physical Review A,* vol. 35, pp. 1778-1785, 1987.

[56]   R. Morrow, "Theory of negative corona in oxygen," *Physical Review A,* vol. 32, pp. 1799-1809, 1985.

[57]   Y. V. Serdyuk, A. Larsson, S. M. Gubanski, and M. Akyuz, "The propagation of positive streamers in a weak and uniform background electric field," *Journal of Physics D: Applied Physics.,* vol. 34, pp. 614-623, 2001.

[58]   Y. V. Serdyuk, "Computer modeling of electrophysical phenomena in high voltage insulation," *Phd Thesis - Chalmers University of Technology,* 2004.

[59]   Y. V. Serdyuk, S. M. Gubanski, J. Blennow, and M. Sjoberg, "Electrical discharge in an air gap with dielectric covered electrodes," *Conference on Electrical Insulation and Dielectric Phenomena,* vol. 1, pp. 397-400, 2000.

[60]   R. Morrow and J. J. Lowke, "Streamer propagation in air," *Journal of Physics D: Applied Physics,* vol. 30, 1997.

[61]   A. Salabas, G. Gousset, and L. L. Alves, *Plasma Sources Science and Technology,* vol. 11, 2002.

[62]   A. A. Kulikovsky, "The role of photoionization in positive streamer dynamics," *Journal of Physics D: Applied Physics,* vol. 33, pp. 1514-1524, 2000.

[63]   A. Luque, U. Ebert, C. Montijn, and W. Hundsdorfer, "Photoionization in negative streamers: Fast computations and two propagation modes," *Applied Physics Letters,* vol. 90, 2007.

[64]   A. Bourdon, V. P. Pasko, N. Y. Liu, S. Célestin, P. Ségur, and E. Marode, "Efficient models for photoionization produced by non-thermal gas discharges in air based on radiative transfer and the Helmholtz equations," *Plasma Sources Science and Technology,* vol. 16, pp. 656-678, 2007.

[65] G. Wormeester, S. Pancheshnyi, A. Luque, S. Nijdam, and U. Ebert, "Probing photoionization: simulations of positive streamers in varying N2 : O2-mixtures," *Journal of Physics D: Applied Physics,* vol. 43, p. 505201, 2010.

[66] M. B. Zhelezniak, A. K. Mnatsakanian, and S. V. Sizykh, "Photoionization of nitrogen and oxygen mixtures by radiation from gas discharge," *High Temperature,* vol. 20, pp. 357–362, 1982.

[67] A. A. Kulikovsky, "Reply to comment on 'The role of photoionization in positive streamer dynamics'," *Journal of Physics D: Applied Physics,* vol. 34, pp. 251-252, 2001.

[68] S. V. Pancheshnyi and A. Y. Starikovskii, "Comments on 'The role of photoionization in positive streamer dynamics'," *Journal of Physics D: Applied Physics,* vol. 34, pp. 248-250, Jan 21 2001.

[69] N. Liu, S. b. Célestin, A. Bourdon, V. P. Pasko, P. Ségur, and E. Marode, "Application of photoionization models based on radiative transfer and the Helmholtz equations to studies of streamers in weak electric fields," *Applied Physics Letters,* vol. 91, 2007.

[70] P. Ségur, A. Bourdon, E. Marode, D. Bessieres, and J. H. Paillol, "The use of an improved Eddington approximation to facilitate the calculation of photoionization in streamer discharges," *Plasma Sources Science and Technology,* vol. 15, pp. 648-660, 2006.

[71] F. Wang, Q. Zhang, Y. Qiu, and E. Kuffel, "Insulator surface charge accumulation under DC voltage," *Conference Record of the 2002 IEEE International Symposium on Electrical Insulation,* pp. 426-429, 2002.

[72] Z. Fang, R. A. Fouracre, and O. Farish, "Investigations of surface charging of DC insulator spacers," *IEEE 1995 Annual Report - Conference on Electrical Insulation and Dielectric Phenomena,* pp. 428-431, 1995.

[73] S. Okabe, "Phenomena and mechanism of electric charges on spacers in gas insulated switchgears," *IEEE Transactions on Dielectrics and Electrical Insulation,* vol. 14, pp. 46-52, Feb 2007.

[74] K. Papailiou and F. Schmuck, *Silicone composite insulators : materials, design, applications*, Springer, 2013.

[75] R. Hackam, "Outdoor high voltage polymeric insulators," *International Symposium on Electrical Insulating Materials, Proceedings,* pp. 1-16, 1998.

[76] C. Johnson, *Numerical solution of partial differential equations by the finite element method*: Dover Publications, 2009.

[77] O. C. Zienkiewicz, R. L. Taylor, and P. Nithiarasu, *The finite element method for fluid dynamics*, Seventh edition. ed. Oxford: Butterworth-Heinemann, 2014.

[78] R. Codina, "Comparison of some finite element methods for solving the diffusion-convection-reaction equation," *Computer Methods in Applied Mechanics and Engineering,* vol. 156, pp. 185-210, Apr 1998.

[79] D. Kuzmin and S. Turek, "Flux correction tools for finite elements," *Journal of Computational Physics,* vol. 175, pp. 525-558, Jan 20 2002.

[80] A. J. Davies and W. Niessen, "The solution of the continuity equations in ionization and plasma growth," *Physics and Applications of Pseudosparks,* vol. 219, pp. 197-217, 1990.

[81] O. Ducasse, L. Papageorghiou, O. Eichwald, N. Spyrou, and M. Yousfi, "Critical analysis on two dimensional point to plane streamer simulations using the finite element and finite volume methods," *IEEE Transactions on Plasma Science,* vol. 35, pp. 1287-1300, Oct 2007.

[82] "COMSOL Multiphysics User Manual," vol. Version 4.4-5.3, 2013-2017.

[83] R. J. LeVeque, *Finite difference methods for ordinary and partial differential equations : steady-state and time-dependent problems*, Society for Industrial and Applied Mathematics, 2007.

[84] C. Montijn, W. Hundsdorfer, and U. Ebert, "An adaptive grid refinement strategy for the simulation of negative streamers," *Journal of Computational Physics,* vol. 219, pp. 801-835, 2006.

[85] M. N. Hirsh and H. J. Oskam, *Gaseous Electronics*, Academic Press, 1978.

[86] T. M. P. Briels, J. Kos, E. M. van Veldhuizen, and U. Ebert, "Positive and negative streamers in ambient air: measuring diameter, velocity and dissipated energy," *Journal of Physics D-Applied Physics,* vol. 41, pp. 234004, 2008.

[87] P. Le Delliou, "Étude des décharges électriques impulsionnelles à pression atmosphérique dans les milieux poreux et/ou alvéolaires," 2014.

[88] A. Starikovskiy, "Fast ionization wave development in atmospheric-pressure air," *IEEE Transactions on Plasma Science,* vol. 39, pp. 2602-2603, 2011.

[89] E. Panousis, L. Papageorghiou, N. Spyrou, J. F. Loiseau, B. Held, and F. Clément, "Numerical modeling of an atmospheric pressure dielectric barrier discharge in nitrogen: electrical and kinetic description," *Journal of Physics D: Applied Physics,* vol. 40, pp. 4168-4180, 2007.

[90] R. Zeng and S. Chen, "The dynamic velocity of long positive streamers observed using a multi-frame ICCD camera in a 57 cm air gap," *Journal of Physics D-Applied Physics,* vol. 46, Dec 4 2013.

[91] A. Pedersen, T. Christen, A. Blaszczyk, and H. Boehme, "Streamer inception and propagation models for designing air insulated power devices," *CEIDP: Annual Report Conference on Electrical Insulation and Dielectric Phenomena,* pp. 571-574, 2009.

[92] E. M. van Veldhuizen, P. C. M. Kemps, and W. R. Rutgers, "Streamer branching in a short gap: The influence of the power supply," *IEEE Transactions on Plasma Science,* vol. 30, pp. 162-163, 2002.

[93] A. Luque and U. Ebert, "Electron density fluctuations accelerate the branching of positive streamer discharges in air," *Physical Review E,* vol. 84, 2011.

[94] M. Akyuz, A. Larsson, V. Cooray, and G. Strandberg, "3D simulations of streamer branching in air," *Journal of Electrostatics,* vol. 59, pp. 115-141, 2003.

[95] A. Rocco, U. Ebert, and W. Hundsdorfer, "Branching of negative streamers in free flight," *Physical Review E,* vol. 66, 2002.

[96] J. Jadidian, M. Zahn, N. Lavesson, O. Widlund, and K. Borg, "Stochastic and deterministic causes of streamer branching in liquid dielectrics," *Journal of Applied Physics,* vol. 114, 2013.

[97] A. A. Kulikovsky, "Comment on ``Spontaneous branching of anode-directed streamers between planar electrodes''," *Physical Review Letters,* vol. 89, 2002.

[98] A. L. Kupershtokh and D. I. Karpov, "Simulation of the development of branching streamer structures in dielectric liquids with pulsed conductivity of channels," *Technical Physics Letters,* vol. 32, pp. 406-409, 2006.

[99] F. Pechereau, P. Le Delliou, J. Jansky, P. Tardiveau, S. Pasquiers, and A. Bourdon, "Large conical discharge structure of an air discharge at atmospheric pressure in a point-to-plane geometry," *IEEE Transactions on Plasma Science,* vol. 42, pp. 2346-2347, 2014.

[100] H. Meyer, F. Mauseth, A. Pederson, and J. Ekeberg, "Streamer propagation in rod-plane air gaps with a dielectric barrier," in *The Conference on Electrical Insulation and Dielectric Phenomena*, 2016.

[101] J. Locher, " The effect of dielectric mist on electrical breakdown in insulating gases," Master Thesis, 2016.